INTRODUCTORY VISUAL LECTURE ON QCD AT LARGE N_c: BOUND STATES, CHIRAL MODELS, AND PHASE DIAGRAM* **

Francesco Giacosa

Institute of Physics, Jan Kochanowski University
Uniwersytecka 7, 25-406, Kielce, Poland
and
Institute for Theoretical Physics, Johann Wolfgang Goethe University
Max-von-Laue-Str. 1, 60438, Frankfurt am Main, Germany

Received 21 February 2024, accepted 17 April 2024, published online 3 June 2024

In these lectures, we present the behavior of conventional $\bar{q}q$ mesons, glueballs, and hybrids in the large-N_c limit of QCD. To this end, we use an approach based on rather simple "NJL-like" bound-state equations. The obtained large-N_c scaling laws are general and coincide with the known results. A series of consequences, such as the narrowness of certain mesons and the smallness of some interaction types, the behavior of chiral and dilaton models at large N_c, and the relation to the compositeness condition and the standard derivation of large-N_c results, are explained. The bound-state formalism shows also that mesonic molecular and dynamically generated states do not form in the large-N_c limit. The same fate seems to apply also to tetraquark states, but here further studies are needed. Next, following the same approach, baryons are studied as bound states of a generalized diquark ($N_c - 1$ antisymmetric object) and a quark. Similarities and differences with regular mesons are discussed. All the standard scaling laws for baryons and their interaction with mesons are correctly reproduced. The behavior of chiral models involving baryons and describing chirally invariant mass generation is investigated. Finally, properties of QCD in the medium at largeN_c are studied: the deconfinement phase transition is investigated along the temperature and the chemical potential directions, respectively. While the critical temperature for deconfinement $T_{\rm dec}$ is N_c-independent, the critical chemical potential is not and increases for growing N_c, thus for very large N_c, one has confined matter below $T_{\rm dec}$ and deconfined above. Yet, in the confined phase but for large densities, one has a 'stiff-matter' phase whose pressure is proportional to N_c (just as a gas of quarks would do) in agreement with a quarkyonic phase. Within the QCD phase diagrams, the features of different models at largeN_c are

* Presented at the LXIII Cracow School of Theoretical Physics *Nuclear Matter at Extreme Densities and High Temperatures*, Zakopane, Poland, 17–23 September, 2023.

reviewed and the location of the critical endpoint is discussed. In the end, the very existence of nuclei and the implications of large-N_c arguments for neutron stars are outlined.

DOI:10.5506/APhysPolB.55.4-A1

1. Introduction

In Quantum Chromodynamics (QCD) each quark can appear in three charges denoted as colors: red (R), green (G), and blue (B). This applies to any of the six quark flavors present in Nature (the light quarks flavors u, d, s and the heavy quark flavors c, b, t [1]). The force carriers, the gluons, can be thought as color–anticolor objects, for a total of $9 - 1 = 8$ combinations [2, 3].

The origin of colors can be better understood by looking at the fundamental properties of QCD, which is a gauge theory built under local invariance of the color group SU(3). The quarks transform under the fundamental representation and the gluons under the adjoint representation.

Why QCD has 3 colors ($N_c = 3$, where N_c stands for the number of colors) and not, *e.g.* 7? At present, there is no compelling answer for that, at least not within the Standard Model (SM). One may eventually ask if the choice $N_c \neq 3$ would allow for stable nuclei, and if this is not the case [4], resort to a kind of anthropic argument.

Yet, here we are not interested in this type of questions, but rather in the study of N_c different from 3, and in particular the study of the limit in which N_c is a 'large' number, in order to understand better our world with $N_c = 3$. This is indeed the so-called QCD in the large-N_c limit, initiated by 't Hooft [5] and further investigated in several review papers and lectures [6–12] (and references therein).

At first, the idea to consider an expansion along N_c may sound strange: how could *anything* valid for, say, $N_c = 101$, be also somewhat relevant for the physical case $N_c = 3$? In other words, how can $N_c = 3$ be considered a 'large' number [6]? As we shall see, that depends. In some (indeed the majority of) cases, the number 3 turns out to be large.

In particular, in these lectures, we intend to revisit the behavior of bound states of QCD in the large-N_c limit. To this end, we recall that quarks and gluons are confined in hadrons, further classified as mesons (bosonic hadrons) and baryons (baryonic hadrons).

Mesons can be divided into conventional ones corresponding to quark–antiquark states (quarkonia), and to exotic or non-conventional types, such as glueballs, hybrids but also mesonic molecules, dynamically generated states, and compact tetraquark states (bound states of diquarks). Quite interestingly, quarkonia, glueballs, and hybrids 'survive' in the large-N_c limit:

this means that their masses are N_c-independent, and their widths decrease with N_c, implying that these objects become stable in the large-N_c limit. We shall revisit these well-known results as well as the specific scaling laws in a novel fashion, that involves the study of bound-state equations. For the latter, we chose the easiest possible approach that describes bound-state equations similar to the ones found in the Nambu–Jona-Lasinio (NJL) model [13–15] (technically, the kernel is separable). Indeed, these bound-state equations are also similar to approaches involving the compositeness conditions, *e.g.* [16–19]. Yet, it should be stressed that our aim is not to actually solve these equations, but just to discuss their large-N_c behavior. The latter is (thought to be) independent of the particular approach and applies also to more advanced methods for bound states, such as the Bethe–Salpeter equations in QCD [20–22]. Quite interestingly, the proposed large-N_c treatment can also help to understand, from a different perspective, various large-N_c features. Namely, we shall re-derive known results in a different and quite simple way. The coupling of bound objects to their constituents is also an intermediate consequence of the chosen approach.

As additional applications, we shall present the large-N_c study of the linear sigma model (LSM) [23, 24], the dilaton [25–28], and their interconnection. Many other properties (weak decay constant, decay chains, *etc.*) shall be discussed as well. The connection of our bound-state approach to the commonly implemented one that uses correlators and currents is also shown.

The fate of mesonic molecular and dynamically generated states is different: they fade away in the large-N_c limit. Indeed, we shall recover this result within the bound-state approach. A peculiar case, not yet fully solved, is if all tetraquark types (among which molecules are only a specific example) fade out as well. It was long believed that this is the case, but this conclusion was revisited by Weinberg in 2013 [29], in which he argued that certain tetraquarks could exist in the large N_c and, if that is the case, their mass scale as N_c^0 and their width as N_c^{-1}, just as regular quarkonia. The work [29] was followed by a series of papers on the subject [12, 30–34]. Up to now, the existence of such peculiar tetraquarks in the large-N_c limit is not settled. We shall discuss what the bound-state approach has to say for tetraquarks as well.

Baryons will be also briefly discussed in this work. We shall concentrate on conventional baryons, which for $N_c = 3$ are made of 3 quarks and for an arbitrary N_c, of N_c quarks. We shall present some interesting similarities between conventional baryons and conventional mesons. To this end, we treat baryons in a way similar to conventional mesons: they shall be seen as a bound state of a quark and of a generalized diquark, the latter being the antisymmetric combination of $N_c - 1$ quarks. Within this context, we

will re-derive the large-N_c scaling for baryons. As an application, we study chiral models implementing baryonic fields and investigate possible ways to generate their mass in a chiral invariant manner and in agreement with large-N_c expectations.

In the end, we recall — concisely — some relevant facts concerning the large-N_c behavior of QCD at finite temperature and density, concentrating on the phase diagram and the quarkyonic phase [35–38], chiral models in the medium [24, 39], nuclear matter [4, 40], and neutron stars [41, 42].

The style of these lectures is focused on the conceptual and qualitative features of QCD at large N_c. Moreover, many pictures shall be presented for a better visualization of the scaling properties. These lectures on large N_c complete previous lectures on chiral models for mesons beyond the quark–antiquark picture given a few years ago [43].

The article is organized as follows. In Section 2, we introduce QCD for an arbitrary number of colors together with the double-line notation and the groups SU(N) and U(N), we discuss the QCD running coupling in the framework of the 't Hooft large-N_c limit, and we qualitatively argue that the main features of the propagators of quarks and gluons are N_c-independent. Next, in Section 3, we study mesons in the large-N_c limit, first the conventional ones (quarkonia) and related topics (chiral models, ...), then the exotic glueballs (together with the dilaton), hybrids, and four-quark objects. In Section 4, we present conventional baryons and their implementation in chiral models. In Section 5, we discuss the main properties of QCD matter at nonzero temperature and chemical potential for large N_c. In Section 6, conclusions are summarized.

2. QCD for arbitrary N_c

2.1. QCD Lagrangian of any N_c

We present the Lagrangian of QCD for an arbitrary number of colors N_c and quark flavors N_f (see, for instance, [2, 3])

$$\begin{aligned} \mathcal{L}_{\rm QCD} &= {\rm Tr}\left[\bar{q}_i(i\gamma^\mu D_\mu - m_i)q_i - \tfrac{1}{2}G_{\mu\nu}G^{\mu\nu}\right], \qquad D_\mu = \partial_\mu - ig_0 A_\mu\,, \\ G^a_{\mu\nu} &= \partial_\mu A_\nu - \partial_\nu A_\mu - ig_0[A_\mu, A_\nu]\,. \end{aligned} \tag{1}$$

Above, A_μ is $N_c \times N_c$ Hermitian matrix, and $q_i(x)$ is a vector in color space for each value of the flavor index $i = 1, \ldots, N_f$ (with N_f being the number of quark flavors), see details below. Moreover, the coupling constant g_0 is an adimensional parameter of the classical Lagrangian and m_i is the bare mass of the $i^{\rm th}$ quark flavor. Note, in the chiral limit ($m_i = 0$, for each i) the Lagrangian is invariant under dilatation transformation since no dimensionful parameter is present in the classical theory. This symmetry is broken by quantum fluctuations (trace anomaly, see Section 3.2).

The part of Eq. (1) containing only gluons is called the Yang–Mills (YM) Lagrangian

$$\mathcal{L}_{\rm YM} = {\rm Tr}\left[-\tfrac{1}{2}G_{\mu\nu}G^{\mu\nu}\right] \ . \tag{2}$$

For $N_c > 1$, the YM Lagrangian contains 3-gluon and 4-gluon vertices. The gluonic self-interactions are a fundamental property of non-Abelian theories. In turn, this feature implies that gluonic bound states, called glueballs, are possible [44–46], see also Section 3.2.

In Nature, $N_c = 3$ and $N_f = 6$. However, depending on the problem, one can consider different values for N_c and N_f. For instance, low-energy QCD is realized for $N_c = 3$ and $N_f = 3$, *i.e.* only light quarks are retained. Moreover, varying N_c is the main goal of large-N_c studies.

In Figs. 1 and 2, we present the Feynman diagrams that follow from the QCD Lagrangian. In particular, in Fig. 1, the fundamental quark–gluon vertex is depicted, while in Fig. 2, the gluonic self-interactions are shown. In both cases, gluons are also represented via the so-called double-line notation, that 'naively speaking' corresponds to a quark and an antiquark. In order to understand this point better, we need to have a closer look at the gluon field.

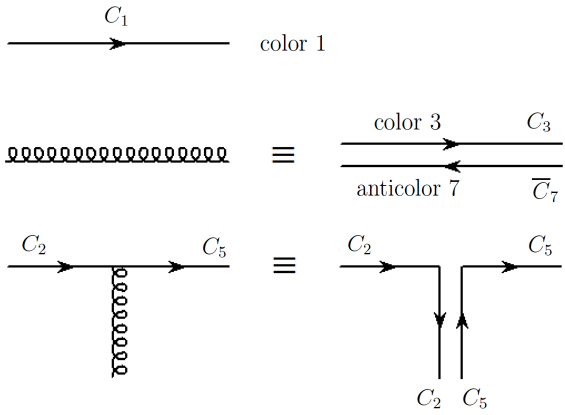

Fig. 1. Free quark, free gluon, and quark-gluon vertex. The double-line notation for the gluons is also shown. The specific choice of colors refers to illustrative examples: the free quark is taken with color C_1, the free gluon carries $\bar{C}_7 C_3$, and the vertex shows how a quark C_2 changes into C_5 via the interaction with a $\bar{C}_2 C_5$ gluon.

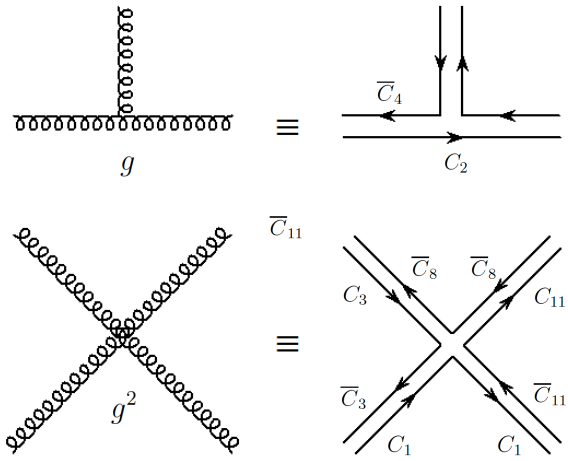

Fig. 2. Three-leg and four-leg in the standard and double-line notation. The specific choice of colors on the right part refers to examples.

The $N_c \times N_c$ Hermitian matrix Yang–Mills field $A_\mu(x)$ can be expressed as

$$A_\mu(x) = \sum_{a=1}^{N_c^2-1} A_\mu^a(x) t^a \,, \tag{3}$$

where t^a is an appropriate set of $N_c^2 - 1$ matrices basis. Usually, they are taken as Hermitian and traceless, see the next subsection. In this way, the coefficients $A_\mu^a(x)$ are real numbers.

The quark field is a vector in color space with

$$q_i = \begin{pmatrix} q_{1,i} \\ q_{1,i} \\ \dots \\ q_{N_c,i} \end{pmatrix} \,, \tag{4}$$

where $i = 1, \dots, N_f$ is the flavor index.

Under SU(N_c) local gauge transformations, these fields transform as

$$q_i \to U(x) q_i \,, \qquad A_\mu(x) \to A'_\mu(x) = U(x) A_\mu(x) U^\dagger(x) - \frac{i}{g_0} U(x) \partial_\mu U^\dagger(x) \,, \tag{5}$$

where $U(x)$ is an arbitrary function of the space-time variable $x \equiv x^\mu \equiv (t, \boldsymbol{x})$.

The Lagrangian $\mathcal{L}_{\rm QCD}$ has been constructed to be invariant under the local gauge transformations of Eq. (5).

A particularly useful limit is the one in which $U(x) = U$ is a constant matrix, leading to

$$q_i \to U q_i \,, \qquad A_\mu(x) \to A'_\mu(x) = U A_\mu(x) U^\dagger \,. \tag{6}$$

In Figs. 1 and 2, a double-line notation for the gluon is presented, according to which the gluon field is described with the help of components carrying two indices

$$A_\mu^{(a,b)}(x) \equiv A_\mu^{(a,b)}(x) \quad \text{with} \quad a, b = 1, \ldots, N_c \,. \tag{7}$$

This point reflects the adjoint Nature of the gluon field that, for what concerns color, can be seen (besides the singlet colorless configuration that is not present) as a quark–antiquark object. For instance,

$$A_\mu^{(2,5)} \equiv \bar{C}_2 C_5 \,, \tag{8}$$

implying that this gluon configuration contains the color C_5 and the anti-color $\bar{C}_2$. Indeed, this choice corresponds to a specific one for the basis of the t^a matrices

$$A_\mu(x) \equiv \sum_{a=1}^{N_c} \sum_{b=1}^{N_c} A_\mu^{(a,b)} t^{(a,b)} \,, \tag{9}$$

where the N_c^2 matrices $t^{(a,b)}$ are given by

$$\left(t^{(a,b)} \right)_{c,d} = \delta_{ac} \delta_{bd} \,. \tag{10}$$

The matrices of this basis are neither Hermitian nor traceless, so the 'coefficients' $A_\mu^{(a,b)}$ are not real, but need to fulfill the following requirements:

$$A_\mu^{(a,b)} = \left(A_\mu^{(b,a)} \right)^* \,, \qquad \sum_{a=1}^{N_c} A_\mu^{(a,a)} = 0 \,. \tag{11}$$

In fact, the former equation guarantees that A^μ is Hermitian, and the latter that it is traceless. Namely, the employed basis contains a matrix 'too much', thus one needs to remove the color singlet (traceless) configuration. Yet, for large N_c this additional contribution is negligible, so we will usually not 'bother' to subtract it. Note, also the tensor $G_{\mu\nu}$ can be expressed in this basis as

$$G_{\mu\nu} = \sum_{a=1}^{N_c} \sum_{b=1}^{N_c} G_{\mu\nu}^{(a,b)} t^{(a,b)} \,. \tag{12}$$

Indeed, while this choice for the matrices t^a may be useful to realize the double-line idea for a gluon, it is not what is usually employed for the specific cases of $N_c = 2$ or $N_c = 3$, see the next subsection.

2.2. Brief recall of SU(N)

Before we continue, it is important to recall some basic properties of the groups U(N) and SU(N) (see *e.g.* Ref. [47]). An element of the group U(N) is a complex $N \times N$ matrix such that

$$U^\dagger U = U U^\dagger = 1_N \,, \tag{13}$$

thus U can be expressed as

$$U = \mathrm{e}^{i\theta_a t^a} \,, \qquad a = 0, 1, \ldots, N^2 - 1 \,, \tag{14}$$

where the matrices t^a are N^2 linearly-independent $N \times N$ Hermitian matrices, implying that Eq. (13) is fulfilled. Following the usual convention, we set

$$t^0 = \frac{1}{\sqrt{2N}} 1_N \,, \tag{15}$$

and for the other matrices, we choose

$$\mathrm{Tr}\left[t^a t^b\right] = \tfrac{1}{2}\delta^{ab} \quad \text{with} \quad a, b = 0, 1, \ldots, N^2 - 1 \,, \tag{16}$$

then

$$\mathrm{Tr}\left[t^a\right] = 0 \quad \text{for} \quad a = 1, \ldots, N^2 - 1 \,. \tag{17}$$

An $N \times N$ matrix U belongs to the SU(N) group if the following two equations are fulfilled:

$$U^\dagger U = U U^\dagger = 1_N \,, \qquad \det U = 1 \,. \tag{18}$$

It is clear that a matrix belonging to SU(N) can be written as

$$U = \mathrm{e}^{i\theta_a t^a} \quad \text{with} \quad a = 1, \ldots, N^2 - 1 \,, \tag{19}$$

(the identity matrix, which is not traceless, is left out). Then

$$\det U = \mathrm{e}^{\mathrm{Tr}\left[i \sum_{a=1}^{N^2-1} \theta_a t^a\right]} = 1 \,. \tag{20}$$

The matrices t^a with $a = 1, \ldots, N^2 - 1$ are the generators of SU(N) and fulfill the algebra

$$\left[t^a, t^b\right] = i f^{abc} t^c \quad \text{with} \quad a, b, c = 1, \ldots, N^2 - 1 \,, \tag{21}$$

where f^{abc} are the corresponding antisymmetric structure constants, see [47] for their explicit form. Namely, the commutator of two Hermitian matrices is anti-Hermitian and traceless, therefore it must be expressed as a sum over t^a for $a = 1, \ldots, N^2 - 1$. By taking this choice, the matrix A_μ is Hermitian and traceless for arbitrary real coefficients A^a_μ in Eq. (3).

For the color local case of QCD, the unitary matrix $U(x)$ can be expressed as

$$U(x) = \mathrm{e}^{i\theta_a(x)t^a}\,, \quad a = 1, \ldots, N_c^2 - 1 \; (= 8 \quad \text{for} \quad N_c = 3)\,, \tag{22}$$

where the quantities $\theta_a(x)$ are arbitrary functions of the spacetime variable x.

It is useful to briefly discuss some particular examples. For $N_c = 2$, the generators are given by the matrices $t^a = \sigma^a/2$, where the σ^a are the Pauli matrices. The structure constants read $f^{abc} = \epsilon^{abc}$. Finally, the matrix A_μ takes the explicit form

$$\begin{aligned} A_\mu &= \sum_{a=1}^{N_c^2-1} A_\mu^a t^a = \sum_{a=1}^{N_c^2-1} A_\mu^a \frac{\tau^a}{2} \\ &= \frac{1}{\sqrt{2}} \begin{pmatrix} \frac{A_\mu^3}{\sqrt{2}} & \frac{A_\mu^1 - iA_\mu^2}{\sqrt{2}} \\ \frac{A_\mu^1 + iA_\mu^2}{\sqrt{2}} & -\frac{A_\mu^3}{\sqrt{2}} \end{pmatrix} \equiv \frac{1}{\sqrt{2}} \begin{pmatrix} \frac{R\bar{R} - G\bar{G}}{2} & R\bar{G} \\ G\bar{R} & \frac{-R\bar{R} + G\bar{G}}{2} \end{pmatrix}, \end{aligned} \tag{23}$$

where it is visible that $\mathrm{Tr}[A_\mu] = 0$ and $A_\mu^\dagger$. The off-diagonal components correspond to the expected double-line assignment. Note, upon including the 0^{th} component (a negligible error for large N_c), we obtain

$$\begin{aligned} A_\mu &= \sum_{a=0}^{N_c^2-1} A_\mu^a t^a = \sum_{a=1}^{N_c^2-1} A_\mu^a \frac{\tau^a}{2} \\ &= \frac{1}{\sqrt{2}} \begin{pmatrix} \frac{A_\mu^0 + A_\mu^3}{\sqrt{2}} & \frac{A_\mu^1 - iA_\mu^2}{\sqrt{2}} \\ \frac{A_\mu^1 + iA_\mu^2}{\sqrt{2}} & \frac{A_\mu^0 - A_\mu^3}{\sqrt{2}} \end{pmatrix} \equiv \frac{1}{\sqrt{2}} \begin{pmatrix} R\bar{R} & R\bar{G} \\ G\bar{R} & G\bar{G} \end{pmatrix} \end{aligned} \tag{24}$$

that corresponds to the double-line notation also along the diagonal elements. Note, in a classical view above, R and G may be thought of as complex numbers that characterize a quark component $\begin{pmatrix} R & G \end{pmatrix}^t$, while the bar quantities are the complex conjugates. The matrix A_μ (that includes the 0^{th} element), corresponds then to

$$A_\mu = \frac{1}{\sqrt{2}} \begin{pmatrix} R \\ G \end{pmatrix} \begin{pmatrix} \bar{R} & \bar{G} \end{pmatrix} \tag{25}$$

which clearly shows the origin of the double-line notation as well as the dual nature of the gluon field.

It is interesting to notice that a similar decomposition holds for the pion triplet

$$\pi = \sum_{a=1}^{N_c^2-1} \pi^a t^a = \frac{1}{\sqrt{2}} \begin{pmatrix} \frac{\pi^3}{\sqrt{2}} & \frac{\pi^1 - i\pi^2}{\sqrt{2}} \\ \frac{\pi^1 + i\pi^2}{\sqrt{2}} & -\frac{\pi^3}{\sqrt{2}} \end{pmatrix}$$
$$= \frac{1}{\sqrt{2}} \begin{pmatrix} \frac{\pi^0}{\sqrt{2}} & \pi^+ \\ \pi^- & -\frac{\pi^0}{\sqrt{2}} \end{pmatrix} = \frac{1}{\sqrt{2}} \begin{pmatrix} \frac{u\bar{u} - d\bar{d}}{2} & u\bar{d} \\ d\bar{u} & \frac{-u\bar{u} + d\bar{d}}{2} \end{pmatrix}, \tag{26}$$

while upon introducing $P^0 = \eta_N = \sqrt{1/2}(u\bar{u} + d\bar{d})$, the full multiplet (quartet) of pseudoscalar states can be described as

$$P = \sum_{a=0}^{N_c^2-1} P^a t^a = \frac{1}{\sqrt{2}} \begin{pmatrix} \frac{\eta_N + \pi^3}{\sqrt{2}} & \frac{\pi^1 - i\pi^2}{\sqrt{2}} \\ \frac{\pi^1 + i\pi^2}{\sqrt{2}} & \frac{\eta_N - \pi^3}{\sqrt{2}} \end{pmatrix}$$
$$= \frac{1}{\sqrt{2}} \begin{pmatrix} \frac{\eta_N + \pi^0}{\sqrt{2}} & \pi^+ \\ \pi^- & \frac{\eta_N - \pi^0}{\sqrt{2}} \end{pmatrix} = \frac{1}{\sqrt{2}} \begin{pmatrix} u\bar{u} & u\bar{d} \\ d\bar{u} & d\bar{d} \end{pmatrix}. \tag{27}$$

The case of $N_c = 3$ can be treated in a similar way. The matrices are $t^a = \lambda^a/2$, with the λ^a being the Gell-Mann matrices for $a = 1, \ldots, 8$.

Finally, we recall also that there is discrete a subgroup of SU(N), denoted as the center $Z(N)$, whose N elements are given by [3]

$$Z = Z_n = \mathrm{e}^{i\frac{2\pi n}{N}} 1_N, \qquad n = 0, 1, 2, \ldots, N-1. \tag{28}$$

Each Z_n corresponds to a proper choice of the parameters θ_a (the case of $Z_0 = 1_N$ corresponds to the simple case of $\theta_a = 0$, the other elements to more complicated choices). This group plays an important role at nonzero temperature as an indicator of confinement, since the $Z(N)$-symmetry is realized in the QCD vacuum and in the confined phase (at small T), but is broken in the deconfined one (at large T) [3, 48].

2.3. Running coupling of QCD

The coupling 'constant' g_0 entering the classical QCD Lagrangian of Eq. (1) turns into a running coupling when QCD is quantized. At one-loop level (which is enough for our illustrative purposes here), one has [2]

$$\mu \frac{\mathrm{d}g}{\mathrm{d}\mu} = -bg^3, \tag{29}$$

with

$$b = \frac{1}{2}\frac{1}{8\pi^2}\left(\frac{11}{3}N_c - \frac{2}{3}N_f\right), \tag{30}$$

and where

$$g_{\rm QCD} \equiv g \equiv g(\mu) \tag{31}$$

refers to the QCD running coupling. In this work, whenever g will be presented, it always refers to the fundamental QCD coupling. Other coupling constants shall carry an appropriate subscript specifying to what they refer. For a detailed description of the QCD running coupling for $N_c = 3$, we refer to Ref. [49] and references therein.

In Nature, $N_c = 3$ and N_f ranges from 2 to 6, in dependence on the number of considered quark flavors; in any case, $b > 0$. Note, $b > 0$ is definitely also true in the large-N_c limit upon keeping N_f fixed, as we shall do here. This is the so-called 't Hooft large-N_c scheme [5].

Upon fixing g_0 at a certain (large, or ultraviolet (UV)) energy scale $\Lambda_{\rm UV}$ and by integrating we obtain

$$\int\limits_g^{g_0} {\rm d}g' \frac{{\rm d}g'}{g'^3} = \left[\frac{g'^{-2}}{-2}\right]_g^{g_0} = -\int\limits_\mu^{\Lambda_{\rm UV}} {\rm d}g' b \frac{{\rm d}\mu'}{\mu'} = -b \ln \frac{\Lambda_{\rm UV}}{\mu} = b \ln \frac{\mu}{\Lambda_{\rm UV}}\,, \tag{32}$$

$$\frac{1}{g_0^2} - \frac{1}{g^2} = -2b \ln \frac{\mu}{\Lambda_{\rm UV}}\,, \tag{33}$$

$$\frac{1}{g^2} = \frac{1}{g_0^2} + 2b \ln \frac{\mu}{\Lambda_{\rm UV}} = \frac{1 + 2bg_0^2 \ln \frac{\mu}{\Lambda_{\rm UV}}}{g_0^2}\,. \tag{34}$$

Hence

$$g^2 = \frac{g_0^2}{1 + 2bg_0^2 \ln \frac{\mu}{\Lambda_{\rm UV}}}\,. \tag{35}$$

Then

$$g^2(\mu) = \frac{g_0^2}{1 + 2bg_0^2 \ln \frac{\mu}{\Lambda_{\rm UV}}} = \frac{g_0^2}{1 + \frac{g_0^2}{8\pi^2}\left(\frac{11}{3}N_c - \frac{2}{3}N_f\right) \ln \frac{\mu}{\Lambda_{\rm UV}}}\,. \tag{36}$$

One has (by construction)

$$g^2(\mu = \Lambda_{\rm UV}) = g_0^2\,. \tag{37}$$

Upon setting the denominator to zero

$$1 + \frac{g_0^2}{8\pi^2}\left(\frac{11}{3}N_c - \frac{2}{3}N_f\right) \ln \frac{\mu}{\Lambda_{\rm UV}} = 0\,, \tag{38}$$

we obtain the so-called $\Lambda_{\rm QCD}$ scale as a Landau pole of the running coupling

$$\Lambda_{\rm QCD} = \Lambda_{\rm UV} \exp\left[-\frac{8\pi^2}{g_0^2\left(\frac{11}{3}N_c - \frac{2}{3}N_f\right)}\right] \ll \Lambda_{\rm UV}\,. \tag{39}$$

The existence of a pole of the coupling at the low energy $\Lambda_{\rm QCD} \ll \Lambda_{\rm UV}$ is an artifact of the one-loop perturbative approach, but it signalizes that the running coupling becomes large. In Ref. [50], using the functional renormalization group (FRG) approach, it is shown that no infinity of the QCD running coupling takes place.

The value of the bare coupling can be expressed as

$$g_0^2 = -\frac{1}{\left(\frac{11}{3}N_c - \frac{2}{3}N_f\right)} \frac{8\pi^2}{\ln \frac{\Lambda_{\rm QCD}}{\Lambda_{\rm UV}}} \,. \tag{40}$$

Here, we intend to study the limit in which the low-energy scale $\Lambda_{\rm QCD}$ is independent of N_c ('t Hooft limit). We require that

$$g_0^2 \propto \frac{1}{N_c} \,, \tag{41}$$

then

$$g_0 \propto \frac{1}{\sqrt{N_c}} \,. \tag{42}$$

Next, upon eliminating the UV scale $\Lambda_{\rm UV}$, we find

$$\begin{aligned} g^2(\mu) &= \frac{g_0^2}{1 + \frac{g_0^2}{8\pi^2}\left(\frac{11}{3}N_c - \frac{2}{3}N_f\right)\ln\frac{\mu}{\Lambda_{\rm UV}}} \\ &= -\frac{-\frac{1}{\left(\frac{11}{3}N_c - \frac{2}{3}N_f\right)}\frac{8\pi^2}{\ln\frac{\Lambda_{\rm QCD}}{\Lambda_{\rm UV}}}}{1 + \left(-\frac{1}{\left(\frac{11}{3}N_c - \frac{2}{3}N_f\right)}\frac{8\pi^2}{\ln\frac{\Lambda_{\rm QCD}}{\Lambda_{\rm UV}}}\right)\frac{1}{8\pi^2}\left(\frac{11}{3}N_c - \frac{2}{3}N_f\right)\ln\frac{\mu}{\Lambda_{\rm UV}}} \\ &= \frac{8\pi^2}{\left(\frac{11}{3}N_c - \frac{2}{3}N_f\right)}\frac{1}{\ln\frac{\mu}{\Lambda_{\rm QCD}}} \,. \end{aligned} \tag{43}$$

Thus, in terms of μ and $\Lambda_{\rm QCD}$, the one-loop running coupling can be expressed as

$$g^2(\mu) = \frac{8\pi^2}{\left(\frac{11}{3}N_c - \frac{2}{3}N_f\right)}\frac{1}{\ln\frac{\mu}{\Lambda_{\rm QCD}}} \,. \tag{44}$$

For large N_c, we get

$$g_{\rm QCD}^2 \equiv g^2(\mu) = \frac{8\pi^2}{\left(\frac{11}{3}N_c\right)}\frac{1}{\ln\frac{\mu}{\Lambda_{\rm QCD}}} \propto \frac{1}{N_c} \,. \tag{45}$$

As for the bare coupling, also the running coupling scales as $1/\sqrt{N_c}$ if $\Lambda_{\rm QCD}$ and N_f are kept N_c-independent. In Fig. 3, the coupling $g(\mu)$ is plotted for $N_c = 3$ and $N_c = 7$.

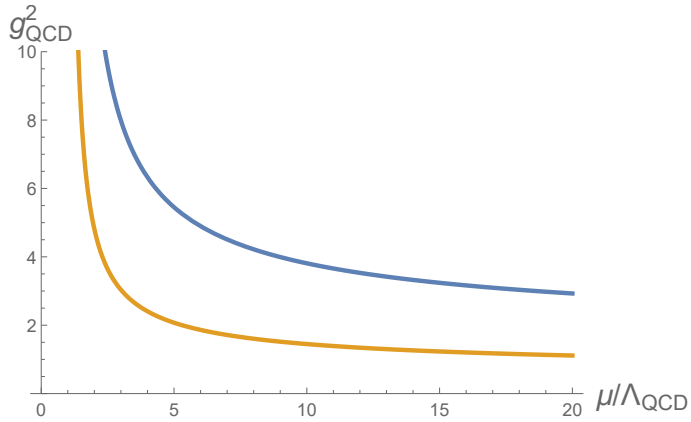

Fig. 3. Running coupling of QCD of Eq. (45) for $N_c = 3$ (upper, blue curve) and for $N_c = 7$ (lower, yellow curve). The Landau pole is the same in both cases, in agreement with the 't Hooft large-N_c limit.

The fact that the coupling g is a function of μ is also at the basis of the so-called trace anomaly: the original classical invariance under dilatation symmetry (which is exact in the chiral limit) is broken by quantum fluctuations that lead to the emergence of the low-energy scale $\Lambda_{\rm QCD}$.

The behavior of the running coupling is in agreement with two crucial properties of QCD: asymptotic freedom and confinement. The former is due to the fact that the coupling becomes smaller at large energies, at which quarks and gluons interact perturbatively. The latter implies that quarks and gluons are confined into hadrons. This is not directly provable, but it fits well with the fact that the coupling becomes large at small energies.

The coupling constant becomes also small in the large-N_c limit, but at the same time, the number of colors grows. Thus, at first, it is hard to say what will happen in this regime. It is assumed (and one finds no contradiction) that many of the properties of QCD are still valid in the large-N_c limit, among which confinement, asymptotic freedom, and spontaneous symmetry breaking (SSB).

For completeness, we summarize below also additional symmetries (besides 'local' color symmetry) of QCD for $m_i = 0$ (more details in Ref. [43]). To this end, the quark field q_i is split into

$$q_i = q_{i,\rm R} + q_{i,\rm L} \tag{46}$$

with

$$q_{i,\rm L} = \frac{1-\gamma^5}{2} q_i \quad \text{and} \quad q_{i,\rm R} = \frac{1+\gamma^5}{2} q_i \,. \tag{47}$$

(i) The dilatation transformation ($x^\mu \to \lambda^{-1} x^\mu$, together with $A_\mu \to \lambda A_\mu$ and $q_i \to \lambda^{3/2} q_i$) is a classical symmetry of QCD in the chiral limit, which is broken by quantum fluctuations (trace anomaly), in turn implying the emergence of the energy scale $\Lambda_{\rm QCD}$ outlined above.

(ii) Chiral symmetry is expressed as

$$\mathrm{U}(N_f)_\mathrm{R} \times \mathrm{U}(N_f)_\mathrm{L} \equiv \mathrm{U}(1)_\mathrm{V} \times \mathrm{SU}(N_f)_\mathrm{V} \times \mathrm{U}(1)_\mathrm{A} \times \mathrm{SU}(N_f)_\mathrm{A}\,.$$

According to it, quark fields transform as

$$q_i = q_{i,\mathrm{L}} + q_{i,\mathrm{R}} \to U_{\mathrm{L},i,j} q_{j,\mathrm{L}} + U_{\mathrm{R},i,j} q_{j,\mathrm{R}}\,, \tag{48}$$

where U_L and U_R are 3×3 unitary matrices that mix flavor (but no color!) degrees of freedom. This symmetry undergoes SSB

$$\mathrm{SU}(N_f)_\mathrm{V} \times \mathrm{SU}(N_f)_\mathrm{A} \to \mathrm{SU}(N_f)_\mathrm{V}\,. \tag{49}$$

(iii) The axial symmetry $\mathrm{U}(1)_\mathrm{A}$ corresponds to the choice $U_\mathrm{L} = U_\mathrm{R}^\dagger = \exp(-i\alpha/2)$. This symmetry is also broken by quantum fluctuations and the corresponding anomaly is called an axial or chiral anomaly.

(iv) There is also an explicit breaking of $\mathrm{U}(1)_\mathrm{A}$ and $\mathrm{SU}(N_f)_\mathrm{A}$ through nonzero bare quark masses. An explicit breaking of $\mathrm{SU}(N_f)_\mathrm{V}$ occurs if the quark masses are different.

In the following, in order to keep the discussion as simple as possible, we will omit — if not stated differently — the flavor index $i = u, d, \ldots$ Yet, the main features of QCD at large N_c are not dependent on the number of flavors. Yet, whenever needed, we will explicitly mention the quark flavors as well.

2.4. Quark and gluon propagators

Here, we shall have a quick look at the quark and gluon propagators. The main message is simple: their main features are retained in the large-N_c limit. It means that they can be "naively" regarded as large-N_c-invariant objects.

Let us be more specific. For the quark propagator, there is an infinity class of diagrams which are large-N_c-independent. They are depicted in Fig. 4. These are the famous 'planar diagrams' since they can be drawn on a plane without intersection [5, 6].

Admittedly, there are also non-planar diagrams which disappear in the large-N_c limit, thus the large-N_c world is slightly simpler than the one for $N_c = 3$. An example of a non-planar (and therefore large-N_c-suppressed)

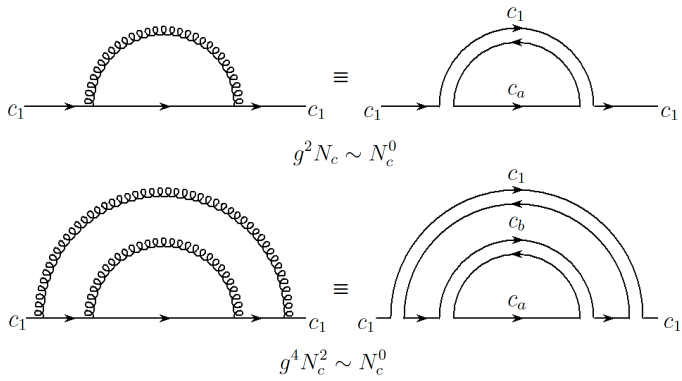

Fig. 4. Two planar diagrams describing the self-energy of the quark (which is taken to have a specific color C_1 for definiteness). Both diagrams are 'mass contributions' and scale as N_c^0. There is an infinity of such planar diagrams.

diagram for the quark propagator can be found in Fig. 5. Yet, the main features are expected to be contained in the large-N_c dominant terms, which survive the limit $N_c \to \infty$.

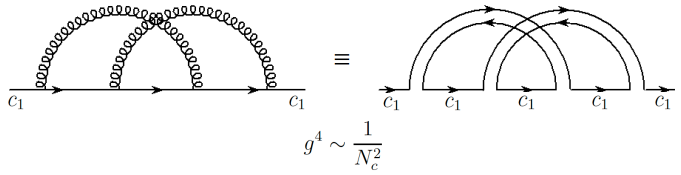

Fig. 5. An example of a non-planar self-energy diagram for the quark propagator. It scales as N_c^{-2} and is thus suppressed.

An important consequence is that the most important properties related to low-energy QCD, among which SSB [51], are still valid for large values of N_c. For instance, the quark u develops a constituent mass due to SSB as [14]

$$m_u^{\text{bare}} \simeq 3 \text{ MeV} \to m_u^* \simeq 300 \text{ MeV}\,, \tag{50}$$

which holds also for arbitrary large values of N_c. Since the dominant contributions to the quark propagator are large-N_c-independent, the constituent mass $m_u^* \simeq 300$ MeV scales as N_c^0. Then, as a consequence, the whole low-energy mesonic phenomenology is quite similar: the pions and kaons are still (quasi-)Goldstone bosons, the vector particles carry a mass of about $2m_u^*$, see later on for more details on mesons. An important exception regards the chiral anomaly, which indeed goes away for $N_c \to \infty$. In the chiral limit, the mass of the singlet η_0 scales as $m_{\eta_0}^2 \propto N_c^{-1}$ [52], thus for $N_f = 3$, a full nonet of Goldstone bosons is actually realized in the chiral limit for large N_c.

The gluon propagator is dressed by large-N_c-independent planar diagrams (see Fig. 6), which are expected to be responsible for its major properties. In this sense, this feature is analogous to the quark propagator. One may roughly speak about an effective gluon mass of about $m_g^* \simeq 800$ MeV [53], even though the term 'mass' should be used with extreme care: one should better refer to an energy scale entering into the propagator without breaking local color gauge invariance [54]. This effective energy scale is N_c-independent. As a consequence, glueballs carry a mass (starting at) about $2m_g^*$, which is also N_c-independent, as we shall discuss in more detail in Section 3.

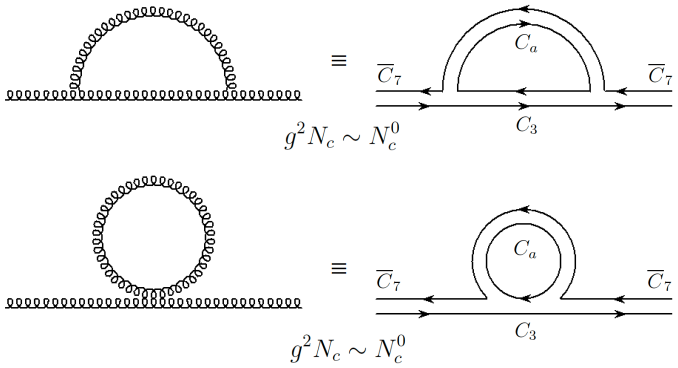

Fig. 6. Two planar diagrams describing the self-energy of the gluon (which is taken to have a specific color $C_3\bar{C}_7$ as an explicit example). Both diagrams are 'mass contributions' and scale as N_c^0.

Summarizing, the quark and gluon propagators contain a class of dominant N_c-independent ($\propto N_c^0$) contributions. For our purposes, these propagators can be seen as independent of the number of colors.

2.5. Brief recall of mesons and baryons at large N_c

Quarks and gluons are not the physical states that hit our detectors. They are confined into hadrons, *i.e.* mesons (integer spin) and baryons (semi-integer spin).

A *conventional meson* is a meson constructed out of a quark and an antiquark. Although it represents only one of (actually infinitely many) possibilities to build a meson, the vast majority of mesons of the PDG [1] can be consistently (and successfully) interpreted as belonging to a quark–antiquark multiplet (see also the results of the quark model [55]). Mesons are classified according to their total spin J, parity P, and charge conjugation C, forming multiplets denoted with J^{PC}.

Moreover, in the quark model, one may express a quark–antiquark state Q using the radial quantum number $n = 1, 2, 3, \ldots$, the angular quantum number $L = 0, 1, 2, 3, \ldots \equiv S, P, D, F, \ldots$, the spin part $S = 0, 1$, the flavor composition, and finally, the color wave function (that is crucial for this work).

Following this spectroscopic notation, a meson is classified as

$$n^{2S+1}L_J\,, \tag{51}$$

where J is the total spin arising from the proper combination of L and S. We remind that P and C are calculated as

$$P = (-1)^{L+1}\,, \qquad C = (-1)^{L+S}\,. \tag{52}$$

In general, the wave function of a quarkonium state Q takes the form

$$\begin{aligned} &\left|Q \text{ with } n\ {}^{2S+1}L_J \text{ and } J^{PC}\right\rangle \\ &= |\text{radial part } n\rangle\,|\text{angular part } L\rangle\,|\text{spin part } S\rangle\,|\text{flavor}\rangle\,|\text{color}\,\rangle\ . \end{aligned} \tag{53}$$

As an example, the wave function of the vector meson $\rho^+ \equiv u\bar{d}$ reads

$$\left|\rho^+\right\rangle = N\,|n=1\rangle\,|L=0\rangle\,|S=1(\uparrow\downarrow+\downarrow\uparrow)\rangle\,\left|u\bar{d}\,\right\rangle\left|\bar{R}R+\bar{G}G+\bar{B}B\right\rangle\ , \tag{54}$$

where N is an overall normalization. The properly normalized color part is

$$|Q\text{-color}\,\rangle = \frac{1}{\sqrt{3}}\left|\bar{R}R+\bar{G}G+\bar{B}B\right\rangle\ . \tag{55}$$

Interestingly, this is the color wave function of any quarkonium, independently of the other quantum numbers. This combination is colorless, in the sense that it is invariant under any (local) SU($N_c = 3$) color transformations.

As we shall prove explicitly later, in the large-N_c limit, quark–antiquark mesons retain their mass but become very narrow. For a generic N_c, the color wave function takes the form

$$|Q\text{-color}\rangle = \frac{1}{\sqrt{N_c}}\left|\bar{C}_1C_1+\bar{C}_2C_2+\ldots+\bar{C}_{N_c}C_{N_c}\right\rangle\ , \tag{56}$$

which is invariant under (local) SU(N_c) color transformations. This fact can be easily seen by considering

$$|Q\text{-color}\rangle \simeq \frac{1}{\sqrt{N_c}}\sum_{a=1}^{N_c}\bar{q}_aq_a\,|0\rangle\ . \tag{57}$$

A generic color transformation implies

$$q_a \to U_{ab} q_b \,, \qquad q_a^\dagger \to (U_{ac} q_c)^\dagger = q_c^\dagger U_{ac}^* = q_c^\dagger \left(U^\dagger\right)_{ca} \,, \tag{58}$$

thus

$$\bar{q}_a q_a \to \bar{q}_c \left(U^\dagger\right)_{ca} U_{ab} q_b = \bar{q}_a q_a \,, \tag{59}$$

where $\left(U^\dagger\right)_{ca} U_{ab} = \delta_{bc}$ follows from $U^\dagger U = 1$ (sum over indices understood).

Other mesons (such as glueballs, hybrids, ...) have more complicated wave functions, see later for their detailed study.

The same procedure above can be carried out for conventional baryon states, where a conventional baryon is a three-quark state. Even if the remaining part of their w.f. is more complicated, the normalized color part is pretty simple

$$|B\text{-color}\rangle = \frac{1}{\sqrt{6}} \left|RGB + BRG + GBR - GRB - BGR - RBG\right\rangle \,, \tag{60}$$

which is invariant under $\mathrm{SU}(N_c = 3)$ color transformations. The extension to a generic number of colors gives

$$|B\text{-color}\rangle = \frac{1}{\sqrt{N_c!}} \varepsilon_{a_1 a_2 \ldots a_{N_c}} \left|C_{a_1} C_{a_2} \ldots C_{a_{N_c}}\right\rangle \tag{61}$$

or, by using quark fields,

$$|B\text{-color}\rangle \simeq \frac{1}{\sqrt{N_c!}} \varepsilon_{a_1 a_2 \ldots a_{N_c}} q_{a_1} q_{a_2} \ldots q_{a_{Nc}} |0\rangle \,. \tag{62}$$

In fact, under $\mathrm{SU}(N_c)$ color transformations, one has

$$\begin{aligned} \varepsilon_{a_1 a_2 \ldots a_{N_c}} q_{a_1} q_{a_2} \ldots q_{N_c} \; &\to \; \varepsilon_{a_1 a_2 \ldots a_{N_c}} U_{a_1 a_1'} U_{a_2 a_2'} \ldots U_{a_{N_c} a_{N_c}'} q_{a_1'} q_{a_2'} \ldots q_{a_{N_c}'} \\ &= \; \varepsilon_{a_1' a_2' \ldots a_{N_c}'} q_{a_1'} q_{a_2'} \ldots q_{a_{N_c}'} \,, \end{aligned} \tag{63}$$

where we have used that

$$\varepsilon_{a_1 a_2 \ldots a_{N_c}} U_{a_1 a_1'} U_{a_2 a_2'} \ldots U_{a_{N_c} a_{N_c}'} = \varepsilon_{a_1' a_2' \ldots a_{N_c}'} \tag{64}$$

being a consequence of $\det U = 1$, namely

$$N! \det U = N! = \varepsilon_{a_1 a_2 \ldots a_{N_c}} \varepsilon_{a_1' a_2' \ldots a_{N_c}'} U_{a_1 a_1'} U_{a_2 a_2'} \ldots U_{a_{N_c} a_{N_c}'} \,. \tag{65}$$

2.6. Large N_c: recall of basic results

We present here a short summary of known large-N_c rules [6, 8]. In the next sections, we will re-derive them following (relatively simple) bound-state equations forming these states.

1. The masses of quark–antiquark states $Q \equiv barqq$, glueballs $G \equiv gg$, and hybrids mesons $H \equiv barqqg$ are constant for $N_c \to \infty$

$$M_Q \propto N_c^0\,, \qquad M_G \propto N_c^0\,, \qquad M_H \propto N_c^0\,. \tag{66}$$

2. The interaction between n_Q quark–antiquark states $Q \equiv |barqq\rangle$ scales as

$$A_{n_Q Q} \propto \frac{N_c}{N_c^{n_Q/2}} \quad \text{for} \quad n_Q \geq 1\,. \tag{67}$$

This implies that the amplitude for an n_Q-meson scattering process becomes smaller and smaller for increasing N_c. In particular, the decay amplitude is realized for $n_Q = 3$, *ergo* $A_{\text{decay}} \propto N_c^{-1/2}$, implying that the width scales as $\Gamma \propto 1/N_c$. Conventional quarkonia become very narrow for large N_c.

3. The interaction amplitude between n_G glueballs is

$$A_{n_G G} \propto \frac{N_c^2}{N_c^{n_G}} \quad \text{for} \quad n_G \geq 1\,, \tag{68}$$

which is smaller than in the quarkonium case.

4. The interaction amplitude between n_Q quarkonia and n_G glueballs behaves as

$$A_{(n_Q Q)(n_G G)} \propto \frac{N_c}{N_c^{n_Q/2} N_c^{n_G}} \quad \text{for} \quad n_Q \geq 1\,, \tag{69}$$

thus the mixing ($n_G = n_Q = 1$) scales as $A_{\text{mixing}} \propto N_c^{-1/2}$. Then, also the glueball–quarkonium mixing is suppressed for $N_c \gg 1$. Note, for $n_G = 0$ one finds the correct interaction for n_Q quarkonia.

5. The amplitude for n_Q quarkonia and n_H hybrids scales as

$$A_{(n_Q Q)(n_H H)} \propto \frac{N_c}{N_c^{n_Q/2} N_c^{n_H/2}} \quad \text{for} \quad n_Q + n_H \geq 1\,. \tag{70}$$

For $n_Q = n_H = 1$, one recovers that the quarkonium–hybrid mixing scales as N_c^0, implying that quarkonia and hybrids behave in the same way at large N_c.

6. For the general case of n_H quarkonia, n_G glueballs, and n_H hybrids, one has

$$A_{(n_Q Q)(n_G G)(n_H H)} \propto \frac{N_c}{N_c^{n_Q/2} N_c^{n_G} N_c^{n_H/2}} \quad \text{for} \quad n_Q + n_H \geq 1\,. \tag{71}$$

7. Four-quark states (both as molecular objects and diquark–anti-diquark objects) tend to fade away at large N_c. In fact, apart from (eventually existing, but not yet proven) peculiar tetraquarks [29], these objects typically do not survive in the large-N_c limit.

8. Baryons are made of N_c quarks for an arbitrary N_c. As a consequence,

$$M_B \propto N_c\,. \tag{72}$$

9. Interactions involving baryons: the baryon–baryon–meson interaction scales as $N_c^{1/2}$, while baryon–baryon scattering goes as N_c. In particular, for an arbitrary number of $\bar{B}B$ pairs, as well as for n_Q quarkonia, n_G glueballs, and n_H hybrids, one has

$$A_{(\bar{B}B\ldots)(n_Q Q)(n_G G)(n_H H)} \propto \frac{N_c}{N_c^{n_Q/2} N_c^{n_G} N_c^{n_H/2}}\,. \tag{73}$$

Summing up, the large-N_c limit is a firm theoretical method which explains why the quark model works. In fact, a decay channel for a certain meson causes quantum fluctuations: the propagator of the meson is dressed by loops of other mesons. For instance, the state ρ^+ decays into $\pi^+\pi^0$, thus the ρ meson is dressed by loops of pions. In the end, one finds that the wave function of the ρ meson is given by

$$\left|\rho^+\right\rangle = a\left|u\bar{d}\right\rangle + b\left|\pi^+\pi^0\right\rangle + \ldots\,, \tag{74}$$

where the full expression of $\left|u\bar{d}\right\rangle$ is given in Eq. (54). Being $a \propto N_c^0$ and $b \propto N_c^{-1/2}$, we understand why the quark–antiquark configuration dominates. Dots refer to further contributions which are even more suppressed.

Yet, for $N_c = 3$, there are some mesons for which the meson–meson component dominates. These are, for instance, the light scalar mesons such as $a_0(980)$, see Section 3.5.

3. Large-N_c results for mesons

In this section, we deal with mesons. First, we discuss conventional quarkonia states, then various exotic configurations: glueballs, hybrids, and (briefly) four-quark states.

3.1. Quark–antiquark mesons

A quark–antiquark meson has a rather simple color wave function, see Eq. (56), that we rewrite here for convenience

$$|Q\text{-color}\rangle = \frac{1}{\sqrt{N_c}} \left| \bar{C}_1 C_1 + \bar{C}_2 C_2 + \ldots + \bar{C}_{N_c} C_{N_c} \right\rangle . \tag{75}$$

How does such a bound state emerge? For simplicity, let us consider the processes that mix two elements of the wave function, for instance,

$$\bar{C}_1 C_1 \to \bar{C}_2 C_2 \, . \tag{76}$$

This particular transition implies that an initial state with color 1 and anticolor 1 transforms into color 2 and anticolor 2. (For $N_c = 3$ that would correspond to *e.g.* $\bar{R}R$ into $\bar{G}G$.) Of course, any other example, such as $\bar{C}_3 C_3 \to \bar{C}_7 C_7$, is equally good. The important point is that we start from a possible component of a quarkonium state and end up in another component of its wave function. This is so because an eventual bound state would couple to any color combination $\bar{C}_a C_a$ with the same strength, and would appear as an intermediate state for processes of the type (76). In particular, close to the mass of the quarkonium, the s-channel becomes dominant. Note, for the moment, we do not 'care' about the normalization $1/\sqrt{N_c}$ entering in Eq. (56), but we simply study the amplitude for the transition of Eq. (76).

The simplest process of this type is depicted in Fig. 7 (upper part), where it is evident that the dominant amplitude for $\bar{C}_1 C_1 \to \bar{C}_2 C_2$ scales as $1/N_c$. Interestingly, loop processes of the type of Fig. 7 (lower part) also scale in this way. Of course, there are also subleading terms that scale as $1/N_c^2$, see Fig. 8, which can be dismissed in the large-N_c limit. In Fig. 9, we show another type of diagrams, which scales also as N_c^{-1} and displays an intermediate loop with any possible color combination.

How to study the emergence of bound states in this context? Of course, the full problem is complicated and one would need a Bethe–Salpeter approach. Yet, a simple and in many respects successful approach makes use of a quartic separable interaction, such as in the NJL model [14, 15]. As previously mentioned, the large-N_c counting is independent on the details of the employed approach, thus the results that we will present are general.

Let us consider a generic 'colorless' current for an arbitrary quarkonium meson Q

$$J_Q(x) = \sum_{a=1}^{N_c} \bar{q}^{(a)} \Gamma q^{(a)} \equiv C_1 \bar{C}_1 + C_2 \bar{C}_2 + \ldots + C_{N_c} \bar{C}_{N_c} \, , \tag{77}$$

where no normalization is considered. (Note, the quantity Γ is an appropriate combination of Dirac matrices and derivatives that varies case by case in

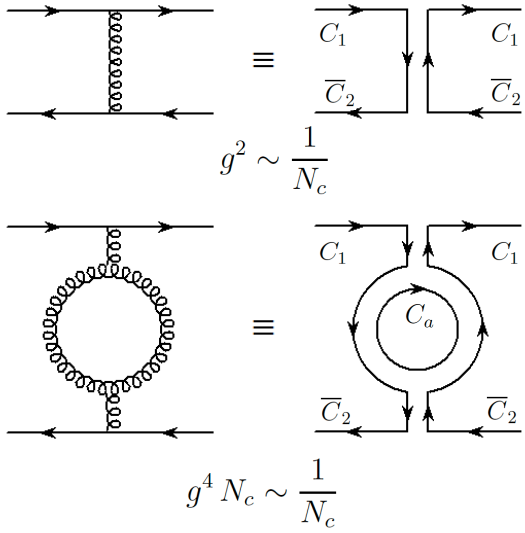

Fig. 7. Examples of dominating diagrams for the scattering process $\bar{C}_1 C_1 \to \bar{C}_2 C_2$. These diagrams scale as N_c^{-1}. Of course, one could take any other color combination, such as $\bar{C}_7 C_7 \to \bar{C}_{11} C_{11}$.
vspace3mm

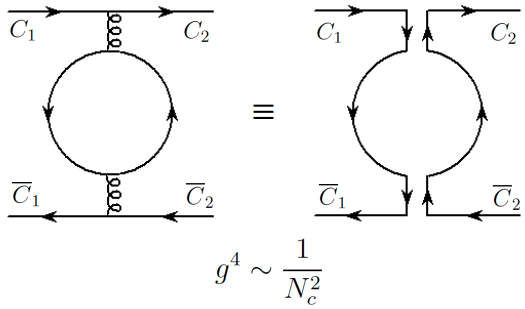

Fig. 8. Example of a subleading diagram for the scattering process $\bar{C}_1 C_1 \to \bar{C}_2 C_2$. These types of diagram scale as N_c^{-2}.

dependence of the mesonic quantum numbers, see Ref. [56]; for instance, for pseudoscalar mesons, one has $\Gamma = i\gamma^5$.) The separable interaction term is proportional to J_Q^2. The corresponding Lagrangian takes the effective form

$$\mathcal{L}_Q = K_Q J_Q^2 \,, \tag{78}$$

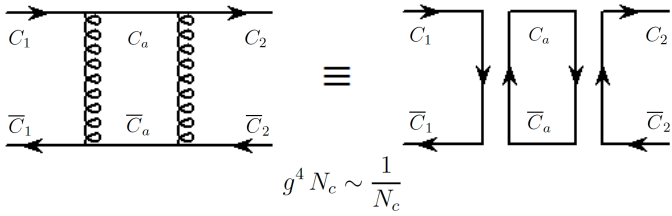

Fig. 9. Another dominating diagram for the scattering process $\bar{C}_1 C_1 \to \bar{C}_2 C_2$ that involves an intermediate state with an arbitrary color $\bar{C}_a C_a$ for $a = 1, \ldots, N_c$. It scales as N_c^{-1}.

where K_Q is a coupling constant. In order to determine the scaling of K_Q, one may consider the illustrative transition $C_1\bar{C}_1 \to C_2\bar{C}_2$ or any other of that type, finding that

$$K_Q \propto g_{\rm QCD}^2 = g^2 \propto N_c^{-1}\,. \tag{79}$$

We then introduce a useful notation: we define $\bar{K}_Q$ as an N_c-independent constant, thus

$$K_Q = \frac{\bar{K}_Q}{N_c}\,. \tag{80}$$

In the following, any quantity with 'bar' shall be regarded as N_c-independent.

The corresponding T-matrix T_Q is obtained by properly resumming the interactions originated by the Lagrangian of Eq. (78), see Fig. 10 for its pictorial representation. It then takes the form

$$iT_Q(s) = iK_Q + iK_Q(-i\Sigma_Q(s))iK_Q + iK_Q(-i\Sigma_Q(s))iK_Q(-i\Sigma_Q(s))iK_Q + \ldots$$

leading to

$$T_Q(s) = K_Q + K_Q\Sigma_Q(s)K_Q + \ldots = \frac{K_Q}{1 - \Sigma_Q(s)K_Q} = \frac{1}{K_Q^{-1} - \Sigma_Q(s)}\,, \tag{81}$$

where $\Sigma_Q(s)$ is the quark–antiquark loop contribution, which scales as

$$\Sigma_Q(s) = N_c\bar{\Sigma}_Q(s)\,. \tag{82}$$

This result is a simple consequence of the N_c possible loops when the quark carries N_c colors. The quantity $\bar{\Sigma}_Q(s)$ is, according to the adopted convention, independent of N_c.

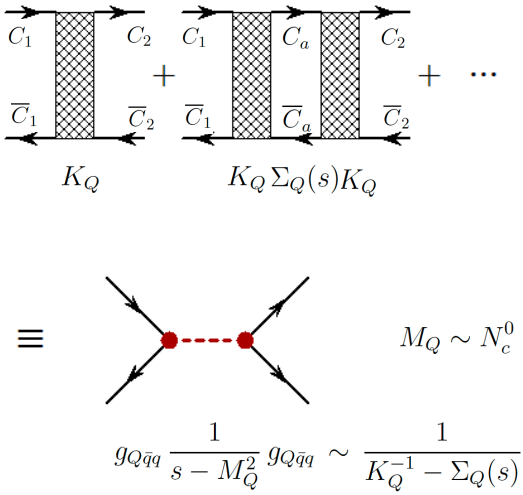

Fig. 10. Generation of a quark–antiquark meson (red dashed line) upon resummation of diagrams for the illustrative process $\bar{C}_1 C_1 \to \bar{C}_2 C_2$.

Next, the amplitude $T_Q(s)$ scales as $1/N_c$ (indeed, each terms in the expansion is of the order of $1/N_c$, as one can easily check). In this specific model, one can also write the explicit form of the loop function $\Sigma_Q(s)$ as

$$\Sigma_Q\left(s=p^2\right) = -iN_c \int \frac{\mathrm{d}^4k}{(2\pi)^4} \mathrm{Tr}\left[S_q\left(\frac{p}{2}+k\right)\Gamma S_q\left(-\frac{p}{2}+k\right)\Gamma\right] f_\Lambda(k)\,. \tag{83}$$

In this sense, the factor N_c is simply a trace over color d.o.f.: this is indeed a general result that does not depend on the model details. The function $f_\Lambda(k)$ stays for a regulator (in turn, this function may arise from a non-local current [18, 19]), but its specification is not needed since no explicit calculation will be performed.

The mass of the quark–antiquark bound states M_Q corresponds to a pole of the resummed amplitude $T_Q(s)$, hence to a zero of its denominator. As such, it is a solution of the equation

$$T_Q(s)^{-1} = 0 \to K_Q^{-1} - \Sigma_Q\left(s=M_Q^2\right) = 0\,. \tag{84}$$

Then, upon using $K_Q = \bar{K}_Q/N_c$ and $\Sigma_Q(s) = N_c\bar{\Sigma}_Q(s)$, the previous equation takes the form

$$\frac{N_c}{\bar{K}_Q} - N_c\bar{\Sigma}_Q\left(s=M_Q^2\right) = 0 \to \frac{1}{\bar{K}_Q} - \bar{\Sigma}_Q\left(s=M_Q^2\right) = 0\,, \tag{85}$$

which is N_c-*independent*. Thus, the mass of the mesonic quarkonium state $Q \equiv \bar{q}q$ scales as

$$M_Q \propto N_c^0 \,. \tag{86}$$

We were able to reproduce this very well known and general result of the large-N_c phenomenology.

Next, let us expand the denominator T_Q around $s = M_Q^2$, finding

$$\begin{aligned} K_Q^{-1} - \Sigma_Q(s) \;&\simeq\; \underbrace{K_Q^{-1} - \Sigma_Q\left(M_Q^2\right)}_{=0} - \left(\frac{\partial \Sigma_Q(s)}{\partial s}\right)_{s=M_Q^2} \left(s - M_Q^2\right) + \dots \\ &\simeq\; -N_c \left(\frac{\partial \bar{\Sigma}_Q(s)}{\partial s}\right)_{s=M_Q^2} \left(s - M_Q^2\right) + \dots \end{aligned} \tag{87}$$

Hence, the amplitude becomes

$$T_Q(s) = \frac{1}{K_Q^{-1} - \Sigma_Q(s)} \simeq \frac{1}{-N_c \left(\frac{\partial \bar{\Sigma}_Q(s)}{\partial s}\right)_{s=M_Q^2} \left(s - M_Q^2\right)} = \frac{(i g_{Q\bar{q}q})^2}{s - M_Q^2} \,, \tag{88}$$

where we identify the coupling of the quarkonium to its constituents, a quark and an antiquark, as

$$g_{Q\bar{q}q} = \frac{1}{\sqrt{N_c \left(\frac{\partial \bar{\Sigma}_Q(s)}{\partial s}\right)_{s=M_Q^2}}} = \frac{1}{\sqrt{N_c}} \bar{g}_{Q\bar{q}q} \,. \tag{89}$$

Again, $\bar{g}_{Q\bar{q}q}$ is N_c-independent. Thus, the coupling of a conventional meson to a quark–antiquark pair $g_{Q\bar{q}q}$ scales as $1/\sqrt{N_c}$. In terms of the composite field Q and the constituent quark fields, one can write an effective interaction Lagrangian

$$\mathcal{L}_{Q\bar{q}q} = g_{Q\bar{q}q} Q J_Q \,. \tag{90}$$

Such interactions enter, for example, in meson-quark chiral models [57, 58], in approaches using the Weinberg compositeness condition [16, 17] (sometimes within nonlocal Lagrangians [18, 19]), as well as at intermediate stages of the hadronization process of quark models such as the NJL one [14].

Many results can be obtained from the previous outcomes. Let us first look at 3-leg meson interactions (see Fig. 11), which is proportional to

$$A_{3Q} \propto g_{Q\bar{q}q}^3 N_c \propto \frac{1}{\sqrt{N_c}} \,. \tag{91}$$

As a consequence, the decay width of a conventional meson into two conventional mesons $Q \to Q_1 Q_2$ scales as

$$\Gamma_{Q\to Q_1Q_2} \propto |A_{3Q}|^2 \propto \frac{1}{N_c}\,. \tag{92}$$

This is also a very well known result of large-N_c phenomenology. Conventional quark–antiquark mesons become stable for $N_c \to \infty$ with a scaling of the type N_c^{-1}.

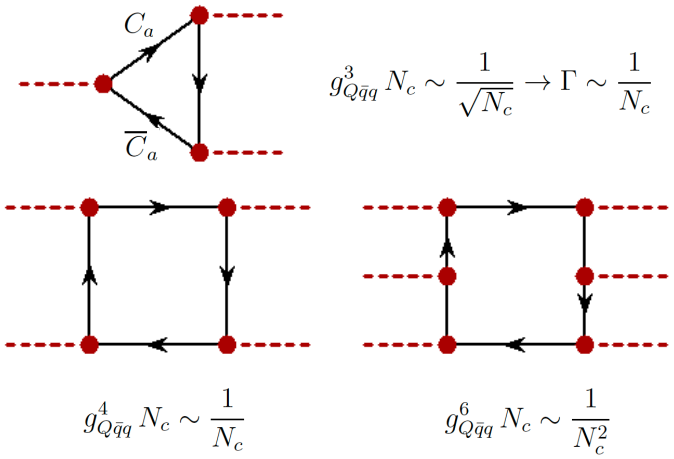

Fig. 11. Conventional $\bar{q}q$ mesons Q are in red (dashed), quarks in black (solid). Top: decay of a conventional $\bar{q}q$ meson into two conventional $\bar{q}q$ mesons via a loop of quarks. The leading amplitude scales as $N_c^{-1/2}$, hence the decay width scales as N_c^{-1}. Bottom: two-body scattering process of conventional Q mesons, whose leading order is N_c^{-1}, thus the cross section goes as N_c^{-2}, and three-body scattering process, whose leading order is N_c^{-2}, thus the cross section goes as N_c^{-4}.

Similarly, the four-leg conventional meson interaction goes as (again Fig. 11)

$$A_{4Q} \propto g^4_{Q\bar{q}q} N_c \propto \frac{1}{N_c}\,. \tag{93}$$

For instance, the four-pion interaction term in an effective Lagrangian should scale as $1/N_c$.

In general, the n_Q^{th}-leg meson interaction among convectional mesons scales as ($n_Q \geq 1$)

$$A_{n_Q Q} \propto g^{n_Q}_{Q\bar{q}q} N_c \propto N_c^{-n_Q/2} N_c = \frac{N_c}{N_c^{\frac{n_Q}{2}}}\,, \tag{94}$$

in agreement with the general result quoted in Section 2.6 (point 2). Note, the case of $n_Q = 1$ generates $A_Q \sim N_c^{1/2}$, which coincides with the vacuum production amplitude (and also with the weak decay constant), see below. The case of $n_Q = 0$ implies $A_0 \sim N_c$ which can be interpreted as the vacuum contribution of quarks. In turn, the pressure generated by quarks scales as N_c, see Section 5.

Next, we examine various additional consequences of the obtained large-N_c scaling behavior.

1. The example of the $\chi_{c,0}$ meson

The $\chi_{c,0}$ meson is the ground-state scalar $\bar{c}c$ state. Its decay width is very small [1]. Can large N_c help us to understand why? Indeed, it does. The dominant decay of the $\chi_{c,0}$ would be decays of the type $\bar{D}D$ or similar ones. The corresponding partial decay widths would be of the order of N_c^{-1}, but cannot take place because it is kinematically forbidden. Schematically,

$$\Gamma_{\chi_{c,0}\to\bar{D}D} \propto g^2_{\chi_{c,0}\bar{D}D} \frac{k_D}{M^2_{\chi_{c,0}}} \Theta(M_{\chi_{c,0}} - 2M_D) = 0\,, \tag{95}$$

where $g_{\chi_{c,0}\bar{D}D}$ goes as $N_c^{-1/2}$ and k_D is the modulus of the three-momentum of an outgoing D-particle. This quantity is N_c-independent but is imaginary for $M_{\chi_{c,0}} < 2M_D$. The step function assures that in these cases the decay simply vanishes.

The $\chi_{c,0}$ can decay into light hadrons, *e.g.* into π mesons. Formally, an analogous expression holds

$$\Gamma_{\chi_{c,0}\to\pi\pi} \propto g^2_{\chi_{c,0}\pi\pi} \frac{k_\pi}{M^2_{\chi_{c,0}}} \Theta(M_{\chi_{c,0}} - 2M_\pi) = g^2_{\chi_{c,0}\pi\pi} \frac{k_\pi}{M^2_{\chi_{c,0}}} \neq 0\,, \tag{96}$$

where $k_\pi = \sqrt{M^2_{\chi_{c,0}}/4 - M^2_\pi} \sim N_c^0$. How does $g_{\chi_{c,0}\pi\pi}$ scale with N_c? A simple diagrammatic analysis, see Fig. 12, shows that

$$g_{g_{\chi_{c,0}\pi\pi}} \propto N_c^{-3/2}\,, \tag{97}$$

thus $\Gamma_{\chi_{c,0}\to\pi\pi} \propto N_c^{-3}$. This result applies to any similar mesonic channel. We thus find that

$$\Gamma_{\chi_{c,0}\to\text{mesons}} \propto N_c^{-3} \tag{98}$$

or even smaller. This explains why these decays are so suppressed. This result holds for any mesons whose (would be large N_c) dominant decays are kinematically forbidden, most notably for the famous charm–anticharm j/ψ state (where, however, because of C-parity, three intermediate gluons

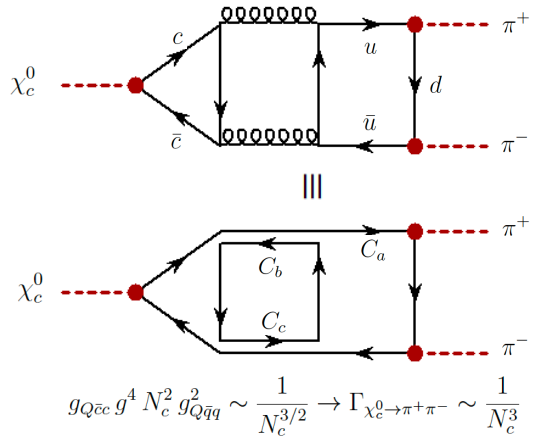

Fig. 12. Decay of the charm–anticharm $\chi_{c,0}$ meson (red, dashed) into two π mesons (also red, dashed). In this case, the leading decay into $\bar{D}D$ mesons as in Fig. 11 cannot take place because it is kinematically forbidden. The subleading diagram scales as $N_c^{-3/2}$, thus the decay width goes as N_c^{-3}, explaining why this charmonium meson is so narrow. Note, the diagrams above also show that the flavor lines (upper part) behave differently than the color ones (lower part).

occur). Indeed, this general outcome is a realization of the so-called OZI (Okubo, Zweig, and Iizuka) rule, *e.g.* [59], according to which diagrams in which the quark lines are disconnected are suppressed. In this respect, the OZI rule can be understood as a consequence of the large-N_c results.

2. Pion decay constant and $\pi^0 \to \gamma\gamma$

The pion decay constant f_π refers to the quark–antiquark annihilation that forms it. It enters as a part of the amplitude of the weak decay of π^+, for which the chain $\pi^+ \to W^+ \to \mu^+\nu_\mu$ takes place, see Fig. 13. It turns out that

$$f_\pi \propto N_c^{1/2}\,. \tag{99}$$

Indeed, this is the same scaling of the chiral condensate, see below. The correct scaling can be also seen by writing the formula for f_π as

$$f_\pi \sim g_{\pi^+ u\bar{d}} \Sigma_\pi \left(s = M_\pi^2\right) = \frac{\bar{g}_{\pi^+ u\bar{d}}}{\sqrt{N_c}} N_c \bar{\Sigma}_\pi \left(s = M_\pi^2\right) \sim \sqrt{N_c}\,. \tag{100}$$

This result is indeed independent on the chosen quark–antiquark meson: the weak decay constant of a generic conventional meson scales as $\sqrt{N_c}$. Note, while the scaling is correct, the expression $g_{\pi^+ u\bar{d}} \Sigma_\pi(s = M_\pi^2)$ has dimension energy^2, but f_π has dimension energy. This is due to the fact that the

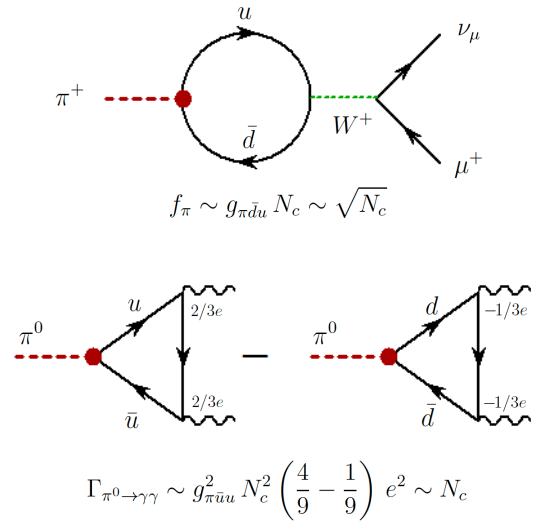

Fig. 13. Schematic diagrams leading to the large-N_c scaling of the weak decay constant f_π and $\pi^0 \to \gamma\gamma$.

expression $g_{\pi^+ u\bar{d}}\Sigma_\pi(s = M_\pi^2)$ is indeed sufficient to determine the large-N_c scaling, but is not enough for an actual calculation of the decay constant. A closer inspection shows that $g_{\pi^+ u\bar{d}}\Sigma_\pi(s = M_\pi^2) \propto M_\pi f_\pi$. For a detailed calculation that includes the large-N_c discussion within a qualitatively similar approach, see Ref. [60]. We also refer to point 3 below for a connection of this quantity to chiral models.

For what concerns the decay of π^0 into $\gamma\gamma$, one obtains the amplitude

$$A_{\pi^0\gamma\gamma} \propto \left[g_{\pi^0\bar{u}u} \left(\frac{2e}{3}\right)^2 + g_{\pi^0\bar{d}d} \left(-\frac{e}{3}\right)^2 \right] N_c \simeq g_{\pi^0\bar{u}u} N_c \left(\frac{4}{9} - \frac{1}{9}\right) , \quad (101)$$

where $g_{\pi^0\bar{d}d} \simeq -g_{\pi^0\bar{u}u}$ has been used (this comes from $|\pi^0\rangle = \frac{1}{\sqrt{2}} |\bar{u}u - \bar{d}d\rangle$.) Since $g_{\pi^0\bar{u}u}$ scales as $N_c^{-1/2}$, one finds

$$\Gamma_{\pi^0\to\gamma\gamma} \propto g^2_{\pi^0\bar{u}u} N_c^2 \propto N_c \,. \quad (102)$$

(If one neglected the scaling of the coupling, a N_c^2 dependence would emerge, but that is not the correct scaling).

The result above is valid as long as the electric charges of the quarks are left untouched. This hypothesis is meaningful if we consider QCD only, yet things change when other interactions are taken into account. In fact, following the scaling rules above, the large-N_c analogous to the proton would

not have charge 1, but rather the charge (for N_c odd and for the number of quarks u exceeding that of quarks d of one unit)

$$\left(\frac{N_c-1}{2}+1\right)\frac{2}{3}-\left(\frac{N_c-1}{2}\right)\frac{1}{3}=\frac{N_c+3}{6}\,. \tag{103}$$

In general, baryons would not have integer charges. For instance, the large-N_c analogous of the Δ^{++} baryon would carry charge $2N_c/3$, which is also not necessarily an integer.

Following the discussion in Refs. [61–63], we impose the subsequent scaling behavior for the charges of the u and d quarks

$$q_u=\frac{1+N_c}{2N_c}\,,\qquad q_d=\frac{1-N_c}{2N_c}\,, \tag{104}$$

out of which any baryon has an integer charge. In particular, the proton carries the charge

$$\left(\frac{N_c-1}{2}+1\right)q_u-\left(\frac{N_c-1}{2}\right)q_d=1\,. \tag{105}$$

The π^+ has still the charge $q_u+q_{\bar{d}}=q_u-q_d=1$, as expected. Then, the amplitude for the π^0 decay reads

$$\begin{aligned}A_{\pi^0\gamma\gamma}&=g_{\pi^0\bar{u}u}N_c\left(q_u^2-q_d^2\right)=g_{\pi^0\bar{u}u}N_c\left(q_u^2-q_d^2\right)\\&=g_{\pi^0\bar{u}u}N_c\left(\left(\frac{1+N_c}{2N_c}\right)^2-\left(\frac{1-N_c}{2N_c}\right)^2\right)=g_{\pi^0\bar{u}u}N_c\frac{4N_c}{4N_c^2}=g_{\pi^0\bar{u}u}\,.\end{aligned} \tag{106}$$

It follows that with this scheme, $\Gamma_{\pi^0\to\gamma\gamma}\sim g^2_{\pi^0\bar{u}u}\sim N_c^{-1}$, just as a regular mesonic decay.

3. Three-body decay: direct process vs. decay chain

We intend to study the three-body decay process

$$Q\to Q_1Q_2Q_3\,. \tag{107}$$

Let us consider two possible models for this decay. For the direct decay, a Lagrangian of the type (we call it 'model A') reads (see Fig. 14, left part)

$$\mathcal{L}_{\rm A}=\lambda QQ_1Q_2Q_3\,, \tag{108}$$

where $\lambda=\bar{\lambda}/N_c$, for which the three-body decay goes as

$$\Gamma_{Q\to Q_1Q_2Q_3}\propto|A_{Q\to Q_1Q_2Q_3}|^2\propto\lambda^2\propto\frac{1}{N_c^2}\,. \tag{109}$$

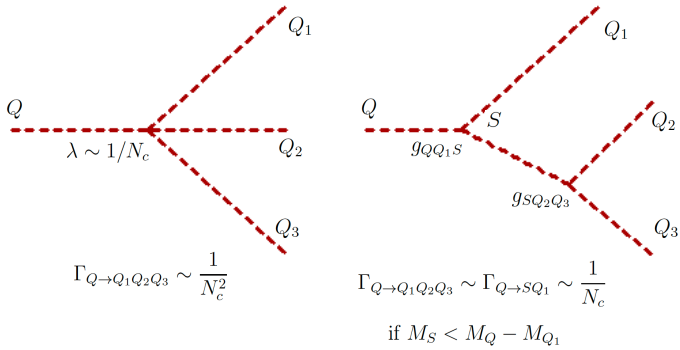

Fig. 14. Direct three-body decay *vs.* decay chain quarkonium Q (red, dashed) into 3 quarkonia states. The decay chain takes place via an intermediate quarkonium state S. Under appropriate conditions, the decay chain dominates in the large-N_c limit.

Next, let us consider the possibility that the decay takes place via an additional intermediate quark–antiquark state S via the Lagrangian (that we shall denote as 'model B', see Fig. 14, right part)

$$\mathcal{L}_{\mathrm{B}} = g_{QQ_1S} Q Q_1 S + g_{SQ_2Q_3} S Q_2 Q_3 \,, \tag{110}$$

where both constants g_{QQ_1S} and $g_{SQ_2Q_3}$ scale as $1/\sqrt{N_c}$. Thus, one has the decay chain

$$Q \to Q_1 S \to Q_1 Q_2 Q_3 \,, \tag{111}$$

where in the second step, $S \to Q_2 Q_3$ has taken place. We assume, for simplicity, that $S \to Q_2 Q_3$ is the only available decay channel for S (the main result holds also when this is not the case).

In scenario B, the decay amplitude takes the form

$$A_{Q\to Q_1Q_2Q_3} \propto g_{QQ_1S} \frac{1}{p_S^2 - M_S^2 + i\Gamma_S M_S} g_{SQ_2Q_3} \,. \tag{112}$$

Since M_S is not dependent on N_c and Γ_S is suppressed as $1/N_c$, at first sight $A_{Q\to Q_1Q_2Q_3}$ scales also as $1/N_c$, thus leading to the same result as in model A (direct decay). Yet, a more careful analysis leads to a different result. Following Refs. [64, 65], the decay chain leads to the integration over final momenta leading to

$$\Gamma_{Q\to Q_1Q_2Q_3} = \int_0^{M_Q - M_1} \mathrm{d}x \Gamma_{Q\to Q_1S}(x) d_S(x) \,, \tag{113}$$

where $\Gamma_{Q\to Q_1 S}(x)$ is the decay width for $Q \to Q_1 S$. The quantity $d_S(x)$ is the mass distribution of the S state with

$$d_S(x) = \frac{\Gamma_S}{2\pi} \frac{1}{(x - M_S)^2 + \Gamma_S^2/4}\,, \tag{114}$$

where x is the running mass of the intermediate state S; only for $x < M_Q - M_1$, a nonzero contribution to $Q \to Q_1 Q_2 Q_3$ is possible. Above, the nonrelativistic Breit–Wigner approximation has been used. This approximation is surely valid for narrow states. Anyway, the result is more general than that (one could use for instance the relativistic Sill distribution of Ref. [65] that takes into account threshold effects, getting the same outcome). In the large-N_c limit, one obtains

$$d_S(x) = \delta(x - M_S)\,, \tag{115}$$

thus

$$\Gamma_{Q\to Q_1 Q_2 Q_3} = \Gamma_{Q\to Q_1 S}(x = M_S) \propto \frac{1}{N_c}\,, \tag{116}$$

instead of N_c^{-2}. It is then evident that in this case, the decay chain dominates. Yet, this term is nonzero only if $M_S \leq M_Q - M_1$. If this is not the case, one should consider the next-to-leading term for $d_S(x)$ that scales as $1/N_c$ which again would lead to an overall $1/N_c^2$ decay of Q. This can be easily seen in the case in which M_S is much larger than M_Q, thus (for x in the range $(0, M_Q - M_1)$)

$$d_S(x) = \frac{\Gamma_S}{2\pi} \frac{1}{M_S^2} + \ldots \propto \frac{1}{N_c}\,, \tag{117}$$

out of which

$$\begin{aligned} \Gamma_{Q\to Q_1 Q_2 Q_3} &= \int_0^{M_Q - M_1} \mathrm{d}x \Gamma_{Q\to Q_1 S}(x) d_S(x) \\ &= \frac{\Gamma_S}{2\pi} \frac{1}{M_S^2} \int_0^{M_Q - M_1} \mathrm{d}x \Gamma_{Q\to Q_1 S}(x) \propto \frac{1}{N_c^2}\,. \end{aligned} \tag{118}$$

(Note, this decay is additionally also suppressed by the assumed large mass M_S).

As anticipated, the outcome is unchanged if S has more than a single decay channel. Namely, in this case, the spectral function refers to the specific decay channel [66] with

$$d_S(x) = \frac{\Gamma_{S\to Q_2Q_3}}{2\pi} \frac{1}{(x-M_S)^2 + \Gamma_S^2/4} \tag{119}$$

which reduces to

$$d_S(x) = \frac{\Gamma_{S\to Q_2Q_3}}{\Gamma_S} \delta(x-M_S) \tag{120}$$

in the large-N_c limit. Then,

$$\Gamma_{Q\to Q_1Q_2Q_3} = \frac{\Gamma_{S\to Q_2Q_3}}{\Gamma_S} \Gamma_{Q\to Q_1S}(x=M_S) \propto \frac{1}{N_c} \tag{121}$$

if, of course, $M_S \leq M_Q - M_1$.

In conclusion, the decay chain is dominant, if appropriate kinematic conditions are met.

4. Chiral models

Let us study the large-N_c scaling in a chiral model. For simplicity, we consider one scalar σ particle and one pseudoscalar π corresponding to the case of a single flavor ($N_f = 1$). (Note, we neglect at first the chiral anomaly, thus π emerges as a Goldstone boson: in this respect, it is more pion-like than η'-like).

The basic chiral 'multiplet' reads

$$\Phi = \sigma + i\pi\,. \tag{122}$$

A chiral transformation amounts to $\Phi \to e^{i\alpha}\Phi$ (it is an $O(2)$ rotation in the plane spanned by (σ, π)), thus the quantity

$$\Phi^\dagger\Phi = \Phi^*\Phi = \sigma^2 + \pi^2 \tag{123}$$

is a chirally-invariant object. For a generic N_f, the quantity Φ is an $N_f \times N_f$ matrix, *e.g.* [23, 67–70], but for $N_f = 1$, it is a scalar, thus $\Phi^\dagger = \Phi^*$. Interestingly, the main large-N_c outcomes that we shall discuss are independent of N_f (with an important exception, the chiral anomaly).

For $N_f = 1$, the chirally invariant potential takes the simple form

$$V(\sigma,\pi) = \frac{m_0^2}{2}\Phi^*\Phi + \frac{\lambda}{4}\left(\Phi^*\Phi\right)^2 = \frac{m_0^2}{2}\left(\pi^2+\sigma^2\right) + \frac{\lambda}{4}\left(\pi^2+\sigma^2\right)^2\,. \tag{124}$$

The large-N_c scaling is an immediate consequence of our previous discussion

$$m_0 \sim N_c^0\,, \qquad \lambda \sim N_c^{-1}\,. \tag{125}$$

For $m_0^2 > 0$, the potential is plotted in Fig. 15 for $m_0^2 = 0.6^2$ GeV^2 and $\lambda = 40$: it has a single minimum for $P_{\rm min} = (\sigma = \pi = 0)$. The masses of the particles correspond to the second derivatives evaluated at the minimum

$$M_\pi^2 = \left.\frac{\partial^2 V}{\partial \pi^2}\right|_{P=P_{\rm min}} = m_0^2 \sim N_c^0\,, \tag{126}$$

$$M_\sigma^2 = \left.\frac{\partial^2 V}{\partial \sigma^2}\right|_{P=P_{\rm min}} = m_0^2 \sim N_c^0\,. \tag{127}$$

Both particles have the same mass m_0. This is a manifest realization of chiral symmetry. Yet, this is not how Nature works. Chiral partners do not have the same mass.

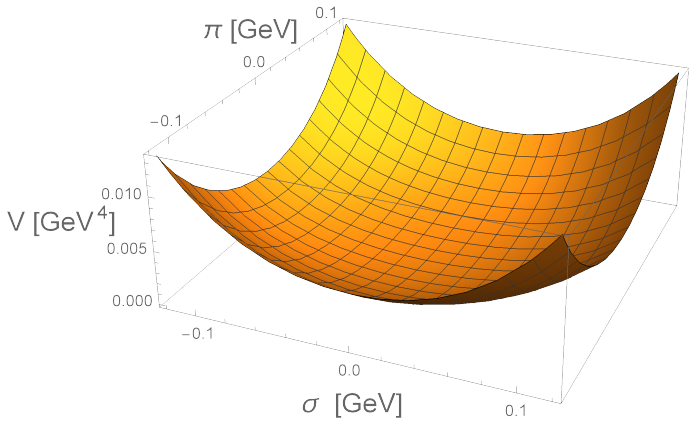

Fig. 15. Form of the chiral potential of Eq. (125) for $m_0^2 > 0$. The (unique and global) minimum sits at the origin.

The splitting of masses is possible without explicit breaking of chiral symmetry by considering $m_0^2 < 0$. The corresponding potential, plotted in Fig. 16 for $m_0^2 = -0.6^2$ GeV^2 and $\lambda = 40$, can be rewritten as

$$V(\sigma,\pi) = \frac{\lambda}{4}\left(\pi^2 + \sigma^2 - F^2\right)^2 - \frac{m_0^4}{4\lambda} \quad \text{with} \quad F = \sqrt{\frac{-m_0^2}{\lambda}} \sim N_c^{1/2} > 0\,. \tag{128}$$

It has the typical shape of a Mexican hat, in which the origin (for $\sigma = \pi = 0$) is not a minimum but a maximum. In fact, upon calculating the masses

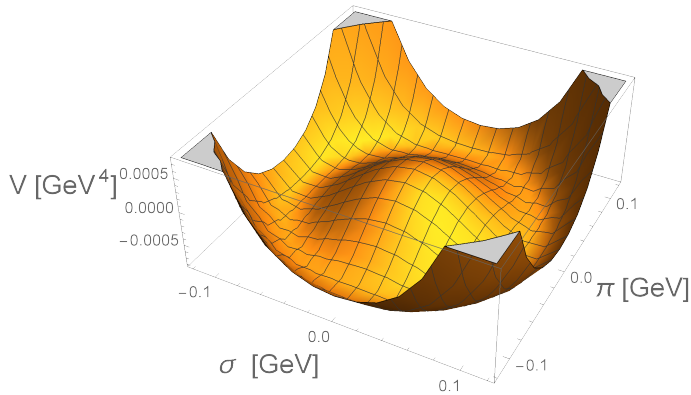

Fig. 16. Form of the chiral potential of Eq. (125) for $m_0^2 < 0$. There is a circle of minima for $\sigma^2 + \pi^2 = F^2 = -m_0^2/\lambda$. The original is a local maximum.

around the origin, they would turn out to be imaginary. There is, however, a circle of equivalent minima for

$$\pi^2 + \sigma^2 = F^2 = -\frac{m_0^2}{\lambda} \sim N_c > 0\,. \tag{129}$$

Moreover, the radius of this circle goes as $N_c^{1/2}$. SSB is realized when a specific minimum is picked up. Following the usual convention, we choose

$$P_{\min} = \left(\sigma_{\min} = \phi_N = \sqrt{-\frac{m_0^2}{\lambda}} = F, 0\right)\,. \tag{130}$$

The quantity $\phi_N = F$ is also denoted as the chiral condensate. Quite remarkably, a closer inspection of chiral models shows that the previously studied pion-decay constant is proportional to ϕ_N

$$\phi_N \sim f_\pi \sim N_c^{1/2}\,. \tag{131}$$

Namely, the coupling to the weak boson $W^\pm$ emerges from an interaction term of the type

$$g_{\text{weak}} \cos\theta_{\text{C}} W_\mu^\pm \sigma \partial^\mu \pi^\mp\,, \tag{132}$$

(θ_{C} is the Cabibbo angle), hence when σ condenses to $\phi_N \sim f_\pi$, the direct W–π mixing

$$W_\mu^\pm \longleftrightarrow \pi^\pm \tag{133}$$

arises.

Within this model, the masses are

$$M_\pi^2 = \left.\frac{\partial^2 V}{\partial \pi^2}\right|_{P=P_{\min}} = 0 \sim N_c^0\,, \tag{134}$$

$$M_\sigma^2 = \left.\frac{\partial^2 V}{\partial \sigma^2}\right|_{P=P_{\min}} = m_0^2 + 3\lambda\phi_N^2 = -2m_0^2 = 2\lambda\phi_N^2 \sim N_c^0 > 0\,, \tag{135}$$

which are not degenerate: the pion has a vanishing mass (it is a Goldstone boson), while the σ is massive. One then realizes how spontaneous chiral symmetry breaking generates different masses for chiral partners. Note, M_σ is proportional to the chiral condensate ϕ_N. Both masses are still $\sim N_c^0$. Yet, as shown in [51], SSB is expected to occur for large N_c, just as it does for $N_c = 3$.

In Nature, the pion has a small but nonzero mass. In order to take this fact into account, the potential is modified as

$$V(\sigma,\pi) = \frac{m_0^2}{2}\left(\pi^2+\sigma^2\right) + \frac{\lambda}{4}\left(\pi^2+\sigma^2\right)^2 - h\sigma\,, \tag{136}$$

where $-h\sigma$ breaks chiral symmetry explicitly. This term follows directly from the mass term $-m\bar{q}q$ in the QCD Lagrangian. We thus expect that $h \propto m_n$, where m_n is the bare quark mass (*e.g.* the average $(m_u + m_d)/2$). The potential, plotted in Fig. 17 (the same parameters as before and $h = m_\pi^2 f_\pi$ with $f_\pi = 92$ MeV and $m_\pi = 135$ MeV) has now a unique minimum for

$$P_{\min} = (\sigma_{\min} = \phi_N, 0) \tag{137}$$

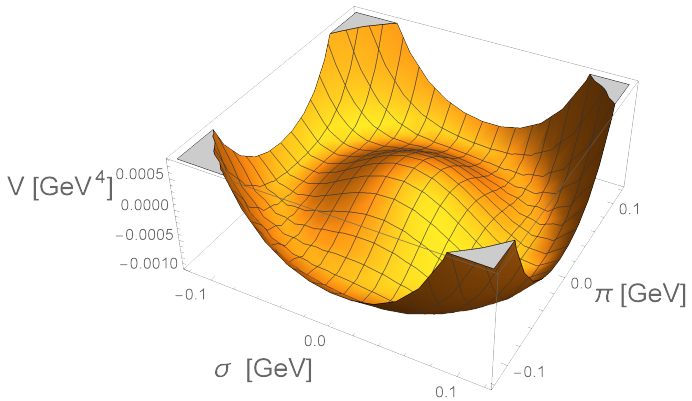

Fig. 17. The same as in Fig. 16 but with the explicit symmetry breaking of Eq. (136). There is now an absolute minimum for $\sigma = \phi_N > 0$ and $\pi = 0$.

with

$$\left.\frac{\partial V(\sigma,0)}{\partial\sigma}\right|_{\sigma=\sigma_{\min}=\phi_N} = m_0^2\phi_N + \lambda\phi_N^3 - h \;= 0\,,$$

which is of third order. (Only one of the three solutions corresponds to an absolute minimum). The pion mass is now nonzero

$$M_\pi^2 = \left.\frac{\partial^2 V}{\partial\pi^2}\right|_{P=P_{\min}} = m_0^2 + \lambda\phi_N^2 = \frac{h}{\phi_N} > 0\,. \tag{138}$$

We realize that the pion mass scales as

$$M_\pi \propto \sqrt{h} \propto \sqrt{m_n}\,. \tag{139}$$

This is indeed a nontrivial dependence since one would naively expect that $M_\pi \propto h \propto m|n$, *i.e.* to the mass of its constituents. This is not the case, signalizing that the tilted Mexican hat form of the potential is actually realized in Nature. This peculiar feature is also confirmed by lattice QCD studies, *e.g.* [71].

In order to fulfill the large-N_c expectation, one must require that

$$h \sim N_c^{1/2} \;\to M_\pi^2 \sim N_c^0\,. \tag{140}$$

This is in agreement with the scaling $f_\pi \propto N_c^{1/2}$. The term $h\sigma$ acts as a source term for σ, thus h scales as $N_c^{1/2}$. Yet, a closer look reveals a kind of problem: h has dimension energy^3 and is proportional to m_n, then one would naively write $h \sim m_n\Lambda_{\rm QCD}^2$, but $\Lambda_{\rm QCD}$ is N_c-independent. How to reconcile that with the required scaling $h \sim N_c^{1/2}$? This point will be clarified in Section 3.2 after discussing the dilaton at large N_c.

The mass of the σ-particle is

$$M_\sigma^2 = \left.\frac{\partial^2 V}{\partial\sigma^2}\right|_{P=P_{\min}} = m_0^2 + 3\lambda\phi_N^2 = M_\pi^2 + 2\lambda\phi_N^2 \sim N_c^0\,. \tag{141}$$

The mass difference $M_\sigma^2 - M_\pi^2 = 2\lambda\phi_N^2 \sim N_c^0 > 0$ does not depend on h. The plot of the potential along the σ-direction is shown in Fig. 18 for two values of N_c.

The chiral condensate $\phi_N \sim f_\pi$ can be related to the quark condensate

$$\langle 0_{\rm QCD}\,|\bar{q}q|\,0_{\rm QCD}\rangle < 0 \tag{142}$$

via the GOR relation (*e.g.* [72])

$$M_\pi^2 f_\pi^2 = -2m_n\,\langle 0_{\rm QCD}\,|\bar{q}q|\,0_{\rm QCD}\rangle\;, \tag{143}$$

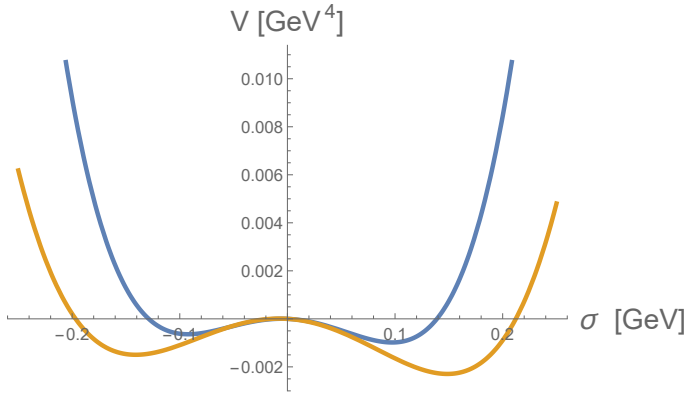

Fig. 18. Potential of Eq. (136) along the σ direction for $N_c = 3$ (upper blue curve) and for $N_c = 7$ (lower yellow curve). The minimum gets deeper on the vertical axis ($V_{\rm min} \sim -N_c$) and its location on the horizontal axis moves to the right ($\phi_N \sim N_c^{1/2}$).

where both members of this equation scale with N_c (the r.h.s. is such because it comes from quark loops, see also Section 5). Note, this equation implies a nontrivial link between the chiral condensate and the quark condensate, ϕ_N^2 scales as $\langle \bar{q}q \rangle$, Moreover, it is also in agreement with $M_\pi^2 \propto m_n$.

The chiral condensate ϕ_N enters also in decays, such as $\sigma \to \pi\pi$. This is determined by performing the shift $\sigma \to \sigma + \phi_N$ and then isolating the term $\lambda \phi_N \sigma \pi^2$, out of which

$$\Gamma_{\sigma\to\pi\pi} = 2\frac{k_\pi}{8\pi M_\sigma^2}\left[\lambda\phi_N\right]^2 \sim N_c^{-1}\,, \tag{144}$$

where $k_\pi = \sqrt{\frac{M_\sigma^2}{4} - M_\pi^2} \propto N_c^0$ is the modulus of the three-momentum of one of the outgoing particle. Also, in this case, the expected scaling is recovered.

In the full $N_f = 3$ version of the model, see *e.g.* Refs. [23, 28], the masses and decays are calculated by following the very same steps. Obviously, there are many more fields and decay channels, but the principles and the basic ideas are exactly the same as those discussed here.

As stated above, in this $N_f = 1$ example, the anomaly has been disregarded. There are however some interesting large-N_c considerations that can be done. The Lagrangian describing the anomaly for any N_f takes the form [73]

$$\mathcal{L}_{\rm A} = -c_1\left(\det\Phi + \det\Phi^\dagger\right) - c_2\left(\det\Phi - \det\Phi^\dagger\right)^2 - c_3\left(\det\Phi + \det\Phi^\dagger\right)^2 \tag{145}$$

which for $N_f = 1$ reduces to

$$\mathcal{L}_{\rm A} = -2c_1\sigma + 4c_2\pi^2 - 4c_3\sigma^2\,. \tag{146}$$

The mass arising from the anomaly scales as $M_\pi^2 \sim N_c^{-1}$. (Actually, the name $M_{\eta_0}^2 \sim N_c^{-1}$ [52] with η_0 being the flavor singlet would be more appropriate, but for simplicity we stick to π.) For $N_f = 1$, the first term is analogous to $h\sigma$ seen before, but the scaling is different, $c_1 \sim N_c^{-1/2}$, so that $M_\pi^2 \sim N_c^{-1}$ follows. For the same reason, $c_2 \sim N_c^{-1}$, $c_3 \sim N_c^{-1}$. The former is evident, for the latter, one needs to calculate the pion mass that turns out to be (for $h = c_1 = c_2 = 0$) $M_\pi^2 = 8c_3$. Thus,

$$c_1 \sim N_c^{-1/2}\,, \qquad c_2 \sim N_c^{-1}\,, \qquad c_3 \sim N_c^{-1}\,. \tag{147}$$

When changing N_f, these scaling behaviors are modified in such a way to preserve $M_{\eta_0}^2 \sim N_c^{-1}$. By properly counting the condensates that scale as $N_c^{1/2}$, one finds

$$c_1 \sim N_c^{-N_f/2}\,, \qquad c_2 \sim N_c^{-N_f}\,, \qquad c_3 \sim N_c^{-N_f}\,. \tag{148}$$

For recent applications and extensions of the axial anomaly, see Refs. [56, 74].

5. Different interaction types: a single trace 'wins'

The study of the full $N_f = 3$ chiral model is not within the scope of this lecture, but there is indeed an interesting point related to large N_c that is worth discussing. To this end, let us introduce the nonet of pseudoscalar states [23, 75] (see also Section 2.2 for $N_f = 2$)

$$P = \begin{pmatrix} \frac{\eta_N+\pi^0}{\sqrt{2}} & \pi^+ & K^+ \\ \pi^- & \frac{\eta_N-\pi^0}{\sqrt{2}} & K^0 \\ K^- & \bar{K}^0 & \eta_S \end{pmatrix} \equiv \begin{pmatrix} u\bar{u} & u\bar{d} & u\bar{s} \\ d\bar{u} & d\bar{d} & d\bar{s} \\ s\bar{u} & s\bar{d} & s\bar{s} \end{pmatrix} \tag{149}$$

with $\pi^0 = \sqrt{1/2}\,(u\bar{u} - d\bar{d})$, and where $\eta(547)$ and $\eta'(958)$ emerge as a mixing of $\eta_N = \sqrt{1/2}\,(u\bar{u} + d\bar{d})$ and $\eta_S = s\bar{s}$. In chiral models such as [23, 70], there are typically two types of quartic interactions that emerge

$$\mathcal{L}_P = -\lambda_2 {\rm Tr}\left[P^4\right] - \lambda_1 \left({\rm Tr}\left[P^2\right]\right)^2\,. \tag{150}$$

Their scaling is depicted in Figs. 19 and 20, respectively, showing that $\lambda_2 \sim N_c^{-1}$ and $\lambda_1 \sim N_c^{-2}$.

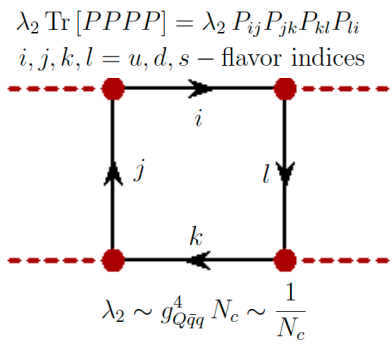

Fig. 19. Large-N_c scaling of the term proportional to λ_2 in the Lagrangian of Eq. (150). Note, the quark loops involves distinct flavors but the usual color factor N_c.

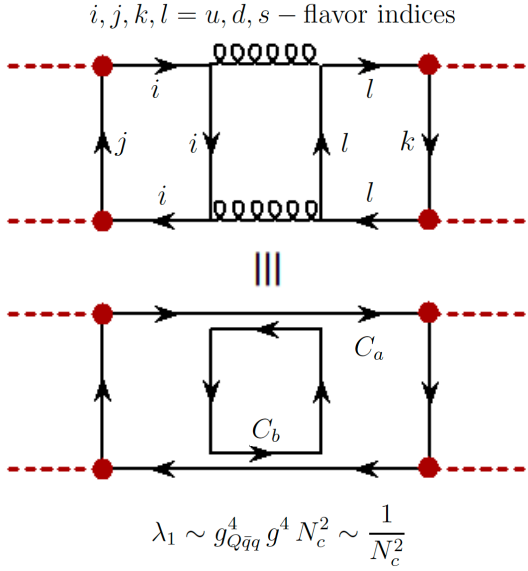

Fig. 20. Large-N_c scaling of the four-leg term proportional to λ_1 in the Lagrangian of Eq. (150).

Note, other terms are possible, as

$$\mathcal{L}'_P = -\lambda_3 \mathrm{Tr}\,[P]\,\mathrm{Tr}\left[P^3\right] - \lambda_4 (\mathrm{Tr}[P])^4\,. \tag{151}$$

The scaling for λ_4 can be determined by drawing the corresponding diagrams of Fig. 21, leading to $\lambda_4 \sim N_c^{-4}$. A similar study for λ_3 leads to $\lambda_3 \sim N_c^{-2}$.

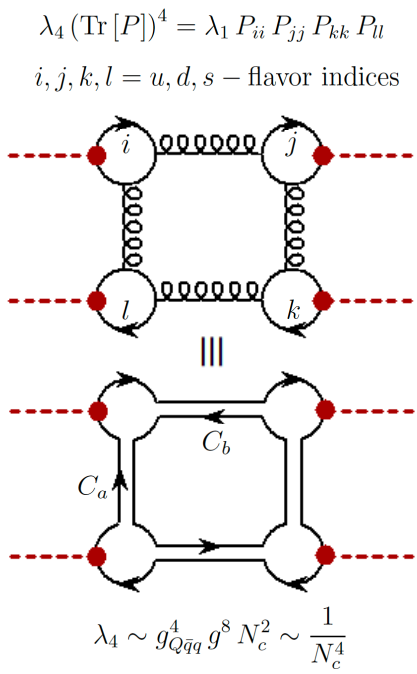

Fig. 21. Large-N_c scaling of the four-leg term proportional to λ_4 in the Lagrangian of Eq. (151).

In conclusion, even if all the terms proportional to $\lambda_{1,2,3,4}$ are quartic terms in the mesonic fields, the large-N_c results show that only one dominates, the one that contains a single trace (the λ_2-term). Interestingly, this result deals with an interplay of flavor and color d.o.f. It is also relevant for models, since it makes clear which terms should be at first kept and which can be disregarded, see *e.g.* [76, 77].

6. Connection to correlations

In [6, 30] as well as other works on QCD at large N_c, the starting point is the correlation function

$$\langle J_Q(x_2) J_Q(x_1) \rangle = -i \int \frac{\mathrm{d}^4 p}{(2\pi)^2} F_Q\left(p^2\right) \mathrm{e}^{ip(x_1 - x_2)} \,, \tag{152}$$

where the quantity $F_Q(p)$ is the loop contribution with total momentum p. Within our framework, at the lowest order, this is just the loop function $-\Sigma_Q(s = p^2)$. Expanding $F_Q(s)$, we get (see Fig. 22 for an illustration of these processes)

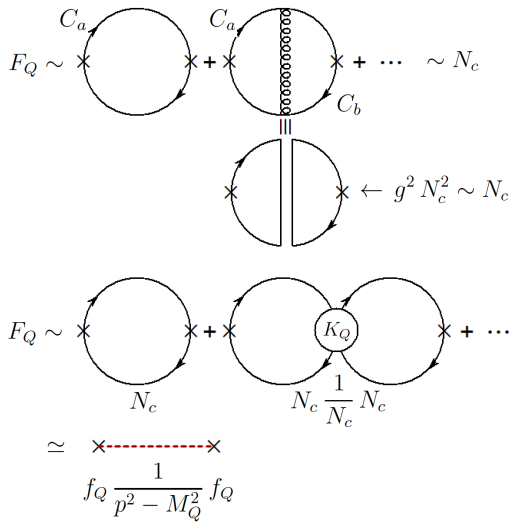

Fig. 22. Large-N_c scaling of the correlator $F_Q(s) \propto N_c$.

$$F_Q\left(s=p^2\right) = -\Sigma_Q\left(s=p^2\right)\left(1+\Sigma_Q(s)K_Q+\ldots\right) = -\frac{\Sigma_Q(s)}{1-\Sigma_Q(s)K_Q} = -\frac{\Sigma_Q(s)}{K_Q}\frac{1}{K_Q^{-1}-\Sigma_Q(s)}\,. \quad (153)$$

The pole is realized for the quarkonium mass M_Q^2 with the already encountered equation $K_Q^{-1} - \Sigma_Q(s = M_Q^2) = 0$. Upon expanding close to the pole, we find

$$F_Q(s) = \frac{\Sigma_Q(s)\Sigma_Q\left(M_Q^2\right)}{\Sigma_Q'\left(M_Q^2\right)\left(s-M_Q^2\right)} \simeq \frac{\Sigma_Q^2\left(M_Q^2\right)g_{Q\bar{q}q}^2}{s-M_Q^2} \simeq \frac{f_Q^2}{s-M_Q^2}\,, \quad (154)$$

where

$$f_Q = \Sigma_Q\left(M_Q^2\right)g_{Q\bar{q}q} = \frac{\Sigma_Q\left(M_Q^2\right)}{\sqrt{\Sigma_Q'\left(s=M_Q^2\right)}} \sim N_c^{1/2} \quad (155)$$

is the amplitude for the vacuum creation of the meson Q. Indeed, this expression has the same large-N_c behavior of the weak decay constant of this meson, see the previous discussion about f_π. (This equivalence does not hold for glueballs or hybrids.)

Since for any given set of quantum numbers an infinity of conventional mesons exists [6], the previous equation may be generalized as

$$F_Q(s) \simeq \sum_{n=1}^{\infty} \frac{f_{Q,n}^2}{s - M_{Q,n}^2} \sim N_c \tag{156}$$

since $f_{Q,n}^2 \sim N_c$ and $M_{Q,n}^2 \sim N_c^0$. This equation can be found in Ref. [6].

7. Connection to the Weinberg compositeness condition

Finally, we study the Weinberg compositeness condition [16, 17] along the large-N_c direction. The starting point is the Lagrangian

$$\mathcal{L}_{Qq} = \mathcal{L}_q + g_{Q\bar{q}q} Q(x) J_Q(x) - \frac{\alpha}{2} Q^2 \,, \tag{157}$$

where Q has no kinetic term and $\mathcal{L}_q$ contains the kinetic part for the quark field as well as eventual other interactions not relevant here. Note, the parameter α is *not* the physical mass squared, see below. The basic assumption is that $g_{Q\bar{q}q} \sim N_c^{-1/2}$.

By using the e.o.m. for the field Q, one gets

$$\frac{\partial \mathcal{L}_{Qq}}{\partial Q} = g_{Q\bar{q}q} J_Q(x) - \alpha Q(x) = 0 \to Q(x) = \frac{g_{Q\bar{q}q}}{\alpha} J_Q(x) \,. \tag{158}$$

Plugging it back into Eq. (157), one obtains a Lagrangian that depends on the quark field q only

$$\mathcal{L}_{Qq} \equiv \mathcal{L}_q + \frac{g_{Q\bar{q}q}^2}{2\alpha} J_Q^2 \,. \tag{159}$$

This is not a surprise, since Q had no kinetic term from the very beginning. One then gets the correspondence

$$K_Q = \frac{g_{Q\bar{q}q}^2}{\alpha} = \frac{1}{\Sigma_Q \left(M_Q^2 \right)} \,, \tag{160}$$

where Eq. (84) has been used. Then,

$$\alpha = \frac{\Sigma_Q \left(M_Q^2 \right)}{\Sigma_Q' \left(M_Q^2 \right)} \sim N_c^0 \,, \tag{161}$$

out of which

$$J_Q(x) = \frac{\alpha}{g_{Q\bar{q}q}} Q(x) = \Sigma_Q \left(M_Q^2 \right) g_{Q\bar{q}q} Q(x) = f_Q Q(x) \,, \tag{162}$$

which shows that the microscopic quark current $J_Q(x)$ is proportional to the composite meson field $Q(x)$, and the constant of proportionality is the amplitude for production of this field in the QCD vacuum. In this way, the correlator $\langle J_Q(x_2)J_Q(x_1)\rangle$ takes the form

$$\langle J_Q(x_2)J_Q(x_1)\rangle = f_Q^2 \langle Q(x_2)Q(x_1)\rangle = -if_Q^2 \int \frac{\mathrm{d}^4p}{(2\pi)^2}\frac{1}{p^2-M_Q^2}\mathrm{e}^{ip(x_1-x_2)}\,, \tag{163}$$

hence

$$F_Q(p) = \frac{f_Q^2}{p^2-M_Q^2} \tag{164}$$

follows consistently.

The formal way to show the result above (especially Eq. (162)) starts from the Lagrangian containing the bare mesonic coupling, mass, and field

$$\mathcal{L}_{Qq} = \mathcal{L}_q + g_{Q_0\bar{q}q}Q_0(x)J_Q(x) - \frac{M_{Q_0}^2}{2}Q_0^2 + \frac{1}{2}\left(\partial_\mu Q_0\right)^2\,, \tag{165}$$

with

$$g_{Q_0\bar{q}q} \sim N_c^{-1/2} \quad \text{and} \quad M_0 \sim N_c^0\,. \tag{166}$$

The propagator of the bare field Q_0 reads

$$\frac{1}{p^2 - M_{Q_0}^2 + g_{Q_0\bar{q}q}^2\Sigma_Q(p^2)} \sim N_c^0\,. \tag{167}$$

The first natural condition is to impose that the pole is realized for the physical mass M_Q^2

$$M_Q^2 - M_{Q_0}^2 + g_{Q_0\bar{q}q}^2\Sigma_Q\left(M_Q^2\right) = 0\,. \tag{168}$$

By expanding the denominator, the propagator of Q_0 reads

$$\begin{aligned}&\frac{1}{\left(p^2-M_Q^2\right)\left(1+g_{Q_0\bar{q}q}^2\Sigma_Q'\left(M_Q^2\right)\right)+g_{Q_0\bar{q}q}^2\tilde{\Sigma}_Q\left(p^2\right)}\\ &\simeq \frac{1}{\left(p^2-M_Q^2\right)\left(1+g_{0,Q\bar{q}q}^2\Sigma_Q'\left(M_Q^2\right)\right)} = \frac{Z_2}{p^2-M_Q^2}\,,\end{aligned} \tag{169}$$

where $\tilde{\Sigma}_Q(p^2)$ contains terms of the type $(p^2-M_Q^2)^2$ and higher powers, which are negligible close to the pole.

In order to obtain a correctly normalized propagator, the field

$$Q = \frac{1}{\sqrt{Z_2}}Q_0 \Leftrightarrow Q_0 = \sqrt{Z_2}Q \tag{170}$$

with the renormalization constant

$$Z_2 = \frac{1}{1 + g^2_{Q_0\bar{q}q}\Sigma'_Q\left(M^2_Q\right)} \sim N_c^0 \tag{171}$$

is introduced.

We impose here $g_{Q_0\bar{q}q} \to \infty$, out of which $Z_2 \to 0$. Intuitively, it means that the dressed field Q is not fundamental, realizing the main idea behind the compositeness condition. The Lagrangian takes the form

$$\begin{aligned}\mathcal{L}_{Qq} &= \mathcal{L}_q + g_{Q_0\bar{q}q}\sqrt{Z_2}Q(x)J_Q(x) - \frac{M^2_{Q_0}}{2}Z_2Q_0^2 + \frac{1}{2}Z_2\left(\partial_\mu Q\right)^2 \\ &= \mathcal{L}_q + g_{Q_0\bar{q}q}\sqrt{Z_2}Q(x)J_Q(x) - \frac{M^2_{Q_0}}{2}Z_2Q^2\,,\end{aligned} \tag{172}$$

where the dynamical term for the field $Q(x)$ has disappeared. Next

$$g_{Q\bar{q}q} = g_{Q_0\bar{q}q}\sqrt{Z_2} = \frac{g_{Q_0\bar{q}q}}{\sqrt{1 + g^2_{Q_0\bar{q}q}\Sigma'_Q\left(M^2_Q\right)}} \overset{g_{Q_0\bar{q}q}\to\infty}{=} \frac{1}{\sqrt{\Sigma'_Q\left(M^2_Q\right)}} \sim N_c^{-1/2} \tag{173}$$

and

$$\alpha = M^2_{Q_0}Z_2 = \frac{g^2_{Q_0\bar{q}q}\Sigma_Q(M^2_Q)}{1 + g^2_{Q_0\bar{q}q}\Sigma'_Q\left(M^2_Q\right)} \overset{g_{0,Q\bar{q}q}\to\infty}{=} \frac{\Sigma_Q\left(M^2_Q\right)}{\Sigma'_Q\left(M^2_Q\right)} \sim N_c^0\,, \tag{174}$$

which coincide with the previous derivation.

3.2. Glueballs

According to lattice QCD, many glueballs with various quantum numbers should exist, see *e.g.* the original predictions within the bag model [45], the review of Ref. [46], and the lattice works of *e.g.* [44, 78] (for a recent compilation and comparison of lattice results, see Ref. [79]). The glueball wave function must be colorless. Considering for definiteness the case of the scalar glueball, the corresponding (local and gauge invariant) current reads

$$J_G = \sum_{a=1}^{N_c^2-1} G^a_{\mu\nu}G^{\mu\nu,a}\,. \tag{175}$$

(For other currents, see *e.g.* [45, 80].) Using the double-line index notation, we may rewrite it as

$$J_G \simeq \sum_{a=1}^{N_c}\sum_{b=1}^{N_c} G^{(a,b)}_{\mu\nu}G^{\mu\nu,(b,a)}\,. \tag{176}$$

Then, the color wave function of this glueball can be written as

$$|G\text{-color}\rangle \simeq \frac{1}{\sqrt{N_c^2-1}} J_G\,|0\rangle\ . \tag{177}$$

Explicitly,

$$|G\text{-color}\rangle \simeq \frac{1}{N_c}\left|\bar{C}_1C_1\bar{C}_2C_2+\bar{C}_1C_1\bar{C}_3C_3+\ldots\right\rangle \simeq \frac{1}{N_c}\sum_{a=1}^{N_c}\sum_{b=1}^{N_c}\left|\bar{C}_aC_a\bar{C}_bC_b\right\rangle\ , \tag{178}$$

where, for simplicity, on the r.h.s. all the combinations are taken into account. Again, there is one combination (the colorless one) that should be subtracted, but this is unimportant for large N_c. Besides that, the previous equation is fully general and applies to any two-gluon glueball.

Following the same procedure as for quark–antiquark states, let us consider the processes leading to the illustrative transition

$$\bar{C}_1C_1\bar{C}_2C_2 \to \bar{C}_3C_3\bar{C}_4C_4 \tag{179}$$

in which all the colors have changed. It is easy to see that the dominant processes leading to this type of transitions scales as N_c^{-2}, see Fig. 23. In fact, a single gluon exchange or the quartic interaction, proportional to g^2, are not sufficient for a switch of all colors, see Fig. 24.

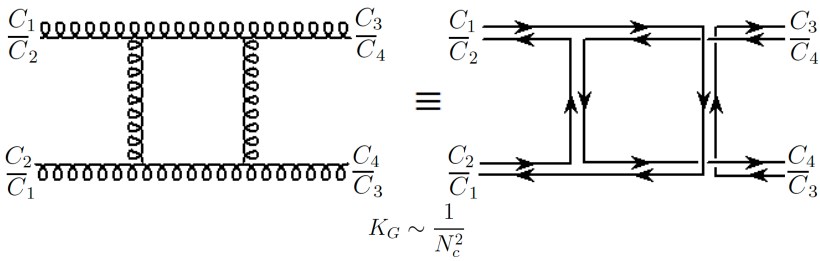

Fig. 23. Example of a leading diagram for the gluon–gluon scattering of the type $C_1\bar{C}_2C_2\bar{C}_1 \to C_3\bar{C}_4C_4\bar{C}_3$. Note, all gluonic colors have switched. The amplitude scales as N_c^{-2} and models the coupling in Eq. (180).

We write down an effective Lagrangian

$$\mathcal{L}_G = K_G J_G^2\,, \tag{180}$$

where

$$K_G \sim g^4 \sim N_c^{-4} \quad \text{thus} \quad K_G = \frac{\bar{K}_G}{N_c^2}\,, \tag{181}$$

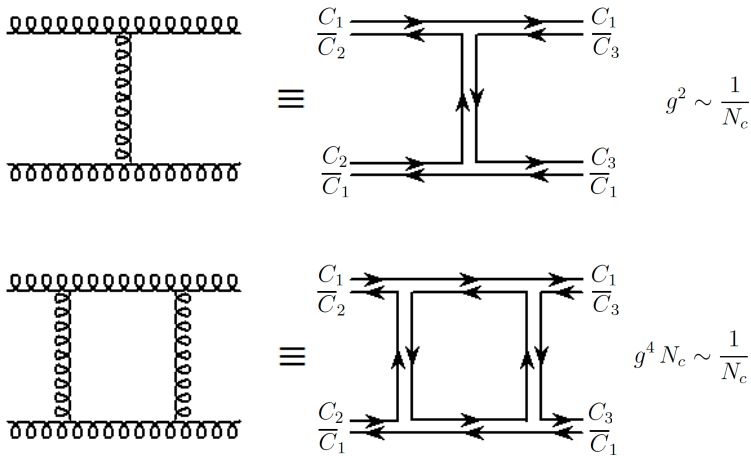

Fig. 24. Example of a leading diagram for the gluon–gluon scattering of the type $C_1\bar{C}_2C_2\bar{C}_1 \to C_1\bar{C}_4C_4\bar{C}_3$. Note, not all colors have switched (C_1 is in the beginning and in the end). This term, whose amplitude goes as N_c^{-1}, does **not** model the constant K_G in Eq. (180).

with $\bar{K}_G$ being N_c-independent. Note, a (nonlocal version of this) Lagrangian was implemented in Ref. [18] to study the mixing of glueballs with quarkonia.

The gluon–gluon scattering matrix for a given selected process such as $\bar{C}_1C_1\bar{C}_2C_2 \to \bar{C}_3C_3\bar{C}_4C_4$ is given by

$$T_G(s) = \frac{1}{K_G^{-1} - \Sigma_G(s)}\,, \tag{182}$$

see Fig. 25 for its pictorial representation. Now, the loop $\Sigma_G(s)$ scales as [18, 81]

$$\Sigma_G(s) = N_c^2\,\bar{\Sigma}_G(s)\,. \tag{183}$$

Then,

$$T_G = \frac{1}{\frac{N_c^2}{\bar{K}_G} - N_c^2\bar{\Sigma}_G(s)}\,. \tag{184}$$

Just as for the quarkonium, the glueball mass is N_c-independent and solves the equation

$$\frac{1}{\bar{K}_G} - \bar{\Sigma}_G\left(s = M_G^2\right) = 0 \to M_G \sim N_c^0\,. \tag{185}$$

Following the same steps, the amplitude can be written as

$$T_G \simeq \frac{(ig_{Ggg})^2}{s - M_G^2}\,, \tag{186}$$

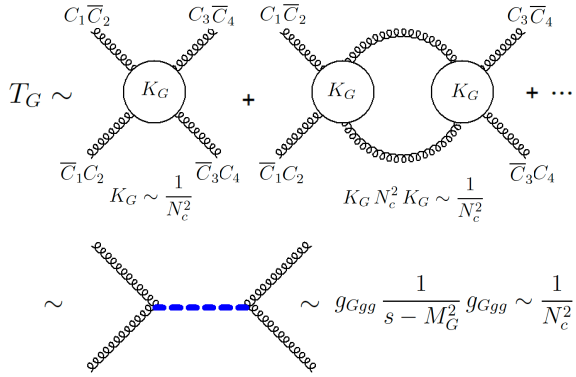

Fig. 25. Resummation of diagrams for the gluon–gluon scattering of the type $C_1\bar{C}_2C_2\bar{C}_1 \to C_3\bar{C}_4C_4\bar{C}_3$ with consequent formation of an intermediate glueball state (blue thick dashed line).

where the coupling of the glueball to its gluonic constituents is

$$g_{Ggg} = \frac{1}{\sqrt{N_c^2 \left(\frac{\partial \bar{\Sigma}_G(s)}{\partial s}\right)_{s=M_G^2}}} = \frac{\bar{g}_{Ggg}}{N_c}\,. \tag{187}$$

From the results above, we can easily derive the phenomenology of glueballs at large N_c.

First, we describe the four- and six-leg purely glueball couplings, which scale as N_c^{-2} and N_c^{-3}, respectively, see Fig. 26. This is in agreement with the general amplitude for n_G glueballs being $A_{n_GG} \propto \frac{N_c^2}{N_c^{n_G}}$, see Section 2.6.

Next, we calculate the interaction of a glueball with mesons. The basic mixing goes as $A_{GQ} \sim N_c^{-1/2}$, while the decay amplitude scales as $A_{GQQ} \sim N_c^{-1}$ (see Fig. 27). It then follows that the glueball decay into two standard mesons is suppressed as

$$\Gamma_{G\to QQ} \sim N_c^{-2}\,, \tag{188}$$

thus even more suppressed than the quarkonium decay.

As additional examples, in Fig. 28, we present the scattering $GG \to QQ$ (two glueballs into two quarkonia) that behaves as N_c^{-2}, and in Fig. 29, the scattering $GGG \to QQ$ scaling with N_c^{-3}.

The general amplitude for n_Q quarkonia and n_G glueballs is

$$A_{(n_QQ)(n_GG)} \propto \frac{N_c}{N_c^{n_Q/2} N_c^{n_G}}.$$

In this way, we confirm the previously quoted results (Section 2.6).

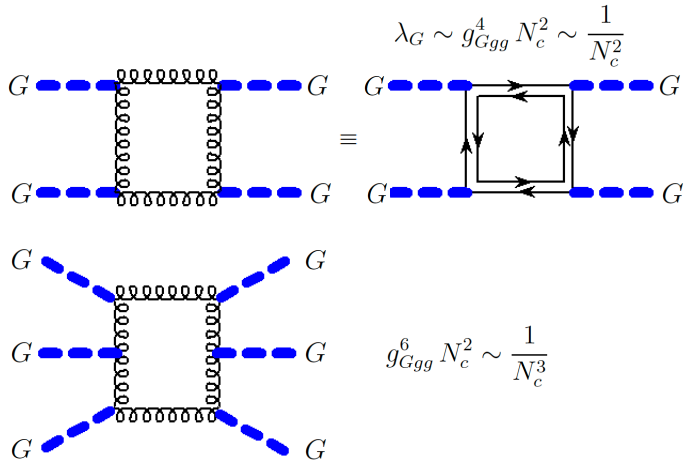

Fig. 26. Examples of processes involving only glueballs as initial and final states. Top: the amplitude $GG \to GG$ goes as N_c^{-2}. Bottom: the amplitude $GGG \to GGG$ goes as N_c^{-3}.

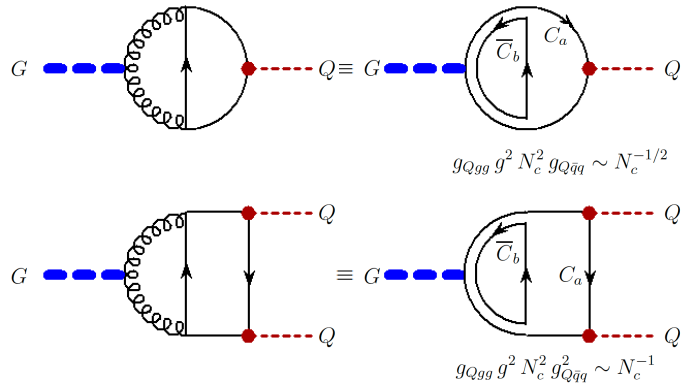

Fig. 27. Top: mixing of a glueball (blue) and a quarkonium (red) via quarks and gluons (black straight and springy lines). The amplitude scales as $N_c^{-1/2}$. Bottom: decay of a glueball (blue) into two quarkonia (red) via quarks and gluons (black). This diagram scales as N_c^{-1}, thus the glueball decay width goes as N_c^{-2}.

An important remark is in order: glueballs with three gluons work just as above. The scaling laws are left unchanged.

Next, we describe additional consequences concerning glueballs.

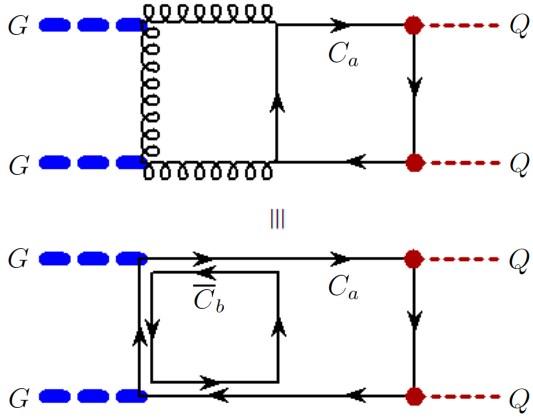

$$g^2_{Ggg}\, g^2\, N_c^2\, g^2_{Q\bar{q}q} \sim \frac{1}{N_c^2}$$

Fig. 28. Leading amplitude for the process $GG \to QQ$ that scales as N_c^{-2}. As usual, glueballs are blue, quarkonia red, quarks and gluons black.

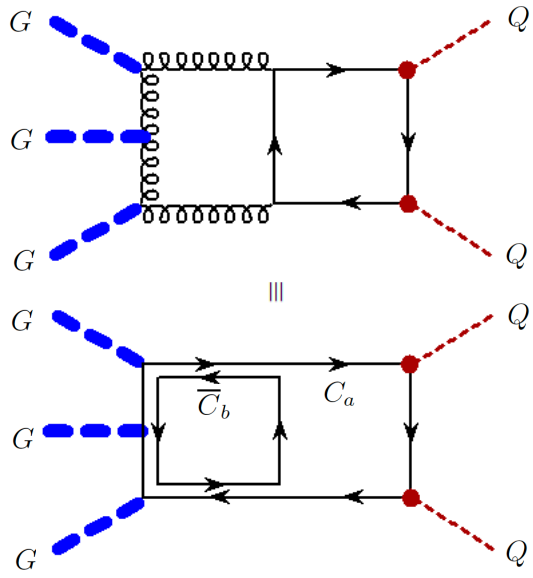

$$g^3_{Ggg}\, g^2\, N_c^2\, g^2_{Q\bar{q}q} \sim \frac{1}{N_c^3}$$

Fig. 29. Leading amplitude for the process $GGG \to QQ$ that scales as N_c^{-3}.

1. The dilaton Lagrangian in the large-N_c limit

The scalar glueball G can be described as a dilaton field, which is an important element of many chiral models (among which the extended linear sigma model [23]).

The dilaton Lagrangian reads [25–28]

$$\mathcal{L}_{\rm dil} = \frac{1}{2}(\partial_\mu G)^2 - V_{\rm dil}(G)\,, \tag{189}$$

with

$$V_{\rm dil}(G) = \frac{1}{4}\lambda_G \left[G^4 \ln\left(\frac{G}{\Lambda_G}\right) - \frac{G^4}{4}\right]\,, \tag{190}$$

which contains the dimensionless constant λ_G and the dimensionful constant Λ_G. The scaling laws, to be explained below, are given by

$$\lambda_G \sim N_c^{-2}\,, \qquad \Lambda_G \sim N_c\,. \tag{191}$$

The potential is shown in Fig. 30 for two different values of N_c (3 and 7, respectively). For $N_c = 3$, the numerical values are given by $\lambda_G = 1.7^2/0.5^2$ and $\Lambda_G = 0.5^2$ GeV^2, corresponding to a glueball mass of 1.7 GeV, in agreement with lattice estimates [44, 78].

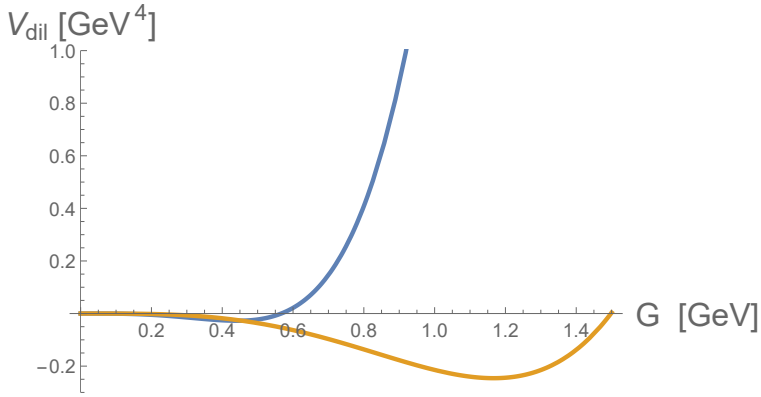

Fig. 30. Function $V_{\rm dil}(G)$ expressed in Eq. (190) for $N_c = 3$ (blue line) and $N_c = 7$ (yellow line). The value of the minimum G_0 increases with N_c, while its depth scales with $-N_c^2$. The numerical values for $N_c = 3$ are: $\Lambda_G = 0.5$ GeV, and $\lambda_G = 1.7^2/\Lambda_G^2$, corresponding to a scalar glueball mass of $M_G = 1.7$ GeV.

The logarithm and the dimensional parameter Λ_G are required for describing the breaking of dilatation symmetry

$$x^\mu \to \lambda^{-1} x^\mu \quad \text{and} \quad G(x) \to G'(x') = \lambda G(x)$$

in the following way:

$$\partial_\mu J^\mu = T^\mu_\mu = -G\partial_G V_{\rm dil}(G) + 4V_{\rm dil}(G) = -\frac{1}{4}\lambda_G G^4\,. \tag{192}$$

This equation resembles the QCD result [2, 27]

$$\left(T^\mu_\mu\right)_{\rm QCD} = -\frac{\alpha_{\rm s}}{16\pi}\left(\frac{11}{3}N_c - \frac{2}{3}N_f\right) G^a_{\mu\nu}G^{a,\mu\nu}\,. \tag{193}$$

Taking the expectation value of the former equation, we get

$$\left\langle\left(T^\mu_\mu\right)_{\rm QCD}\right\rangle = -\frac{\alpha_{\rm s}}{16\pi}\left(\frac{11}{3}N_c - \frac{2}{3}N_f\right) \left\langle G^a_{\mu\nu}G^{a,\mu\nu}\right\rangle\,, \tag{194}$$

which scales as N_c^2 because the gluon condensate $\left\langle G^a_{\mu\nu}G^{a,\mu\nu}\right\rangle \sim N_c^2$ and $\alpha_{\rm s} \sim N_c^{-1}$ (for a numerical estimate of the gluon condensate for $N_c = 3$, see Ref. [82]). Does the dilaton potential reproduce this scaling? In order to see that, let us expand the dilaton potential around the minimum, which is realized for $G_0 = \Lambda_G$. Upon performing the shift $G \to G_0 + \Lambda_G$, we obtain [83]

$$V_{\rm dil}(G) = -\lambda_G\Lambda_G^4 + \frac{1}{2}\lambda_G\Lambda_G^2 G^2 + \frac{5\lambda_G\Lambda_G}{3!}G^3 + \frac{11\lambda_G}{4!}G^4 + \dots\,, \tag{195}$$

where $V_{\rm dil}(G = \Lambda_G) = -\lambda_G\Lambda_G^4 \sim N_c^2$ has been used. From the term proportional to G^4, it follows that

$$\lambda_G \sim N_c^{-2}\,. \tag{196}$$

The glueball mass reads

$$M_G^2 = \lambda_G\Lambda_G^2 \sim N_c^0 \to \Lambda_G \sim N_c\,. \tag{197}$$

Note, the G^3 terms scales as $\lambda_G\Lambda_G \sim N_c^{-1}$, which is in agreement with the previous general rules. Going to a higher order in the expansions would also generate terms in agreement with those rules (for instance, G^5 goes as $\lambda_G/\Lambda_G \sim N_c^{-3}$ as expected, *etc.*).

The fact that the energy parameter Λ_G scales as N_c implies that it can be intuitively expressed as

$$\Lambda_G \sim N_c\Lambda_{\rm QCD}\,. \tag{198}$$

Finally, let us have a look at the condensate of the dilaton field

$$\left\langle T^\mu_\mu\right\rangle = -\frac{1}{4}\lambda_G\left\langle G^4\right\rangle = -\frac{1}{4}\lambda_G\Lambda_G^4 \sim -N_c^2 \tag{199}$$

in agreement with the QCD scaling of Eq. (194).

The scalar glueball is the lightest gluonic state predicted by lattice QCD and is a natural element of the chiral models with dilatation invariance [23, 28]. Presently, the resonance $f_0(1710)$ is a good candidate for being predominantly the scalar glueball, see *e.g.* [28, 84–88] and references therein.

2. Coupling the dilaton to other glueballs

The lightest scalar glueball is special since it is related to dilatation symmetry and its breaking, but other fields can be easily introduced. For illustrative purposes, let us couple the dilaton to the pseudoscalar glueball $\tilde{G}$ and the tensor glueball $T_{\mu\nu}$

$$\mathcal{L} = \mathcal{L}_{\rm dil} + \mathcal{L}_{\rm kin} - \frac{\lambda_{\tilde{G}G}}{2}\tilde{G}^2 G^2 - \lambda_{\tilde{G}}\tilde{G}^4 + \frac{\lambda_{TG}}{2} T_{\mu\nu}T^{\mu\nu}G^2 + \frac{\lambda_T}{2}\left(T_{\mu\nu}T^{\mu\nu}\right)^2 + \dots , \tag{200}$$

where Λ_G is the only dimensionful parameter entering in $\mathcal{L}_{\rm dil}$. All the λ parameters scale as N_c^{-2}, since each of them describes a four-leg interaction between glueballs.

When considering the $G \to \Lambda_G + G$ shift, the other glueballs get a mass: $m_{\tilde{G}}^2 = \lambda_{\tilde{G}G}\Lambda_G^2 \sim N_c^0$ and $m_T^2 = \lambda_{TG}\Lambda_G^2 \sim N_c^0$. For an explicit study of the scattering of tensor glueballs using the Lagrangian above, see Ref. [79].

3. Coupling the dilaton to the LSM

We consider, again for simplicity, the case of $N_f = 1$. The potential for the chiral model containing both the dilaton as well as the chiral multiplet $\Phi = \sigma + i\pi$ is given by

$$V(G, \sigma, \pi) = V_{\rm dil}(G) + \frac{a}{2}G^2\Phi^*\Phi + \frac{\lambda}{4}\left(\Phi^*\Phi\right)^2 . \tag{201}$$

Again, Λ_G is the only dimensionful parameter. Above, the constant a scales as

$$a \sim N_c^{-2} , \tag{202}$$

since it parameterizes a vertex with two glueballs and two quarkonia. The realistic $N_f = 3$ treatment of this model can be found in Ref. [28].

The search for the minimum of the model is more complicated than in the LSM case, since now two scalar fields are present and can condense. Namely, by setting the pion field to zero ($\pi = 0$), one has

$$V(G, \sigma, 0) = \frac{1}{4}\lambda_G\left[G^4 \ln\left(\frac{G}{\Lambda_G}\right) - \frac{G^4}{4}\right] + \frac{a}{2}G^2\sigma^2 + \frac{\lambda}{4}\sigma^4 , \tag{203}$$

with

$$\lambda_G \sim N_c^{-2} , \qquad \Lambda_G \sim N_c , \qquad a \sim N_c^{-2} , \qquad \lambda \sim N_c^{-1} . \tag{204}$$

The minimum is searched for

$$\partial_G V(G,\sigma,0) \;=\; \lambda_G G^3 \ln\left(\frac{G}{\Lambda_G}\right) + aG\sigma^2 = 0\,, \tag{205}$$

$$\partial_\sigma V(G,\sigma,0) \;=\; aG^2\sigma + \lambda\sigma^3 = 0\,. \tag{206}$$

For $a > 0$, the minimum is realized for $G_0 = \Lambda_G \neq 0$, $\sigma_0 = 0$, but as explained above, this is not what we have in Nature.

For $a < 0$, the minimum is realized for $G_0 \neq 0$, $\sigma_0 \neq 0$: the spontaneous breaking of chiral symmetry (on top of the breaking of dilatation symmetry) is realized. In particular, one has

$$\sigma_0^2 = -\frac{aG_0^2}{\lambda} \to \sigma_0 = \sqrt{\frac{-m_0^2}{\lambda}} \sim N_c^{1/2} \quad \text{with} \quad m_0^2 = aG_0^2 < 0\,. \tag{207}$$

The equation for G_0 reads

$$\lambda_G G_0^3 \ln\left(\frac{G_0}{\Lambda_G}\right) = -aG_0\sigma_0^2 = \frac{a^2 G_0^3}{\lambda}\,, \tag{208}$$

or

$$\ln\left(\frac{G_0}{\Lambda_G}\right) = \frac{a^2}{\lambda\lambda_G}\,, \tag{209}$$

hence

$$G_0 = \Lambda_G\, \mathrm{e}^{\frac{a^2}{\lambda\lambda_G}} \geqslant \Lambda_G\,. \tag{210}$$

In terms of large N_c, we have

$$G_0 \sim N_c\, \mathrm{e}^{1/N_c} \sim N_c\left(1 + \frac{1}{N_c} + \ldots\right)\,. \tag{211}$$

Thus, in the large-N_c limit,

$$G_0 = \Lambda_G \propto N_c\,. \tag{212}$$

How far is G_0 from Λ_G? For $N_c = 3$ that depends on the numerical values, but typically $G_0 \simeq \Lambda_G$ is well fulfilled [83].

Finally, let us briefly discuss the explicit symmetry breaking. That can be achieved by a term of the type

$$\lambda_n m_n G^2 \sigma\,, \tag{213}$$

where the coupling constant λ_n scales as

$$\lambda_n \sim N_c^{-3/2} \tag{214}$$

since it represents the coupling to two glueballs to an ordinary meson.

Then, the parameter h in Eq. (136) turns out to be (upon dilaton condensation ($G = G_0$))

$$h = \lambda_n m_n G_0^2 \simeq \lambda_n m_n \Lambda_G^2 \sim N_c^{1/2} \,, \tag{215}$$

as required for getting a pion mass that does not depend on N_c. This result shows that this is the appropriate way to model the explicit chiral symmetry breaking.

Another interesting consequence of this toy model is the decay of G into pions [83]

$$\begin{aligned} \Gamma_{G\to\pi\pi} &= 2\frac{k_\pi}{8\pi M_\sigma^2}\left[aG_0\right]^2 = 2\frac{k_\pi}{8\pi M_\sigma^2}\left[\frac{-m_0^2}{G_0}\right]^2 \\ &\simeq 2\frac{k_\pi}{8\pi M_\sigma^2}\left[\frac{M_\sigma^2}{2\Lambda_G}\right]^2 \sim N_c^{-2} \,, \end{aligned} \tag{216}$$

where $k_\pi = \sqrt{\frac{M_G^2}{4} - M_\pi^2}$. The scaling laws, that follow from $\Lambda_G \sim N_c$, are in agreement with the expected results.

All in all, a fully consistent picture, that is correctly embedded in chiral models with the dilaton, is obtained in the large-N_c limit.

4. Decays of other glueballs

Other glueballs also decay into conventional quark–antiquark mesons. A special case is given by the pseudoscalar glueball, whose coupling to mesons may be written down as [89]

$$\mathcal{L}_{\tilde{G}} = ic_{\tilde{G}}\tilde{G}\left(\det\Phi - \det\Phi^\dagger\right) \,, \tag{217}$$

where

$$c_{\tilde{G}} \propto N_c^{-1/2-N_f/2} \,. \tag{218}$$

A numerical evaluation of $c_{\tilde{G}}$ via instantons can be found in Ref. [74]. The recently discovered resonance $X(2600)$ by the BESIII Collaboration is a promising candidate for being the pseudoscalar glueball [90].

For the study of various glueball masses and decays, we refer to chiral models of Refs. [89, 91, 92] and to the Witten–Sakai–Sugimoto approach (which also makes use of large-N_c arguments) of Refs. [87, 93, 94] (for additional holographic considerations related to the spectrum, see Ref. [95]).

5. Connection to correlations

When considering the correlation involving glueball currents

$$\langle J_G(x_2) J_G(x_1)\rangle = -i \int \mathrm{d}^4 p F_G\left(s=p^2\right) \mathrm{e}^{ip(x_1-x_2)}\,, \tag{219}$$

$F_G(s)$ is the loop contribution with total momentum p. At the lowest order, this is just the loop function $-\Sigma_G(s=p^2)$. Evaluating $F_G(p)$ according to Fig. 31, we get

$$\begin{aligned} F_G(p) &= -\Sigma_G\left(s=p^2\right)\left(1+\Sigma_G(s) K_G+\ldots\right) \\ &= -\frac{\Sigma_G(s)}{1-\Sigma_G(s) K_G} = -\frac{\Sigma_G(s)}{K_G} \frac{1}{K_G^{-1}-\Sigma_G(s)}\,. \end{aligned} \tag{220}$$

The pole takes place (just as previously) for $K_G^{-1}-\Sigma_G(s=M_G^2)=0$. Upon

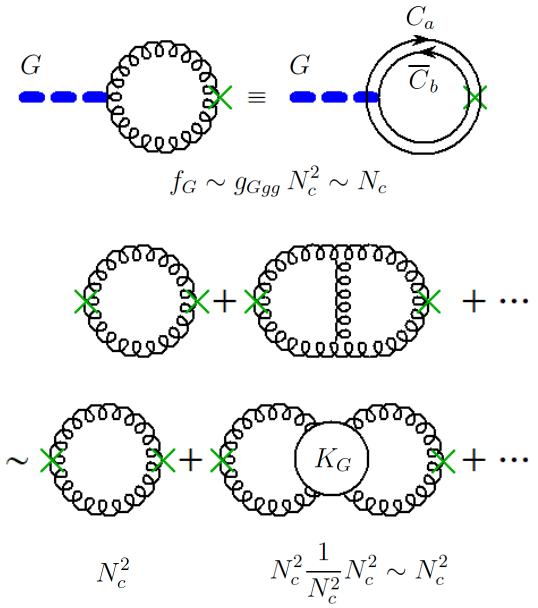

Fig. 31. Top: amplitude for the production of the glueball, denoted as f_G, scales with N_c. Bottom: correlator due to colorless sources of gluon–gluon states (glueballs): the bubbles scale as N_c^2. One may understand this process with a (tower of) glueball(s) as intermediate states, see Eq. (3.2).

expanding close to the pole, we find

$$F_G(p) = \frac{\Sigma_G(s)\Sigma_G\left(M_G^2\right)}{\Sigma_G'\left(M_G^2\right)\left(s-M_G^2\right)} \simeq \frac{\Sigma_G^2\left(M_Q^2\right) g_{Ggg}^2}{s-M_G^2} \simeq \frac{f_G^2}{s-M_Q^2}\,, \tag{221}$$

where

$$f_G = g_{Ggg}\Sigma_G\left(M_G^2\right) \sim N_c^{-1}\, N_c^2 \sim N_c \tag{222}$$

is the vacuum production/annihilation amplitude of the glueball G. In some cases, f_G may also be referred to as a 'decay constant', yet it should be stressed that this is not the weak decay constant. This is so because $W^{\pm}$ and Z^0 couple directly to quarks and not to gluons. In order to obtain the weak decay constant of glueballs, an additional suppression of N_c enters, leading to

$$f_G^{\text{weak}} \sim N_c^0\,. \tag{223}$$

Indeed, the same result can be obtained starting with an external glueball G, which transforms to a Q (mixing proportional $N_c^{-1/2}$), which then annihilates weakly (process proportional to $f_Q \sim N_c^{1/2}$). The scaling goes as $f_G^{\text{weak}} \sim N_c^{-1/2}\, f_Q \sim N_c^0$.

3.3. Hybrids

Hybrids are bound states containing a quark–antiquark pair and a gluon, see the review of Ref. [96] and the lattice results in Ref. [97]. As an example of a hybrid current, we consider the lightest 1^{-+} hybrid case

$$J_H^{\mu} = \sum_{a=1}^{N_c^2-1} \bar{q} G^{a,\mu\nu} t^a \gamma^5 \gamma_\nu q\,. \tag{224}$$

The quantity $\bar{q}G^{a,\mu\nu}t^a\gamma^5\gamma_\nu q$ is a scalar in color space. Schematically (and neglecting Lorentz indices and Dirac matrices), the hybrid current in the double-line notation reads

$$J_H = \sum_{a=1}^{N_c}\sum_{b=1}^{N_c} \bar{q}^{(a)} A^{(a,b)} q^{(b)} = C_1\left(\bar{C}_1 C_2\right)\bar{C}_2 + C_3\left(\bar{C}_3 C_4\right)\bar{C}_4 + \ldots \tag{225}$$

The corresponding interaction Lagrangian for the hybrid formation is expressed as

$$\mathcal{L}_H = K_H J_H^2\,. \tag{226}$$

In line with the previous cases, let us consider a specific transition (see Fig. 32)

$$C_1\left(\bar{C}_1 C_2\right)\bar{C}_2 \to C_3\left(\bar{C}_3 C_4\right)\bar{C}_4 \tag{227}$$

in which all colors have been switched.

The basic (connected) interaction turns out to be of the order of (see Fig. 32)

$$K_H \propto g^4 \propto N_c^{-2} \to K_H = \frac{\bar{K}_H}{N_c^2}\,. \tag{228}$$

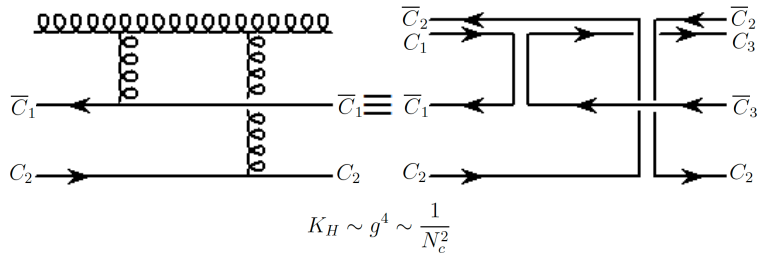

Fig. 32. Amplitude for gluon–quark–antiquark (hybrid) scattering of the type $(C_1\bar{C}_2)C_2\bar{C}_1 \to (C_4\bar{C}_3)C_3\bar{C}_4$. Then the initial gluon is $(C_1\bar{C}_2)$ and the final one $(C_4\bar{C}_3)$. Note, all colors have switched. The corresponding amplitude scales as N_c^{-2} and models the constant K_H appearing in the interaction Lagrangian of Eq. (226).

We then proceed as before by resumming over loop diagrams, see Fig. 33, finding

$$T_H(s) = \frac{1}{K_H^{-1} - \Sigma_H(s)}\,. \tag{229}$$

Now, the loop $\Sigma_H(s)$ scales as

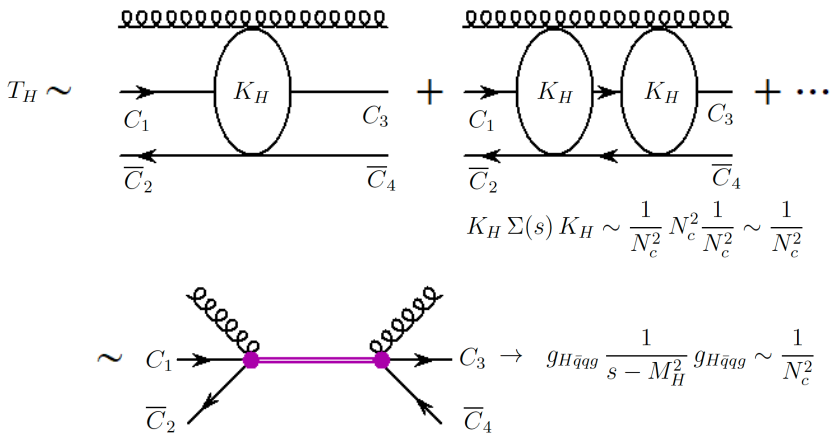

Fig. 33. Resummed diagrams leading to the formation of a hybrid meson (purple, double-solid line).

$$\Sigma_H(s) = N_c^2\,\bar{\Sigma}_H(s)\,. \tag{230}$$

Then

$$T_H = \frac{1}{\frac{N_c^2}{K_H} - N_c^2\,\bar{\Sigma}_H(s)}\,. \tag{231}$$

Just as for quarkonia and glueballs, the hybrid mass is N_c-independent

$$\frac{1}{\bar{K}_H} - \bar{\Sigma}_H\left(s = M_H^2\right) = 0 \to M_H \sim N_c^0\,. \tag{232}$$

Following analogous steps, the T-amplitude can be written as

$$T_H \simeq \frac{\left(i g_{H\bar{q}qg}\right)^2}{s - M_H^2}\,, \tag{233}$$

where the coupling of an hybrid meson to its constituents is

$$g_{H\bar{q}qg} = \frac{1}{\sqrt{N_c^2 \left(\frac{\partial \bar{\Sigma}_G(s)}{\partial s}\right)_{s=M_G^2}}} = \frac{\bar{g}_{H\bar{q}qg}}{N_c}\,. \tag{234}$$

We list some phenomenological consequences of hybrids at large N_c. The most important one is that the mixing of a hybrid state H with a quarkonium state Q (with the same quantum numbers, of course) scales as

$$A_{HQ} \sim \frac{1}{N_c} N_c^2 \frac{1}{\sqrt{N_c}} \frac{1}{\sqrt{N_c}} \sim N_c^0\,, \tag{235}$$

which is N_c-independent! (This case is depicted in Fig. 34.) This result means that hybrids behave as quarkonia in the large-N_c limit.

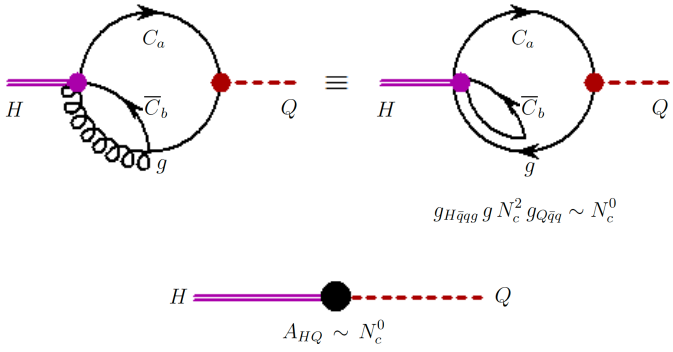

Fig. 34. The mixing of a hybrid meson H (purple, double-solid line) with a conventional quarkonium Q (red, dashed line) scales as N_c^0, implying that hybrids and quarkonia can freely mix at large N_c and therefore behave (mostly) in a similar way.

For example, the decay of a hybrid into two standard quarkonia mesons (see Fig. 35) scales as

$$A_{HQQ} \sim \frac{1}{N_c} N_c^2 \frac{1}{\sqrt{N_c}} \left(\frac{1}{\sqrt{N_c}}\right)^2 = \frac{1}{\sqrt{N_c}}\,, \tag{236}$$

just as a regular quark–antiquark mesonic decay.

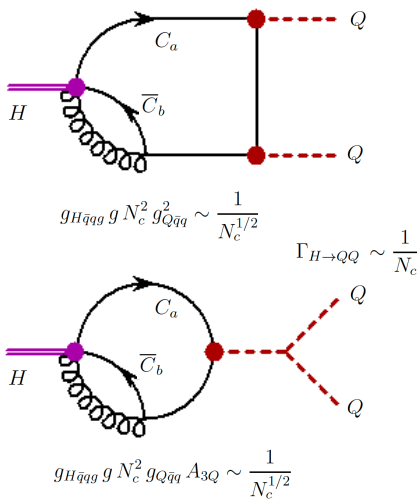

Fig. 35. Top: decay of a hybrid meson H (purple double-solid line) into two quarkonia mesons Q (red dashed lines) via quarks and gluons (black lines). The amplitude scales as $N_c^{-1/2}$, just as for the standard decay of a quarkonium. Bottom: the same result is obtained by converting a hybrid H into a quarkonium Q, which then decays into two quarkonia. Even simpler, one could just use the previous result concerning mixing and study the chain $H \to Q \to QQ$ that goes as $N_c^{-1/2}$.

The same applies to interactions with an arbitrary number of hybrids, that scales as $N_c/N_c^{n_H/2}$, as well as of hybrids and quarkonia that goes as $N_c/\left(N_c^{n_Q/2}N_c^{n_H/2}\right)$. In the case of $n_Q = 0$ and $n_H = 1$, one obtains $N_c^{1/2}$, which corresponds to the weak decay constant of a hybrid meson. Namely, the hybrid production/annihilation amplitude goes as

$$f_H \sim g_{Hqqg}\Sigma_H\left(M_H^2\right) \sim N_c^{-1}\, N_c^2 \sim N_c\,, \tag{237}$$

but the weak decay goes with an additional suppression of $N_c^{1/2}$ (the gluon needs to disappear)

$$f_H^{\text{weak}} \sim N_c^{1/2}\,. \tag{238}$$

This result is also obtained by taking an external H, which converts to Q (amplitude N_c^0), which subsequently annihilates (amplitude $N_c^{1/2}$), resulting in $N_c^{1/2}$.

Indeed, hybrids can form nonets just as regular mesons, and thus can be embedded into chiral approaches [98, 99].

The interaction of hybrids and glueballs can also be studied, see Fig. 36 for the explicit case of the decay of a hybrid meson into two glueballs, that scales as $N_c^{-3/2}$.

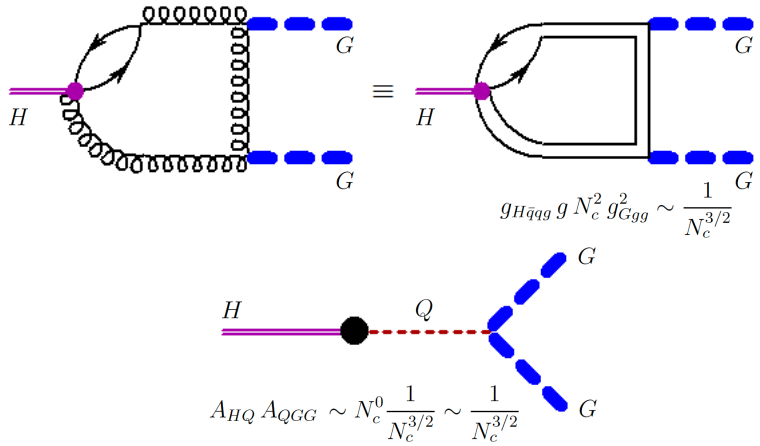

Fig. 36. Top: decay of a hybrid meson H (purple double-solid line) into two glueballs G (blue thick dashed lines) via quarks and gluons (black lines). The amplitude scales as $N_c^{-3/2}$. Bottom: the same result is obtained by converting a hybrid into a quarkonium which then converts into two glueballs.

3.4. Summary of the scaling for an arbitrary number of Q, G, H states

Putting all the results together, we recover the general scaling law for the amplitude with n_Q quarkonia, n_G glueballs, and n_H hybrids (see Section 2.6) as

$$A_{(n_Q Q)(n_G G)(n_H H)} \propto \frac{N_c\, N_c^{2(1-\mathrm{sign}(n_Q+n_H))}}{N_c^{n_Q/2} N_c^{n_G} N_c^{n_H/2}}\,, \tag{239}$$

where $\mathrm{sign}(x)$ is the sign function with $\mathrm{sign}(0) = 1/2$. If $n_Q + n_H > 0$, thus at least one quarkonium or a hybrid is present, $N_c\, N_c^{2(1-\mathrm{sign}(n_Q+n_H))} = N_c$, while for $n_Q = n_H = 0$, the purely gluonic case is recovered:

$$N_c\, N_c^{2(1-\mathrm{sign}(n_Q+n_H))} = N_c^2.$$

3.5. Four-quark states

The treatment of four-quark states in the large-N_c limit is subject to an ongoing debate, see [12] for a review. Some of the questions related to it are unsettled yet. The first question is what one can understand under four-quark states, since different possibilities are available.

As a specific example, we shall consider the meson $a_0(980)$, for which different interpretations have been proposed in the literature, that we briefly review in the following.

1. Molecular states, such as the binding of two colorless quark–antiquark mesons

For the illustrative state $a_0^+(980)$, this amounts to considering a bound state of K^+ and $\bar{K}^0$ [100, 101] resulting in the state

$$\left|a_0^+(980)\right\rangle = \left|K^+\bar{K}^0\right\rangle . \tag{240}$$

In general, such a molecule is of the type $|QQ\rangle$ and its current can be expressed as $J_{QQ}(x) = Q^2(x)$. The basic interaction takes the form

$$\mathcal{L}_{QQ} = K_{QQ} J_{QQ}^2(x) , \tag{241}$$

where

$$K_{QQ} \sim N_c^{-1} \to K_{QQ} \simeq \frac{\bar{K}_{QQ}}{N_c} , \tag{242}$$

being a quartic interaction between conventional mesonic fields.

Upon repeating the previous steps, the resummed T-matrix for the eventual formation of QQ bound states (see Fig. 37) reads

$$T_{QQ}(s) = \frac{1}{K_{QQ}^{-1} - \Sigma_{QQ}(s)} \tag{243}$$

with $\Sigma_{QQ}(s) = \bar{\Sigma}_{QQ}(s)$ being large-N_c-independent (it is the loop of two colorless states). The mass of the molecular states corresponds to a solution

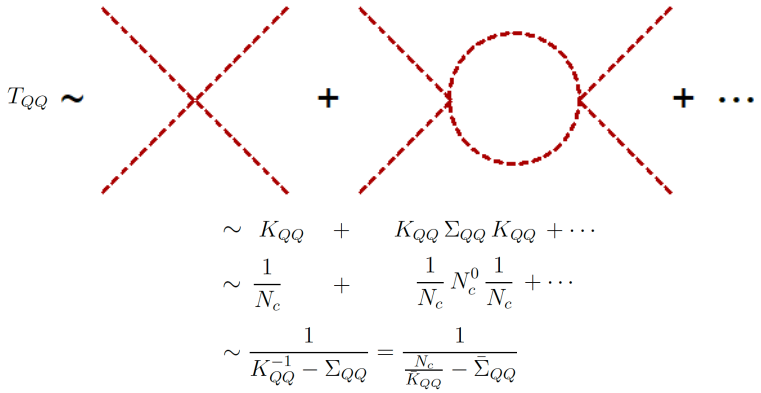

Fig. 37. Resummation of regular meson–meson scattering diagrams needed to investigate the eventual emergence of a molecular bound state. While for $N_c = 3$ these states can form, this is not the case for large N_c. Namely, the attraction decreases as N_c^{-1} but the intermediate states in the bubble are colorless, thus the loop function cannot compensate for the decrease of attraction. See the text for more details.

of the equation

$$\frac{N_c}{\bar{K}_{QQ}} - \bar{\Sigma}_{QQ}\left(s = M_{QQ}^2\right) = 0\,. \tag{244}$$

This equation might have a solution for $N_c = 3$, but this is not the case of large N_c.

Let us first consider the case of a genuine molecular state whose mass M_{QQ} is below the threshold $2M_Q$ for $N_c = 3$. The function $\Sigma_{QQ}(s)$ is real below the threshold and has a maximum (cusp) just at it. If the bound state exists for $N_c = 3$ for a value $M_{QQ} < 2M_Q$ below the threshold, there is a maximal value $N_c^{\max}$ for which the molecular state forms just at the threshold, $M_{QQ} = 2M_Q$. Yet, upon increasing N_c further, the state ceases to form. Indeed, this is very intuitive: by increasing N_c, the attraction decreases and there is no N_c factor to compensate it. Molecular states of this type fade away for large N_c.

Indeed, the previous argumentation may be extended also to molecular resonances with mass above $2M_Q$, since $\Sigma_{QQ}(s)$ is a non-diverging function. In any case, for N_c large enough, one has $T_{QQ}(s) \simeq K_{QQ} \simeq \bar{K}_{QQ}/N_c$, thus no bound state is possible.

Molecular states may also emerge from glueballs or hybrids. The case of glueball molecular states, so-called glueballonia, has been recently studied in Ref. [83]. Quite remarkably, the bound state of two scalar glueballs may be stable in pure Yang–Mills and be a resonance in full QCD for $N_c = 3$. Yet, for large N_c, it fades away even faster than QQ molecular states. In fact, one has

$$\mathcal{L}_{GG} = K_{GG} J_{GG}^2(x)\,, \tag{245}$$

where $J_{GG} = G^2(x)$ and

$$K_{GG} \sim N_c^{-2} \to K_{GG} \simeq \frac{\bar{K}_{GG}}{N_c^2}\,, \tag{246}$$

as it follows from being a quartic interaction between glueballs. Then

$$T_{GG}(s) = \frac{1}{K_{GG}^{-1} - \Sigma_{GG}(s)} = \frac{1}{\frac{N_c^2}{\bar{K}_{GG}} - \bar{\Sigma}_{GG}(s)} \tag{247}$$

with $\Sigma_{GG}(s) = \bar{\Sigma}_{GG}(s)$ being N_c-independent. This result shows that no glueballonium can form at large N_c. It is important to note that the same large-N_c scaling for the glueballonium formation is obtained in the more advanced approach of Ref. [83], where two unitarization methods have been used to study its formation. This fact shows again that the rather simple separable interaction considered above is fully consistent with general

large-N_c results and is therefore suitable to study the large-N_c scaling. Additional bound states of regular mesons with glueballs and/or hybrids can be studied [102], but for the very same reason, they shall also not survive in the large-N_c domain.

2. Dynamically generated states: the example of companion poles

A specific example of a dynamically generated state is the so-called emergence of a companion pole, as it was presented for the case of the meson $a_0(980)$ in Refs. [103, 104]. The starting point is a Lagrangian which contains a single conventional scalar quark–antiquark bare state, roughly corresponding to $a_0 \equiv a_0(1450)$. One then writes the interaction term as

$$\mathcal{L}_{\rm int} = g_{a_0 KK} a_0^+ K^- K^0 + g_{a_0 \pi\eta} a_0^+ \pi^- \eta + \dots \,, \tag{248}$$

with the standard scaling

$$g_{a_0 KK} \sim N_c^{-1/2} \,, \qquad g_{a_0 \pi\eta} \sim N_c^{-1/2} \,. \tag{249}$$

Then, upon studying mesonic loops, the full-dressed propagator of $a_0(1450)$ arising from the decays into $\bar{K}K$, $\pi\eta$, *etc.*, takes the form

$$\frac{1}{p^2 - M_{a_0}^2 + g_{a_0 KK}^2 \Sigma_{KK}(p^2) + g_{a_0 \pi\eta}^2 \Sigma_{\pi\eta}(p^2) + \dots} \tag{250}$$

with $M_{a_0} \simeq 1.4$ GeV$\sim N_c^0$. The coupling constants are set to reproduce the physical results for the resonance $a_0(1450)$ for the physical case of $N_c = 3$.

Then, upon solving the pole equation in the complex plane

$$p^2 - M_{a_0}^2 + g_{a_0 KK}^2 \Sigma_{KK}\left(p^2\right) + g_{a_0 \pi\eta}^2 \Sigma_{\pi\eta}\left(p^2\right) + \dots = 0 \,, \tag{251}$$

two poles are found (in this specific case on the third and second Riemann sheets, respectively, but this aspect is not relevant to our analysis).

One pole is close to the expected bare quarkonium result and corresponds to $a_0(1450)$: when increasing N_c, this pole converges toward the real axis, that is its imaginary part decreases as N_c^{-1}, as expected for a regular $\bar{q}q$ quarkonium state.

The second pole appears close the $\bar{K}K$ threshold and corresponds to $a_0(980)$. In the large-N_c limit, it behaves differently: its width increases instead of decreasing, showing that this additional state is not an ordinary quark–antiquark object. Eventually, it disappears from the original (second) Riemann sheet.

These features concerning dynamically generated companion poles are quite general and apply, with minor changes, to other states as well, such as the scalar resonances $f_0(500)$ [105, 106] and $K_0^*(700)$ [107, 108], or the famous $X(3872)$ (as a virtual pole) [109].

It should be also stressed that companion poles are not the only possibility for dynamically generated states, see *e.g.* [106, 110] but it shows a quite general feature: these solutions fade away in the large-N_c limit[1].

3. Genuine tetraquark state as a bound state of two diquarks

Referring to $a_0(980)$ as our example, we may interpret it as a bound state of a good diquark and a good anti-diquark [113, 114], where a good diquark state is antisymmetric in both color and flavors, *e.g.*

$$|us, \text{good}\rangle = |\text{space: } L=0\rangle\, |\text{spin: } S=0\rangle\, |\text{color: } RG-GR\rangle\, |\text{flavor: } us-su\rangle\,.$$

Then

$$\left|a_0^+(980)\right\rangle = |us, \text{good}\rangle\, \left|\bar{d}\bar{s}, \text{good}\right\rangle\,. \tag{252}$$

Indeed, one can build nonets of states and describe these objects in a chiral context [70, 115–117].

What about the large-N_c scaling of these configurations? The issue is that the straightforward generalization of the good diquark is an object that contains $N_c - 1$ quarks, *e.g.* [33]. This object may be used to construct baryons in the large-N_c limit (see the next section for its explicit implementation), but is not useful for building tetraquarks states (with 'tetra' in the sense of four).

In the classic lecture of Coleman [9], it is stated that tetraquarks (of whatever type) do not exist in the large-N_c limit because four-quark states preferably arrange themselves into two free mesons, see Fig. 38.

Weinberg realized years later [29] that one should rather look at connected diagrams, hence certain tetraquarks states might exist and show scaling laws similar to regular mesons. A debate has followed [12, 30–34], basically confirming the Weinberg point of view but always stressing that it is not clear if such tetraquark states do form in the large-N_c limit. Indeed, in [32], it is argued that they eventually do not.

Does the bound-state approach discussed in these lectures help? Here, we just make some basic considerations that are not conclusive, but may be the starting point for future investigations. To this end, let us consider the most general four-quark current [33]

$$J_T = C_1 \delta^{ac}\delta^{bd} q^a q^b \bar{q}^c \bar{q}^d + C_2 \delta^{ad}\delta^{bc} q^a q^b \bar{q}^c \bar{q}^d\,. \tag{253}$$

[1] A word of caution is required; in some cases, one may obtain certain mesons as solutions of bound-state equations out of effective Lagrangians. Yet, these mesons can be ordinary quark–antiquark states, but the way they have been obtained would make them look like molecular states that do not survive the large-N_c limit. We refer to Ref. [111] (see also [112]) for this subtlety and for the related notion of 'dynamical reconstruction'.

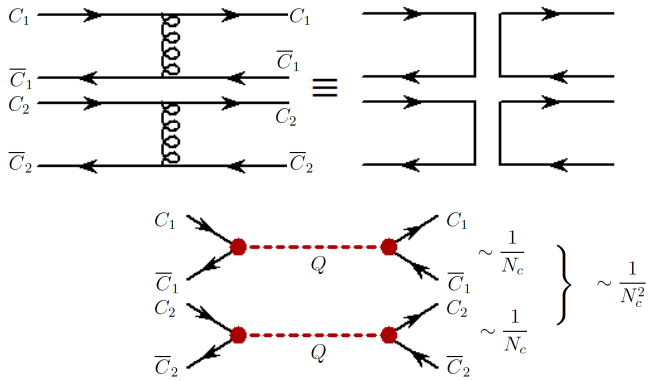

Fig. 38. Disconnected diagram for the reaction $C_1\bar{C}_1C_2\bar{C}_2 \to C_3\bar{C}_3C_4\bar{C}_4$. All the colors have switched, but these diagrams (properly resummed) eventually generate two intermediate conventional Q states. Indeed, the scaling N_c^{-2} is in agreement with this interpretation.

Then, the separable interaction takes the form

$$\mathcal{L}_T = K_T J_T^2(x)\,, \tag{254}$$

where we need to discuss the large-N_c scaling of K_T. If one considers a connected four-quark diagram, one obtains (see Fig. 39)

$$K_T \sim N_c^{-3} \to K_T \simeq \frac{\bar{K}_T}{N_c^3}\,, \tag{255}$$

since it is a quartic interaction between conventional mesonic fields. Namely, a disconnected diagram, in which the two quark–antiquark parts interact separately, would scale as N_c^{-2}, see again Fig. 38, but this is not what we search for.

Then, the resummed T-matrix for the eventual formation of a tetraquark state state, see Fig. 40, reads

$$T_T(s) = \frac{1}{K_T^{-1} - \Sigma_T(s)}\,, \tag{256}$$

where $\Sigma_T(s)$ scales as N_c^2. Namely, whatever is the specific tetraquark configuration, the order is always N_c^2. (If, for example, we consider only antisymmetric diquark color configurations, there are $N_c(N_c-1)/2 \sim N_c^2$ choices for the diquark color.) Hence, $\Sigma_T(s) \simeq N_c^2\bar{\Sigma}_T(s)$, leading to

$$T_T(s) = \frac{1}{\frac{N_c^3}{K_T} - N_c^2\bar{\Sigma}_T(s)}\,. \tag{257}$$

This result suggests that no tetraquark binds for large N_c, since the interaction strength decreases too fast, just as mesonic molecular states.

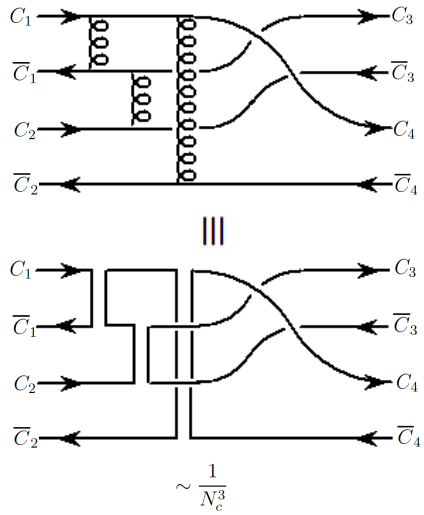

Fig. 39. Connected diagram for the reaction $C_1\bar{C}_1C_2\bar{C}_2 \to C_3\bar{C}_3C_4\bar{C}_4$. All the colors have been switched. It scales as N_c^{-3}.

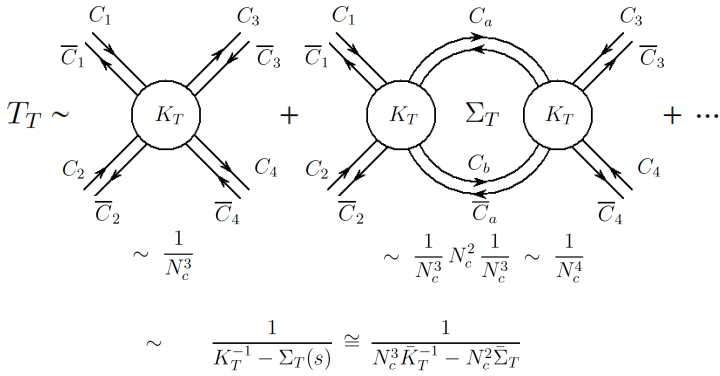

Fig. 40. Tentative resummation of connected diagrams with a colorless four-quark configuration in the initial and final states. The attraction seems to decrease too fast to allow for a bound-state (a genuine tetraquark state) formation.

Note, if we would study the tetraquark correlator $\langle J_T(x_2)J_T(x_1)\rangle$, one should indeed remove the disconnected part $\Sigma_T(s) \sim N_c^2$, hence the lowest order contribution $\Sigma_T(s)K_T^{-1}\Sigma_T(s)$ scales as N_c, as expected. Future studies are needed to check if the present heuristic arguments against the emergence of tetraquarks can be made rigorous.

4. Brief study of baryons at large N_c

The topic of baryons at large N_c cannot be fully covered in these lectures. Here, our aim is to show that an approach similar to the one applied to mesons (bound state formation) is also consistent with baryonic large-N_c scaling properties. To this end, let us introduce the generalized 'diquark' D^{a_1} for $a_1 = 1, \ldots, N_c$ as a $N_c - 1$ quark object with the structure

$$D^{a_1} = \frac{1}{\sqrt{(N_c-1)!}} \sum_{a_2,a_3,\ldots,a_{N_c}=1}^{N_c} \varepsilon_{a_1 a_2 \ldots a_{N_c}} q^{a_2} q^{a_3} \ldots q^{a_{N_c}} \,. \tag{258}$$

There are N_c generalized diquarks, just as there are N_c antiquarks. Indeed, under color transformations, D^{a_1} transforms as an antiquark. Then, one may interpret the baryon as a bound state of such a generalized diquark and a quark. The current is given by

$$J_B = \sum_{a_1=1}^{N_c} D^{a_1} q^{a_1} \,. \tag{259}$$

Following the mesonic case, we write down the interaction Lagrangian as

$$\mathcal{L}_B = K_B J_B^2 \,. \tag{260}$$

The determination of the scaling of K_B can be deduced from Fig. 41. Since at the lowest order no gluon is involved because a simple switch of quarks suffices to change the color of both D and q (this is due to the fact that D contains already $N_c - 1$ colors), it then follows that:

$$K_B \sim N_c^0 \,, \tag{261}$$

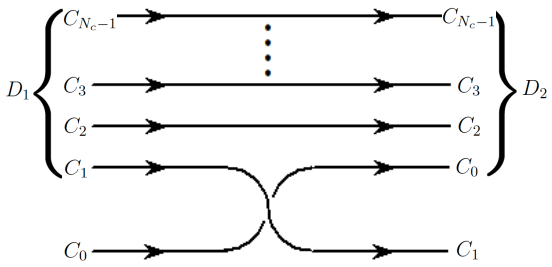

Fig. 41. Scattering of a generalized diquark D_1 and a quark with color C_1 into D_2 and C_2 (thus color 'changed'). A simple switch of quarks does the job, thus at leading order no gluon is present and the amplitude goes with N_c^0.

hence $K_B \simeq \bar{K}_B$. On the other hand, the loop $\Sigma_B(E)$ involving D–q goes with N_c for what concerns the color circulating in it, but contains also a dependence on the mass of the generalized diquark D with $m_D \propto N_c - 1$. Since m_D is very large, we resort to nonrelativistic propagators and use the energy E (and not $s = E^2$) as an argument of the loop $\Sigma_B(E)$. This function can be expanded in E finding

$$\Sigma_B(E) \simeq N_c \left(\frac{c_1}{m_D} + c_2 \frac{E}{m_D^2} + \dots \right) , \tag{262}$$

which scales as $N_c^0 + N_c^{-1} + \dots$ The T-matrix for the illustrative scattering process $D^1 q^1 \to D^2 q^2$ reads (Fig. 42)

$$T_B = \frac{1}{K_B^{-1} - \Sigma_B(E)} . \tag{263}$$

The pole equation reads

$$\bar{K}_B^{-1} - N_c \left(\frac{c_1}{m_D} + c_2 \frac{E}{m_D^2} + \dots \right) = 0 , \tag{264}$$

leading to

$$\frac{N_c}{m_D} c_1 + c_2 \frac{N_c}{m_D} \frac{E}{m_D} + \dots = \bar{K}_B^{-1} , \tag{265}$$

thus

$$c_2 \frac{N_c}{m_D} \frac{E}{m_D} = \bar{K}_B^{-1} - \frac{N_c}{m_D} c_1 \sim N_c^0 . \tag{266}$$

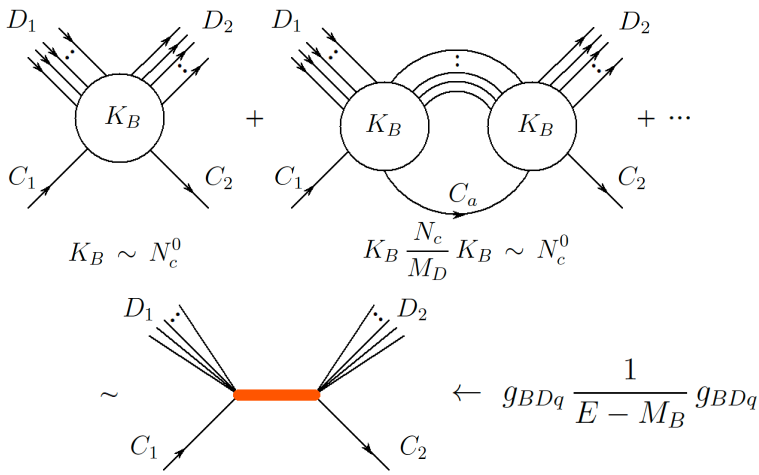

Fig. 42. Resummation of the scattering $D_1 C_1 \to D_2 C_2$ with consequent formation of one baryon (brown thick line) as intermediate state.

It then follows that

$$E \equiv M_B \sim m_D \frac{m_D}{N_c} \sim m_D \sim N_c \,. \tag{267}$$

In other words, we find that, if $m_D \sim N_c$, then $M_B \sim m_D \sim N_c$ as well, being a consistent (and expected) result.

Upon expanding around the pole, we find

$$T_B \simeq \frac{(i g_{BDq})^2}{E - M_B} \tag{268}$$

with

$$g_{BDq} \simeq \sqrt{\frac{1}{\Sigma_B'(E = M_B)}} \simeq \sqrt{\frac{1}{\frac{N_c c_2}{m_D^2} + \ldots}} \sim \sqrt{\frac{1}{\frac{1}{N_c}}} \sim N_c^{1/2} \,, \tag{269}$$

thus the baryon coupling to its generalized diquark D and quark q increases as $N_c^{1/2}$.

From these scaling laws, one can determine all the others. The quarkonium–baryon coupling goes as (see Fig. 43 as well as Ref. [118])

$$g_{\bar{B}BQ} \sim N_c^{1/2} \,. \tag{270}$$

The scaling is the same for any number of $\bar{B}B$ pairs.

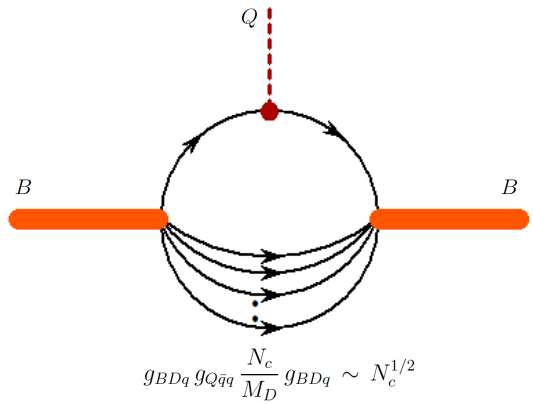

Fig. 43. Vertex of two baryons B (brown thick lines) and one conventional meson Q (red dashed line). The amplitude that corresponds to the generic meson–baryon–baryon coupling scales with $N_c^{1/2}$.

By increasing the number of quarkonia to n_Q, we find (see Fig. 44 for two examples) that the generic amplitude

$$A_{(\bar{B}B\bar{B}B\cdots)(n_Q Q)} \sim \frac{N_c}{N_c^{n_Q/2}} \,. \tag{271}$$

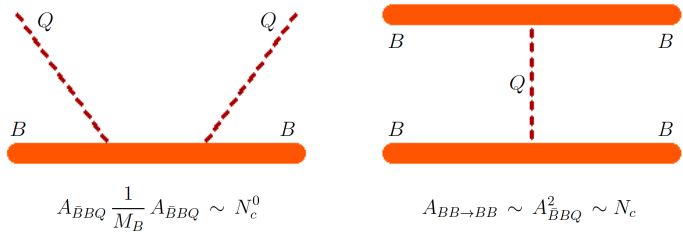

Fig. 44. Left: baryon–meson scattering, which goes with N_c^0 (note, the intermediate baryon gives a N_c^{-1} contribution). Right: baryon–baryon scattering that scales as N_c. Baryons are brown thick lines, quarkonia are red dashed lines.

The coupling to a single glueball goes as (see Fig. 45)

$$g_{\bar{B}BG} \sim N_c^0\,, \tag{272}$$

and then the one to n_G glueballs as

$$A_{(\bar{B}B\bar{B}B\cdots)(n_G G)} \sim \frac{N_c}{N_c^{n_G}}\,. \tag{273}$$

The coupling to hybrid meson is identical to quark–antiquark ones

$$g_{\bar{B}BH} \sim N_c^{1/2}\,, \tag{274}$$

$$A_{(\bar{B}B\bar{B}B\cdots)(n_H H)} \sim \frac{N_c}{N_c^{n_H/2}}\,. \tag{275}$$

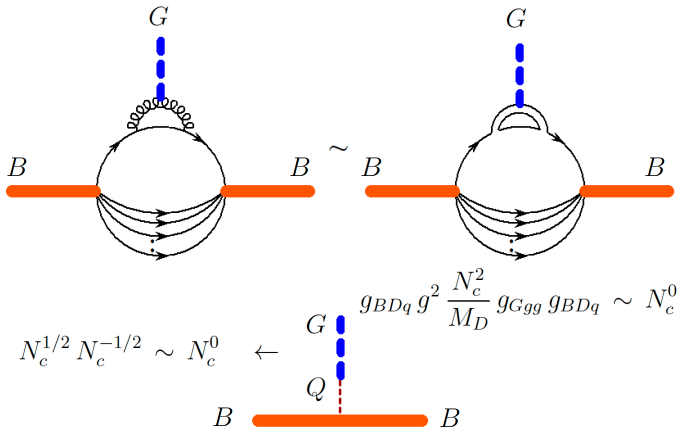

Fig. 45. Coupling of a baryon (brown thick lines) to a glueball (blue thick dashed line). This is shown both at the level of intermediate quarks and gluons (upper left) and color double-line notation (upper right). This interaction scales with N_c^0. At the bottom, the very same result can be obtained by coupling the baryon to a quarkonium Q (red dashed line) and subsequently Q to G.

The final coupling of an arbitrary number of baryon–antibaryon pairs to n_Q quarkonia, n_G glueballs, and n_H hybrid mesons is

$$A_{(\bar{B}B\bar{B}B\cdots)(n_Q Q)(n_G G)(n_H H)} \sim \frac{N_c}{N_c^{n_Q/2} N_c^{n_G} N_c^{n_H/2}} \,. \tag{276}$$

What about the scattering of baryons? Following the same 'visual' approach (Fig. 44), the amplitude for the process $BB \to BB$ goes as

$$A_{BB\to BB} \sim N_c \,. \tag{277}$$

Indeed, it does not change for any arbitrary number of baryons, provided that the initial number of baryons is equal to the final one (baryon number conservation). In turn, it is equal to the amplitude with n_B baryons and n_B antibaryons, and can be formally recovered from the previous case of Eq. (276) upon setting $n_Q = n_G = n_H = 0$.

How to implement baryons in a chiral model? In line with previous simplified treatments, we consider a single flavor (and disregard the chiral anomaly). We introduce a nucleon field Ψ_1, which is as usual split into right-handed and left-handed parts as

$$\Psi_{1,\mathrm{R}} = \frac{1+\gamma^5}{2}\Psi_1 \,, \qquad \Psi_{1,\mathrm{L}} = \frac{1-\gamma^5}{2}\Psi_1 \,. \tag{278}$$

A chiral transformation at the level of the nucleon amounts to

$$\Psi_{1,\mathrm{R}} \to \mathrm{e}^{i\alpha/2}\Psi_{1,\mathrm{R}} \,, \qquad \Psi_{1,\mathrm{L}} \to \mathrm{e}^{-i\alpha/2}\Psi_{1,\mathrm{L}} \,, \tag{279}$$

where the right and left pieces transform with a different sign of the phase (for equal sign, one has a simple U(1) baryon-number transformation). Due to this chiral transformation, a mass term of the type

$$\bar{\Psi}_1\Psi_1 = \bar{\Psi}_{1,\mathrm{R}}\Psi_{1,\mathrm{L}} + \bar{\Psi}_{1,\mathrm{L}}\Psi_{1,\mathrm{R}} \tag{280}$$

is *not* chirally-invariant! Thus, it seems that the nucleon needs to be — at first — massless.

As indeed well known, one can generate a massive nucleon by fulfilling chiral symmetry upon coupling the nucleon field to the mesonic field Φ, which transforms as $\Phi \to \mathrm{e}^{i\alpha}\Phi$. Then, an invariant term that generates a mass (via SSB) is obtained as (*e.g.* [119])

$$\mathcal{L}_{\Psi_1\Phi} = -g_{\Psi_1\Phi}\left(\bar{\Psi}_{1,\mathrm{R}}\Phi\Psi_{1,\mathrm{L}} + \bar{\Psi}_{1,\mathrm{L}}\Phi^\dagger\Psi_{1,\mathrm{R}}\right) \,, \tag{281}$$

where

$$g_{\Psi_1\Phi} \sim N_c^{1/2} \,. \tag{282}$$

When Φ condenses via SSB to $\phi_N \sim N_c^{1/2}$, a nucleon mass proportional to the chiral condensate ϕ_N is generated as

$$M_N \sim g_{\Psi_1 \Phi} \phi_N \sim N_c^{1/2}\, N_c^{1/2} \sim N_c \tag{283}$$

with the expected large-N_c behavior, see Fig. 46 for a pictorial representation of this result.

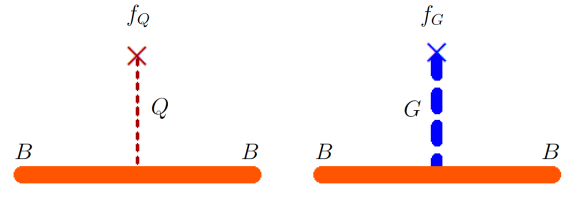

Fig. 46. Contribution to the mass of the baryon emerging from its interaction to a scalar quarkonium field Q and to a scalar glueball G. One obtains that, in both cases, when the scalar quarkonium field condenses or the scalar glueball field (the dilaton) condenses, the mass of the baryon scales with N_c, as expected. These results are implemented in the context of chiral models for the nucleon: the left one corresponds to the standard LSM, the second one to the so-called mirror assignment (see the text).

Note, the mesonic loop mass correction contributes with N_c^0 to the nucleon mass and is thus suppressed, as shown in Fig. 47. The 'bulk' mass dominates the formation of the nucleon mass.

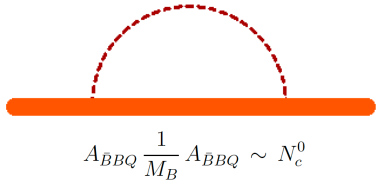

Fig. 47. The contribution to the mass of a baryon generated by a meson emission and absorption is suppressed in the large-N_c limit.

If the only mass term is the one of Eq. (283), it means that the nucleon mass disappears when the chiral condensate vanishes (as *e.g.* in a confined but chirally restored phase of matter, see the next section).

Interestingly, there is a second chiral way to give mass to the nucleon. To this end, a second nucleon field (the chiral partner of the nucleon, with opposite parity w.r.t. the bare nucleon field Ψ_1) is considered, see, for example, [120–126] and references therein. We consider its chiral transformation

as being mirror-like

$$\Psi_{2,\mathrm{R}} \to \mathrm{e}^{-i\alpha/2}\Psi_{2,\mathrm{R}}\,, \qquad \Psi_{2,\mathrm{L}} \to \mathrm{e}^{i\alpha/2}\Psi_{2,\mathrm{L}}\,. \tag{284}$$

Besides a standard interaction

$$\mathcal{L}_{\Psi_2\Phi} = g_{\Psi_2\Phi}\left(\bar{\Psi}_{2,\mathrm{R}}\Phi^\dagger\Psi_{2,\mathrm{L}} + \bar{\Psi}_{2,\mathrm{L}}\Phi\Psi_{2,\mathrm{R}}\right)\,, \tag{285}$$

an invariant mass term is obtained as [123, 125]

$$\begin{aligned}\mathcal{L}_{\mathrm{mirror,mass}} &= -c_N G\left(\bar{\Psi}_{1,\mathrm{L}}\Psi_{2,\mathrm{R}} - \bar{\Psi}_{1,\mathrm{R}}\Psi_{2,\mathrm{L}} - \bar{\Psi}_{2,\mathrm{L}}\Psi_{1,\mathrm{R}} - \bar{\Psi}_{2,\mathrm{R}}\Psi_{1,\mathrm{L}}\right)\\ &= -c_N G\left(\bar{\Psi}_1\gamma^5\Psi_2 - \bar{\Psi}_2\gamma^5\Psi_1\right)\,,\end{aligned} \tag{286}$$

where $c_N \sim N_c^0$ is a dimensionless constant independent of N_c and G is, as usual, the dilaton/scalar glueball field. Hence, a chirally-invariant mass terms

$$m_{N,0} = c_N G_0 \simeq c\Lambda_{\mathrm{QCD}} \sim N_c \tag{287}$$

emerge with the correct scaling, see Fig. 46.

The mass of the nucleon and its chiral partners are obtained by properly diagonalizing the system, finding

$$\begin{pmatrix} N \\ N^* \end{pmatrix} = \frac{1}{\sqrt{2\cosh\delta}}\begin{pmatrix} \mathrm{e}^{\delta/2} & \gamma^5\mathrm{e}^{-\delta/2} \\ \gamma^5\mathrm{e}^{-\delta/2} & \mathrm{e}^{\delta/2} \end{pmatrix}\begin{pmatrix} \Psi_1 \\ \Psi_2 \end{pmatrix} \tag{288}$$

with

$$M_{N,N^*} = \sqrt{m_{N,0}^2 + \frac{1}{4}\left(g_{\Psi_1\Phi} + g_{\Psi_2\Phi}\right)^2\phi_N^2} \pm \frac{1}{2}\left(g_{\Psi_1\Phi} - g_{\Psi_2\Phi}\right)\phi_N \sim N_c \tag{289}$$

and

$$\cosh\delta = \frac{M_N + M_{N^*}}{2m_{N,0}} \sim N_c^0\,. \tag{290}$$

Note, for $m_{N,0} = 0$, one has $M_N = g_{\Psi_1\Phi}\phi_N$ and $M_{N^*} = g_{\Psi_2\Phi}\phi_N$, as expected. On the other hand, if $\phi_N = 0$, the chiral partners are degenerate with $M_N = M_{N^*} = m_{N,0}$.

There is another interesting aspect of chiral models that regards the axial coupling constant of the nucleon. In the model above, for $m_{N,0} = 0$, the axial coupling constant turns out to be one, $g_{\mathrm{A}}^N = 1$. If $m_{N,0}$ is nonzero, the mixing sets in with

$$g_{\mathrm{A}}^N = \frac{1}{2\cosh\delta}\left(\mathrm{e}^{\delta/2} - \mathrm{e}^{-\delta/2}\right) \sim N_c^0\,. \tag{291}$$

Yet, the Skyrme model predicts $g_{\mathrm{A}}^N \sim N_c$ [38]. How to reconcile these different results?

The key is to consider vector and axial-vector mesons. We introduce

$$R^\mu = \rho^\mu - a_1^\mu \,, \qquad L^\mu = \rho^\mu + a_1^\mu \tag{292}$$

(recall that we are in the one-flavor case, so we could have as well used ω^μ and f_1^μ instead), which under a chiral transformation are separately invariant: $R^\mu \to R^\mu$, $L^\mu \to L^\mu$. However, under parity: $R^\mu \Leftrightarrow L^\mu$. Hence, the chirally- and parity-invariant coupling to (axial-)vector states is

$$\begin{aligned} \mathcal{L}_{(\text{axial}-)\text{vector}} \;=\; & c_{\Psi_1} R_\mu \bar{\Psi}_{1,\mathrm{R}} \gamma^\mu \Psi_{1,\mathrm{R}} + c_{\Psi_1} L_\mu \bar{\Psi}_{1,\mathrm{L}} \gamma^\mu \Psi_{1,\mathrm{L}} \\ & + c_{\Psi_2} R_\mu \bar{\Psi}_{2,\mathrm{R}} \gamma^\mu \Psi_{2,\mathrm{R}} + c_{\Psi_2} L_\mu \bar{\Psi}_{2,\mathrm{L}} \gamma^\mu \Psi_{2,\mathrm{L}} \,, \end{aligned} \tag{293}$$

where

$$c_{\Psi_1} \sim N_c^{1/2} \,, \qquad c_{\Psi 2} \sim N_c^{1/2} \,. \tag{294}$$

The exact calculation of the axial coupling constants goes beyond the scope of these lectures, since it involves subtle issues, such as the mixing of the a_1 and π occurring in chiral models with (axial-)vector mesons [23, 28, 67–69]. Yet, we can provide the final results of this calculation. The previous expression for the axial coupling g_A is modified into

$$g_\mathrm{A}^N = \frac{1}{2\cosh\delta} \left(g_\mathrm{A}^{(1)} \mathrm{e}^{\delta/2} + g_\mathrm{A}^{(2)} \mathrm{e}^{-\delta/2} \right) \tag{295}$$

with

$$g_\mathrm{A}^{(1)} = 1 - \frac{c_{\Psi_1}}{g_1} \left(1 - \frac{1}{Z^2} \right) \,, \qquad g_\mathrm{A}^{(2)} = -1 + \frac{c_{\Psi_2}}{g_1} \left(1 - \frac{1}{Z^2} \right) \,, \tag{296}$$

where $g_1 \sim N_c^{-1/2}$ is the coupling of one vector meson to two pseudoscalar ones (hence a standard QQQ vertex that scales as $N_c^{-1/2}$), and

$$Z = \left(1 - \frac{g_1^2 \phi_N^2}{M_{a_1}^2} \right)^{-1/2} \sim N_c^0 \tag{297}$$

is a constant that appears when dealing with the mixing between the pion and the a_1 meson [23, 28, 67–69]. It then follows that:

$$g_\mathrm{A}^{(1)} \sim N_c \quad \text{and} \quad g_\mathrm{A}^{(2)} \sim N_c \tag{298}$$

thus

$$g_\mathrm{A}^N \sim N_c \,, \tag{299}$$

in agreement with the Skyrme approach. This result implies that, in the present case, one cannot neglect axial-vector mesons, otherwise basic large-N_c properties might be lost.

5. Brief description of QCD at nonzero temperature and densities at large N_c

The QCD phase diagram at large N_c is a rich topic that would deserve a series of lectures on its own. Here, we present a summary of some basic facts and some interesting recent developments.

As shown in [35], when N_c is large, gluons dominate: a first-order phase transition between the deconfined and confined phases at $T_{\rm dec} \simeq 300 \propto N_c^0$ MeV (see [79] for a compilation of results) is expected for any value of the chemical potential. This is utterly different from the QCD phase diagram for $N_c = 3$ [3], which is cross-over along the T direction and first order along the μ one.

In the following, we first concentrate on the main expected properties of confinement/deconfinement phase transition for varying N_c and then on four snapshots concerning large-N_c properties in the medium.

Since it is relevant to our purposes, we write down the vacuum contribution of the dilaton-LSM confined matter, see Section 3.1 (consequence 3) and Section 3.2 (consequence 1)

$$\begin{aligned} V_{\rm vac} &= V(G = G_0, \sigma = \sigma_0 = \phi_N, 0) \\ &= \frac{1}{4}\lambda_G G_0^4 \left[\ln\left(\frac{G_0}{\Lambda_G}\right) - \frac{1}{4}\right] + \frac{a}{2}G_0^2\sigma_0^2 + \frac{\lambda}{4}\sigma_0^4\,, \end{aligned} \tag{300}$$

with

$$G_0 = \Lambda_G\, {\rm e}^{\frac{a^2}{\lambda\lambda_G}} \sim N_c\,, \qquad \sigma_0^2 = -\frac{aG_0^2}{\lambda} \sim N_c\,. \tag{301}$$

Hence,

$$V_{\rm vac} = V_{G,{\rm vac}} + V_{\sigma,{\rm vac}}\,, \tag{302}$$

with

$$V_{G,{\rm vac}} = \frac{1}{4}\lambda_G\Lambda_G^4\, {\rm e}^{\frac{4a^2}{\lambda\lambda_G}} \left[\frac{a^2}{\lambda\lambda_G} - \frac{1}{4}\right] \sim N_c^2\left[N_c^{-1} - \frac{1}{4}\right] \sim -N_c^2 < 0\,, \tag{303}$$

and

$$V_{\sigma,{\rm vac}} = \frac{a}{2}G_0^2\sigma_0^2 + \frac{\lambda}{4}\sigma_0^4 = -\frac{a^2}{4\lambda}G_0^4 \sim -N_c < 0\,. \tag{304}$$

We may then express the QCD vacuum pressure as a function of N_c by two terms

$$P_{\rm QCD,vac} = P_{G,{\rm vac}} + P_{\sigma,{\rm vac}} \tag{305}$$

with

$$P_{G,{\rm vac}} \simeq \bar{B}_G N_c^2 > 0\,, \qquad P_{\sigma,{\rm vac}} \simeq \bar{B}_\sigma N_c > 0\,. \tag{306}$$

Now, strictly speaking, this pressure should be added (as a positive term) to the confined phase, as it is derived from a confined model of QCD. We however follow the usual convention of subtracting this term from the QCD vacuum, thus at zero temperature and density, the pressure of the confined phase vanishes. One has then to subtract this term from the corresponding quark–gluon plasma (QGP) phase.

Hence, the (schematic and simplified) pressure of the QGP can be expressed as [127]

$$\begin{aligned} P_{\rm QGP}(T) &= 2N_c^2\frac{\pi^2}{90}T^4 + \frac{7}{4}N_cN_f\frac{\pi^2}{90}T^4 - P_{G,\rm vac} \\ &= 2N_c^2\frac{\pi^2}{90}T^4 + \frac{7}{4}N_cN_f\frac{\pi^2}{90}T^4 - \bar{B}_GN_c^2 - \bar{B}_\sigma N_c\,, \end{aligned} \tag{307}$$

where it is visible that gluons dominate for N_c large enough. The pressure for the confined phase (referred to as Hadron Resonance Gas (HRG) [3]) reads

$$P_{\rm HRG}(T) = \sum_n P_n(T)\,, \tag{308}$$

with

$$P_n(T) = -T\varsigma_n\int_k \ln\left[1-\exp\left[-\frac{\sqrt{k^2+M_n^2}}{T}\right]\right] \text{ if } n \text{ is a meson}\,, \tag{309}$$

$$P_n(T) = T\varsigma_n\int_k \ln\left[1+\exp\left[-\frac{\sqrt{k^2+M_n^2}}{T}\right]\right] \text{ if } n \text{ is a baryon}\,, \tag{310}$$

where ς_n is the appropriate degeneracy factor and M_n is the mass of the $n^{\rm th}$ hadron. Clearly, mesons dominate at large N_c since baryons are very heavy in this limit. Hence,

$$P_{\rm HRG}(T) \simeq P_{\rm HRG}^{\rm mesons}(T) \sim N_c^0\,. \tag{311}$$

Note,

$$P_{\rm HRG}(T=0) = 0 \tag{312}$$

in agreement with the adopted normalization.

The confinement/deconfinement phase transition takes place for $T = T_{\rm dec}$ given by (see Fig. 48)

$$P_{\rm HRG}(T_{\rm dec}) = P_{\rm QGP}(T_{\rm dec})\,. \tag{313}$$

It is easy to understand that this is the case for

$$T_{\rm dec} \sim N_c^0\,. \tag{314}$$

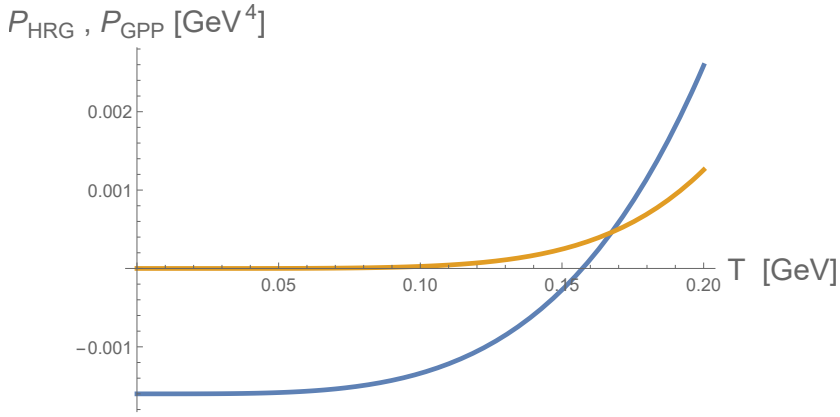

Fig. 48. Schematic representation of the pressure in the confined and deconfined phases. In the confined one, the pressure $P_{\rm HRG}$ (Eq. (308), yellow line, the upper one for low T) of the hadron resonance gas scales as N_c^0 and vanishes at $T = 0$. Then, the quark–gluon pressure $P_{\rm QGP}$ (Eq. (307), blue line, the lower one for low T) contains the free parts of quarks and gluons that scale as N_c and N_c^2, respectively, as well as the vacuum part that has two similar terms, but with opposite signs. Thus, in order the QGP to be realized, the QGP pressure needs first to become positive: this occurs for a temperature of the order of N_c^0. Shortly after, the QGP pressure overcomes the HRG one, realizing deconfinement.

Namely, at large N_c, the gluons dominate and the transition takes place basically just after the QGP pressure comes positive

$$T_{\rm dec} \gtrsim \frac{\bar{B}_G}{2\frac{\pi^2}{90}} \sim N_c^0 \,. \tag{315}$$

Note, the present simple treatment is not able to correctly guess the order of the transition, which is by construction a first-order, but in reality, it is known to be a cross-over [3].

Moreover, it is also expected that the phase transition for chiral restoration takes place for a similar temperature as the deconfined one, as supported by models, *e.g.* [3, 57, 128].

Next, let us consider zero temperature and finite density. To this end, we introduce the quark chemical potential μ_q and the baryon chemical potential $\mu_B = N_c\mu_q$. In the confined phase, one has only baryons. We follow here one possible choice described in Ref. [42] that corresponds to a confined stiff matter with the speed of sound equal to the speed of light. Intuitively, it corresponds to an interaction-dominated gas. In this case, the pressure in

the baryonic phase is (for large values of the baryonic chemical potential)

$$P_B = a_B \mu_B^2 \,, \tag{316}$$

where a_B is a constant with dimension energy^2, whose N_c dependence must be established[2].

The baryon density follows as

$$n_B = \frac{\mathrm{d}P_B}{\mathrm{d}\mu_B} = 2 a_B \mu_B \,, \tag{317}$$

while the energy density as

$$\varepsilon_B = n_B P_B - P_B = P_B \,, \tag{318}$$

hence the speed of sound is

$$v_B = \sqrt{\mathrm{d}P_B/\mathrm{d}\varepsilon_B} = 1 \,. \tag{319}$$

This result is indeed in agreement with the high-density limit of nuclear matter described in Ref. [129], which takes place when vector-meson-driven interaction dominates. Within, since a_B has energy^2 and since the appropriate dimension is constructed by $m_V^2/g_{\bar{B}BV}^2$ with $g_{\bar{B}BV} \sim N_c^{1/2}$ being the baryon–baryon–vector coupling and m_V the mass of the vector meson (such as the ω meson), one gets

$$a_B \sim \frac{m_V^2}{g_{\bar{B}BV}^2} \sim N_c^{-1} \to a_B = \frac{\bar{a}_B}{N_c} \,. \tag{320}$$

In fact, the pressure as a function of the density can be written as

$$P_B = \frac{n_B^2}{4 a_B} \simeq \frac{1}{2} \frac{g_{\bar{B}BV}^2}{m_V^2} n_B^2 \,, \tag{321}$$

where the right-hand side follows from Section 4.11 of Ref. [129] (high-density limit). It thus shows the direct proportionality of a_B to $m_V^2/g_{\bar{B}BV}^2$.

Finally, in terms of the quark chemical potential, we may write the baryonic pressure

$$P_B(\mu_q) = N_c \bar{a}_B \mu_q^2 \tag{322}$$

implying that we have a confined phase whose pressure scales with N_c. This is in agreement with the quarkyonic phase discussed in Refs. [35, 36, 40], and also with the result of the Walecka-type model at large N_c and for high densities, see Ref. [4].

[2] In a more realistic treatment, one may consider at high density $P_B = a_B \mu_B^\alpha - K$ (with α a free parameter) which needs to be matched to the known equation of state of nuclear matter at about $2n_0$ [42]. The large-N_c behavior is not affected.

Next, let us consider the QGP phase, which contains only quarks as d.o.f. (gluons are not present at $T = 0$) as well as the already discussed vacuum contribution

$$P_{\rm QGP}(\mu_q) = P_q(\mu_q) = \frac{N_c N_f}{12\pi^2}\mu_q^4 + P_{\rm QCD,vac} = \frac{N_c N_f}{12\pi^2}\mu_q^4 - \bar{B}_G N_c^2 - \bar{B}_G N_c \,. \tag{323}$$

The deconfinement phase transition takes place for $P_B(\mu_{q,\rm dec}) = P_q(\mu_{q,\rm dec})$, leading to

$$\mu_{q,\rm dec} \sim N_c^{1/4} \,, \tag{324}$$

thus the deconfinement phase transition takes place at higher and higher densities when N_c increases. Here, one expects a different behavior of the chiral phase transition, which should take place for $\mu_{q,c} \sim N_c^0$. There is therefore a wide range of μ_q for which matter is chirally-restored but confined, the already mentioned quarkyonic phase [35, 36] (see also the large-N_c considerations of [130, 131]).

Additional topics related to large N_c in the medium are briefly discussed below.

1. Chiral mesonic models at nonzero T: a problem and how to cure it

If a purely mesonic model as the one of Eq. (136) is considered, chiral restoration can be studied by evaluating the chiral condensate as a function of the temperature, $\phi_N \to \phi_N(T)$. For large T, $\phi_N(T)$ tends to zero and the way it does also specifies the order of the chiral phase transition. For $N_c = 3$, one expects a smooth cross-over [3, 128, 132].

What about the behavior of the chiral phase transition at large N_c? One indeed expects that the critical temperature for chiral restoration, denoted as $T_{\rm c}$, should be N_c-independent

$$T_{\rm c} \sim T_{\rm dec} \sim \Lambda_{\rm QCD} \sim N_c^0 \,. \tag{325}$$

Yet, in purely mesonic models, the contribution of the interaction to the effective potential (or equivalently to the pressure) scales as $1/N_c$ and is therefore suppressed. Correspondingly, one finds [39]

$$T_c \sim f_\pi \sim N_c^{1/2} \,, \tag{326}$$

hence chiral restoration takes place at larger and larger N_c. This result is depicted in Fig. 49 (left), in which the vacuum diagrams give rise to the contribution for the pressure, see Ref. [128] and references therein. It seems therefore that such models cannot describe the expected large-N_c results.

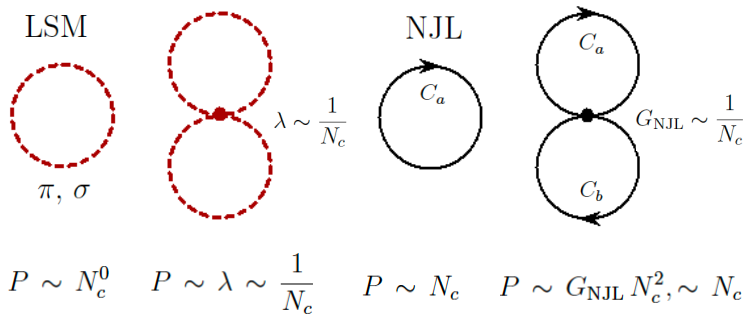

Fig. 49. Vacuum diagrams can be used to establish the scaling of different contribution to the pressure. Left: in the LSM, the pressure of free mesons goes with N_c^0, while the interaction contribution goes as N_c^{-1}. This is why in the large-N_c limit chiral restoration takes place at higher and higher T. Right: in the NJL model, the free quarks give rise to a pressure proportional to N_c, just as the interaction terms. Accordingly, the critical temperature for chiral restoration is N_c-independent, as it should.

How to reconcile chiral models with the expected large-N_c scaling? In Ref. [39], some recipes were put forward. An intuitive heuristic approach consists in considering the following potential with an explicit dependence on the temperature T:

$$\begin{aligned} V(\sigma,\pi) &= \frac{m_0^2}{2}\left(1-\frac{T^2}{T_0^2}\right)\Phi^*\Phi + \frac{\lambda}{4}\left(\Phi^*\Phi\right)^2 \\ &= \frac{m_0^2}{2}\left(1-\frac{T^2}{T_0^2}\right)\left(\sigma^2+\pi^2\right) + \frac{\lambda}{4}\left(\sigma^2+\pi^2\right)^2 , \end{aligned} \tag{327}$$

where $T_0 \sim \Lambda_{\rm QCD} \sim N_c^0$. In this way, the chiral restoration is enforced by this modification. At $T = T_0$, the bare potential is such that only the quartic interaction is present. With this *ad hoc* modification, $T_{\rm c} \sim N_c^0$ is obtained.

A more formal way of achieving this result is realized by coupling the chiral multiplet Φ to the expectation value of the Polyakov loop (see, *e.g.*, [3, 48]). This quantity, denoted as $l(T)$, describes effectively the gluonic sector, more specifically the restoration of the symmetry under $Z(N_c)$ transformations in the vacuum. In particular, $|l(T)| = 1$ at large temperature (in the deconfined phase), while it vanishes at small T. One can couple the Polyakov loop to the LSM in the following way:

$$V(\sigma,\pi,l) = \frac{m_0^2}{2}\left(1-c_l T^2\left|l(T)\right|^2\right)\Phi^*\Phi + \frac{\lambda}{4}\left(\Phi^*\Phi\right)^2 , \tag{328}$$

where $c_l \sim N_c^0$ is a dimensionless constant. Indeed, the proper description of the Polyakov loop at large N_c is not an easy task, but certain relatively simple choices are possible [24, 48]. Within the LSMs with Polyakov loop, the critical temperature for chiral restoration scales as $T_c \propto N_c^0$, as expected.

The already mentioned famous NJL model [13, 14] contains only quarks with a chiral interaction of the type

$$V_{\rm NJL}(\sigma,\pi,l) = G_{\rm NJL}\left[\left(\bar{\psi}\psi\right)^2 + \left(\bar{\psi}i\gamma^5\psi\right)^2\right] , \tag{329}$$

where the chiral transformation (in this one-flavor case) is $\psi \to {\rm e}^{i\alpha\gamma^5/2}\psi$, and where $G_{\rm NJL} \sim N_c^{-1}$ (this is just as the constant K_Q studied in the case of the quarkonium formation in Sec. 3.1; indeed, the NJL model has been widely used to study $\bar{q}q$ bound states [14, 15]). Here, the interaction type is of the same order of the free quark ones. The SSB takes place if $G_{\rm NJL}$ is large enough and chiral restoration takes place at nonzero T, with $T_c \sim N_c^0$, see Fig. 49 (right).

The last case that we mention is the one that involves the quark-meson type model [24, 57, 58], in which both mesons and quarks are present

$$V_{\rm LSM,quarks}(\sigma,\pi,l) = g_\sigma\sigma\left(\bar{\psi}\psi\right) + g_\pi\pi\left(\bar{\psi}i\gamma^5\psi\right) . \tag{330}$$

In this case, the interaction contribution to the pressure is also of the order of N_c just as the quarks, thus $T_c \sim N_c^0$, see Fig. 50.

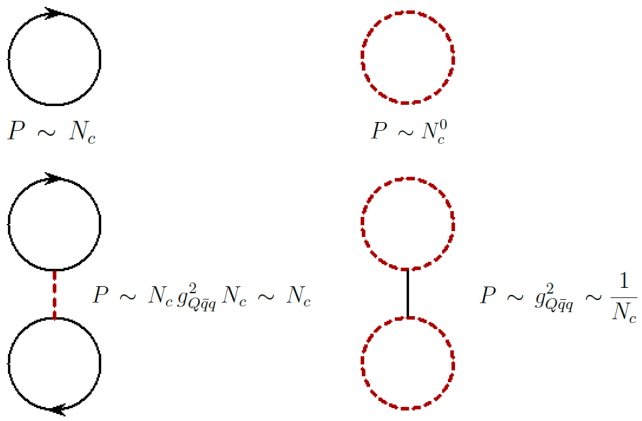

Fig. 50. Quark-level LSM. The free part contains two contributions for the pressure, the meson one (N_c^0) and the quark one (N_c). Two interaction terms are outlined: one with quark loops, whose pressure contribution goes as N_c (just as the free quark part) and one with mesonic loops, whose pressure contribution goes as N_c^{-1}. Quarks dominate in both cases, and the final outcome is similar to the NJL model: the critical temperature for chiral restoration scales as N_c^0.

2. Critical endpoint CEP at large N_c

It is well known that the confinement/deconfinement as well as the chiral phase transition(s) are of cross-over type along the T direction and first order along the μ_q one. At least one critical point is therefore expected, whose search is important for both theoretical and experimental investigations, *e.g.* [3, 57, 134, 135].

Yet, at large N_c, as shown in detail in [24] using an extended linear sigma model with quarks and Polyakov loop, the phase diagram turns out to be utterly different: one has a first-order transition along T and a cross-over one along μ_q. A critical point is present at about $(T_{\rm CEP}, \mu_{q,\rm CEP})$, where $T_{\rm CEP} \propto \Lambda_{\rm QCD} \sim N_c^0$, while $\mu_{q,\rm CEP}$ increases for increasing N_c). Quite remarkably, for intermediate N_c (from 4 up to about 50), only cross-over phases are present in the whole phase diagram [24].

The pressure at very large N_c resembles the expected behavior, in particular, we have the following areas, see Fig. 51 as well as the detailed explanations in Ref. [24]:

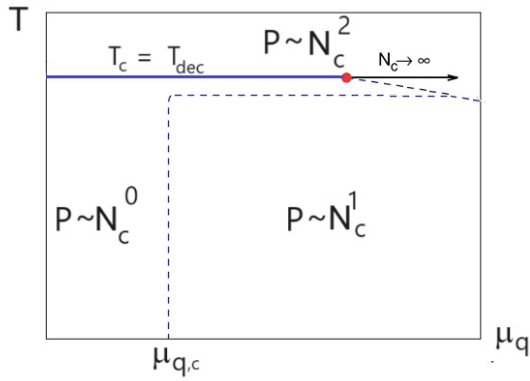

Fig. 51. Schematic and simplified representation of the QCD phase diagram for large N_c. For low T and μ, a confined and chirally broken (SSB) phase with pressure proportional to N_c^0 is present. If the temperature is above $T_{\rm c} = T_{\rm dec}$, for any chemical potential μ, a deconfined phase with pressure proportional to N_c^2 is realized. Here, chiral symmetry is also restored. For large μ but $T < T_{\rm dec} = T_{\rm c}$, the system is still confined but chiral symmetry is restored: the pressure is proportional to N_c (as a gas of quarks would have). Important aspects: the type of the chiral phase transition is a first-order one along T (solid line) and a cross-over along μ (dashed line). Along T, the chiral and the deconfinement transitions coincide. Along μ, they do not: the chiral one takes place for $\mu_{q,c} \sim N_c^0$, the deconfinement one moves toward infinity. The critical endpoint (red dot in the figure) also tends to infinity along the μ direction. For more details, see Ref. [24].

(i) $P \sim N_c^0$ for low T and low μ_q within the confined and chirally broken phase.

(ii) $P \sim N_c$ for low T and high μ_q within the confined and chirally restored (quarkyonic) phase. Note, in this phase, the nucleons do not need to be massless, see the discussion in Section 4.

(iii) $P \sim N_c^2$ for high T and high μ_q within the deconfined QGP phase.

Finally, along the T line and for small μ_q, the chiral and the deconfinement phase transitions coincide ($T_{\rm dec} = T_{\rm c}$), while along the μ_q line and for small T, the chiral transition occurs for $\mu_{q,c} \sim N_c^0$ and the deconfinement one for $\mu_{q,\rm dec}$ increasing N_c.

In the recent work of Ref. [133], the effect of the chiral anomaly on the phase diagram is discussed. Yet, anomaly terms decrease fast for increasing N_c, thus they shall not modify the overall large-N_c picture outlined above.

3. Nuclear matter at large N_c

Does nuclear matter bind at large N_c? This question was already posed in the introduction, and at first put aside since quite (too?) philosophical. Yet, is $N_c = 3$ somewhat special?

Indeed, the issue is quite subtle. In the easiest scenario, one considers a standard σ–ω model coupled to the nucleon

$$V = g_{\sigma N} \bar{\Psi}_1 \Psi_1 + g_{\omega N} \omega_\mu \bar{\Psi}_1 \gamma^\mu \Psi_1 \,, \tag{331}$$

with

$$g_{\sigma N} \sim N_c^{1/2} \quad \text{and} \quad g_{\omega N} \sim N_c^{1/2} \,, \tag{332}$$

where σ corresponds to $f_0(500)$ and ω to $\omega(782)$. If the masses of these fields behave as N_c^0 (as quark–antiquark regular states), then the mean-field equations show that nuclear matter forms for any N_c (and becomes more and more bound).

Yet, it is well known that $f_0(500)$ is *not* predominantly a $\bar{q}q$ [106]. Considering this fact, changes the picture completely: nuclear matter does not form, already for $N_c \geq 4$.

Indeed, for very large N_c, the pion cannot be neglected and being *de facto* massless should generate a kind of loosely bound nuclear matter similar to atomic matter (basically an attractive almost Coulomb force would act among nucleons in this limit). The detailed study of this hypothetical state of matter is a task for the future.

4. Neutron stars at large N_c

One may apply the previous discussion about baryonic and quark matter to neutron stars, see Ref. [42] for details.

Using the baryonic equation of state of Eq. (322) that corresponds to stiff matter (speed of sound equal 1), for $N_c = 3$, the maximal mass of a neutron star turns out to be about

$$M_{\rm NS}^{\rm max} \simeq 2.2 M_\odot \,. \tag{333}$$

Namely, for higher masses, a phase transition to the deconfined quark phase takes place inside the neutron star, which is however unstable because quark matter cannot sustain the gravitational pressure [136]. (The maximal value quoted above can be increased if the vacuum pressure is increased.)

When increasing N_c, the phase transition to quark matter takes place at higher and higher density. Already for $N_c \gtrsim 5.5$, quark matter plays no role, and the maximum mass of a neutron star is about $3M_\odot$.

6. Conclusions

In these lectures, we have revisited the main features of QCD at large N_c for both mesons and baryons. To this end, we have used a bound-state approach in which a simple separable Ansatz has been applied. This is indeed similar to certain approaches of QCD, such as the NJL model. Yet, the large-N_c scaling laws that can be derived are fully general and do not depend on this specific Ansatz. In this way, we could recover all the large-N_c scaling behavior for regular mesons, glueballs, and hybrid mesons. Also, their mutual interactions, decays, and mixing could be properly described.

Many consequences of these results have been investigated, among which the reason why certain mesons are narrow, how dominant and subdominant interaction terms arise, and most importantly, how chiral models behave in the large-N_c limit. Also, the behavior of the dilaton/scalar glueball field and its coupling to chiral models has been reviewed in some detail. An overall nice and consistent picture of large-N_c QCD has emerged.

Four-quark states were briefly discussed. Molecular states and dynamically generated states do not form in the large-N_c limit, as our bound-state approach easily shows. Yet, the case of tetraquark objects is more complicated. Our present results suggest that all of them share the same fate: they do not form in the large-N_c limit, but this last statement is not yet conclusive.

Baryons were presented following the same line applied to mesons, upon interpreting them as bound states of a generalized diquark built with $N_c - 1$ quarks and a quark. Upon taking the mass of the generalized diquark as

increasing with N_c, it was possible to recover the known large-N_c results for baryons. Chiral models have been studied for baryons as well: the chirally-invariant mass generation via the quark condensate and via the dilaton condensate (the latter in the so-called mirror assignment) fulfill the expected large-N_c properties.

Finally, we have discussed the main features of the phase diagram of QCD in the large-N_c domain. Simple scaling laws show that at large N_c, gluons dominate if the temperature is high enough. The temperature for confinement/deconfinement transition is N_c-independent, but the chemical potential increases for increasing N_c. This means that in the large-N_c limit, matter is confined below a certain $T_{\rm dec}$ and deconfined above, for any chemical potential. Yet, for high density, one may have a confined and chirally restored matter whose pressure is proportional to N_c, which well fits with the concept of a quarkyonic phase. These results also imply that the phase diagram at large N_c looks quite different than the one for the real $N_c = 3$ world.

Moreover, we have also discussed some related issues, such as the failure of certain chiral models at large N_c and how to improve them, the formation (or non-formation) of nuclear matter, and implications for neutron stars.

In conclusion, large-N_c QCD is an interesting theoretical framework, often the only one available, to understand certain properties of QCD. It offers a consistent picture, somewhat simplified from our physical one, but definitely not trivial.

Coming back to our original question: is $N_c = 3$ large? We have shown that in most cases it is, but not in all of them. There is therefore not a simple and always valid answer to that seemingly naive question but one needs, case by case, to study the consequences of increasing N_c and see how much the outcomes depart from the real world. Yet, in many cases, the lesson gained from large N_c is very useful for understanding our world with $N_c = 3$.

The author thanks A. Pilloni, G. Pagliara, Gy. Kovacs, P. Kovacs, C. Fischer, R. Pisarski, G. Torrieri, L. Bonanno, S. Jafarzade, E. Trotti, J. Peláez, L. McLerran, D. Rischke, A. Koenigstein, and V. Shastry for very useful discussions that extended over the last 15 years. The author also acknowledges useful remarks to the first version of these lectures by M. Praszałowicz, J.M. Gerard, and S. Leupold. *Acta Phys. Pol. B* is thanked for help in preparing a new version of the figures. Financial support from the National Science Centre (NCN), Poland via the OPUS project 2019/33/B/ST2/00613 is acknowledged.

REFERENCES

[1] Particle Data Group (R.L. Workman *et al.*), «Review of Particle Physics», *Prog. Theor. Exp. Phys.* **2022**, 083C01 (2022) and 2023 update.

[2] A.W. Thomas, W. Weise, «The Structure of the Nucleon», *Wiley-VCH*, Berlin, Germany 2001, p. 389.

[3] C. Ratti, R. Bellwied, «The Deconfinement Transition of QCD: Theory Meets Experiment», *Lect. Notes Phys.* **981**, 1 (2021).

[4] L. Bonanno, F. Giacosa, «Does nuclear matter bind at large N_c?», *Nucl. Phys. A* **859**, 49 (2011), arXiv:1102.3367 [hep-ph].

[5] G. 't Hooft, «A planar diagram theory for strong interactions», *Nucl. Phys. B* **72**, 461 (1974).

[6] E. Witten, «Baryons in the 1/N expansion», *Nucl. Phys. B* **160**, 57 (1979).

[7] G. 't Hooft, «Large N», in: «Phenomenology of Large Nc QCD», *Proceedings from the Institute for Nuclear Theory*, World Scientific 2002, pp. 3–18.

[8] R.F. Lebed, «Phenomenology of Large N_c QCD», *Czech. J. Phys.* **49**, 1273 (1999), arXiv:nucl-th/9810080.

[9] S.R. Coleman, «1/N» in: «17$^{\text{th}}$ International School of Subnuclear Physics: Point-like Structures Inside and Outside Hadrons», Erice, Italy, 31 July–10 August 1979, SLAC-PUB-2484.

[10] B. Lucini, M. Panero, «Introductory lectures to large-N QCD phenomenology and lattice results», *Prog. Part. Nucl. Phys.* **75**, 1 (2014), arXiv:1309.3638 [hep-th].

[11] C. Bonanno, M. D'Elia, B. Lucini, D. Vadacchino, «Towards glueball masses of large-N SU(N) pure-gauge theories without topological freezing», *Phys. Lett. B* **833**, 137281 (2022), arXiv:2205.06190 [hep-lat].

[12] W. Lucha, D. Melikhov, H. Sazdjian, «Tetraquarks in large-N_c QCD», *Prog. Part. Nucl. Phys.* **120**, 103867 (2021), arXiv:2102.02542 [hep-ph].

[13] Y. Nambu, G. Jona-Lasinio, «Dynamical Model of Elementary Particles Based on an Analogy with Superconductivity. I.», *Phys. Rev.* **122**, 345 (1961).

[14] T. Hatsuda, T. Kunihiro, «QCD phenomenology based on a chiral effective Lagrangian», *Phys. Rep.* **247**, 221 (1994), arXiv:hep-ph/9401310; S.P. Klevansky, «The Nambu–Jona-Lasinio model of quantum chromodynamics», *Rev. Mod. Phys.* **64**, 649 (1992); U. Vogl, W. Weise, «The Nambu and Jona-Lasinio model: Its implications for Hadrons and Nuclei», *Prog. Part. Nucl. Phys.* **27**, 195 (1991).

[15] M.K. Volkov, A.E. Radzhabov, «The Nambu–Jona-Lasinio model and its development», *Phys. Usp.* **49**, 551 (2006), arXiv:hep-ph/0508263.

[16] S. Weinberg, «Evidence That the Deuteron Is Not an Elementary Particle», *Phys. Rev. B* **137**, 672 (1965).

[17] K. Hayashi *et al.*, «Compositeness Criteria of Particles in Quantum Field Theory and S-Matrix Theory», *Fortsch. Phys.* **15**, 625 (1967).

[18] F. Giacosa, T. Gutsche, A. Faessler, «A Covariant constituent quark/gluon model for the glueball–quarkonia content of scalar–isoscalar mesons», *Phys. Rev. C* **71**, 025202 (2005), arXiv:hep-ph/0408085.

[19] A. Faessler *et al.*, «Pion and sigma meson properties in a relativistic quark model», *Phys. Rev. D* **68**, 014011 (2003), arXiv:hep-ph/0304031.

[20] R. Alkofer, L. von Smekal, «The Infrared behavior of QCD Green's functions: Confinement dynamical symmetry breaking, and hadrons as relativistic bound states», *Phys. Rep.* **353**, 281 (2001), arXiv:hep-ph/0007355.

[21] C.S. Fischer, «Infrared properties of QCD from Dyson–Schwinger equations», *J. Phys. G: Nucl. Part. Phys.* **32**, R253 (2006), arXiv:hep-ph/0605173.

[22] G. Eichmann *et al.*, «Baryons as relativistic three-quark bound states», *Prog. Part. Nucl. Phys.* **91**, 1 (2016), arXiv:1606.09602 [hep-ph].

[23] D. Parganlija *et al.*, «Meson vacuum phenomenology in a three-flavor linear sigma model with (axial-)vector mesons», *Phys. Rev. D* **87**, 014011 (2013), arXiv:1208.0585 [hep-ph].

[24] P. Kovács, G. Kovács, F. Giacosa, «Fate of the critical endpoint at large N_c», *Phys. Rev. D* **106**, 116016 (2022), arXiv:2209.09568 [hep-ph].

[25] A.A. Migdal, M.A. Shifman, «Dilaton effective lagrangian in gluodynamics», *Phys. Lett. B* **114**, 445 (1982).

[26] A. Salomone, J. Schechter, T. Tudron, «Properties of scalar gluonium», *Phys. Rev. D* **23**, 1143 (1981).

[27] J.R. Ellis, J. Lanik, «Is scalar gluonium observable?», *Phys. Lett. B* **150**, 289 (1985).

[28] S. Janowski, F. Giacosa, D.H. Rischke, «Is $f_0(1710)$ a glueball?», *Phys. Rev. D* **90**, 114005 (2014), arXiv:1408.4921 [hep-ph].

[29] S. Weinberg, «Tetraquark Mesons in Large-N Quantum Chromodynamics», *Phys. Rev. Lett.* **110**, 261601 (2013), arXiv:1303.0342 [hep-ph].

[30] R.F. Lebed, «Large-N Structure of tetraquark mesons», *Phys. Rev. D* **88**, 057901 (2013), arXiv:1308.2657 [hep-ph].

[31] T.D. Cohen, R.F. Lebed, «Tetraquarks with exotic flavor quantum numbers at large N_c in QCD(AS)», *Phys. Rev. D* **89**, 054018 (2014), arXiv:1401.1815 [hep-ph].

[32] T.D. Cohen, R.F. Lebed, «Are there tetraquarks at large N_c in QCD(F)?», *Phys. Rev. D* **90**, 016001 (2014), arXiv:1403.8090 [hep-ph].

[33] T. Cohen, F.J. Llanes-Estrada, J.R. Peláez, J. Ruiz de Elvira, «Nonordinary light meson couplings and the $1/N_c$ expansion», *Phys. Rev. D* **90**, 036003 (2014), arXiv:1405.4831 [hep-ph].

[34] M. Knecht, S. Peris, «Narrow tetraquarks at large N», *Phys. Rev. D* **88**, 036016 (2013), arXiv:1307.1273 [hep-ph].

[35] L. McLerran, R.D. Pisarski, «Phases of cold, dense quarks at large N_c», *Nucl. Phys. A* **796**, 83 (2007), arXiv:0706.2191 [hep-ph].

[36] T. Kojo, Y. Hidaka, L. McLerran, R.D. Pisarski, «Quarkyonic chiral spirals», *Nucl. Phys. A* **843**, 37 (2010), arXiv:0912.3800 [hep-ph].

[37] L. McLerran, K. Redlich, C. Sasaki, «Quarkyonic matter and chiral symmetry breaking», *Nucl. Phys. A* **824**, 86 (2009), arXiv:0812.3585 [hep-ph].

[38] L. McLerran, «The Phase Diagram of QCD and Some Issues of Large N_c», *Nucl. Phys. B Proc. Suppl.* **195**, 275 (2009), arXiv:0906.2651 [hep-ph].

[39] A. Heinz, F. Giacosa, D.H. Rischke, «Restoration of chiral symmetry in the large-N_c limit», *Phys. Rev. D* **85**, 056005 (2012), arXiv:1110.1528 [hep-ph].

[40] Y. Hidaka, T. Kojo, L. McLerran, R.D. Pisarski, «The dichotomous nucleon: Some radical conjectures for the large-N_c limit», *Nucl. Phys. A* **852**, 155 (2011), arXiv:1004.2261 [hep-ph].

[41] L. McLerran, S. Reddy, «Quarkyonic Matter and Neutron Stars», *Phys. Rev. Lett.* **122**, 122701 (2019) arXiv:1811.12503 [nucl-th].

[42] F. Giacosa, G. Pagliara, «Neutron stars in the large-N_c limit», *Nucl. Phys. A* **968**, 366 (2017), arXiv:1707.02644 [nucl-th].

[43] F. Giacosa, «Mesons Beyond the Quark–Antiquark Picture», *Acta Phys. Pol. B* **47**, 7 (2016), arXiv:1511.04605 [hep-ph].

[44] Y. Chen *et al.*, «Glueball spectrum and matrix elements on anisotropic lattices», *Phys. Rev. D* **73**, 014516 (2006), arXiv:hep-lat/0510074.

[45] R.L. Jaffe, K. Johnson, Z. Ryzak, «Qualitative features of the glueball spectrum», *Ann. Phys.* **168**, 344 (1986).

[46] V. Mathieu, N. Kochelev, V. Vento, «The Physics of Glueballs», *Int. J. Mod. Phys. E* **18**, 1 (2009), arXiv:0810.4453 [hep-ph].

[47] A. Zee, «Group Theory in a Nutshell for Physicists», *Princeton University Press*, 2016.

[48] K. Fukushima, V. Skokov, «Polyakov loop modeling for hot QCD», *Prog. Part. Nucl. Phys.* **96**, 154 (2017), arXiv:1705.00718 [hep-ph].

[49] A. Deur, S.J. Brodsky, G.F. de Teramond, «The QCD running coupling», *Nucl. Phys.* **90**, 1 (2016), arXiv:1604.08082 [hep-ph].

[50] H. Gies, «Running coupling in Yang–Mills theory: A flow equation study», *Phys. Rev. D* **66**, 025006 (2002), arXiv:hep-th/0202207.

[51] S.R. Coleman, E. Witten, «Chiral-Symmetry Breakdown in Large N Chromodynamics», *Phys. Rev. Lett.* **45**, 100 (1980).

[52] E. Witten, «Current algebra theorems for the U(1) "Goldstone boson"», *Nucl. Phys. B* **156**, 269 (1979).

[53] J.F. Donoghue, «The gluon "mass" in the bag model», *Phys. Rev. D* **29**, 2559 (1984).

[54] D. Binosi, D. Ibanez, J. Papavassiliou, «The all-order equation of the effective gluon mass», *Phys. Rev. D* **86**, 085033 (2012), arXiv:1208.1451 [hep-ph]; S. Strauss, C.S. Fischer, C. Kellermann, «Analytic Structure of the Landau-Gauge Gluon Propagator», *Phys. Rev. Lett.* **109**, 252001 (2012), arXiv:1208.6239 [hep-ph].

[55] S. Godfrey, N. Isgur, «Mesons in a relativized quark model with chromodynamics», *Phys. Rev. D* **32**, 189 (1985). See also the summary on 'quark model' in Ref. [1].

[56] F. Giacosa, A. Koenigstein, R.D. Pisarski, «How the axial anomaly controls flavor mixing among mesons», *Phys. Rev. D* **97**, 091901 (2018), arXiv:1709.07454 [hep-ph].

[57] P. Kovács, Z. Szép, G. Wolf, «Existence of the critical endpoint in the vector meson extended linear sigma model», *Phys. Rev. D* **93**, 114014 (2016), arXiv:1601.05291 [hep-ph].

[58] R.A. Tripolt, N. Strodthoff, L. von Smekal, J. Wambach, «Spectral functions for the quark-meson model phase diagram from the functional renormalization group», *Phys. Rev. D* **89**, 034010 (2014), arXiv:1311.0630 [hep-ph].

[59] H.J. Lipkin, «The OZI rule in charmonium decays above $D\bar{D}$ threshold», *Phys. Lett. B* **179**, 278 (1986).

[60] M.K. Volkov, A.A. Osipov, A.A. Pivovarov, K. Nurlan, «$1/N_c$ approximation and universality of vector mesons», *Phys. Rev. D* **104**, 034021 (2021), arXiv:2105.02160 [hep-ph].

[61] J.M. Gérard, T. Lahna, «The asymptotic behavior of the $\pi^0\gamma^*\gamma^*$ vertex», *Phys. Lett. B* **356**, 381 (1995), arXiv:hep-ph/9506255.

[62] O. Bar, U.J. Wiese, «Can one see the number of colors?», *Nucl. Phys. B* **609**, 225 (2001), arXiv:hep-ph/0105258.

[63] P. Bickert, S. Scherer, «$\eta^{(\prime)} \to \pi^+\pi^-\gamma^{(*)}$ in large-N_c chiral perturbation theory», *Phys. Rev. D* **104**, 074021 (2021), arXiv:2106.12482 [hep-ph].

[64] F. Giacosa, G. Pagliara, «Spectral functions of scalar mesons», *Phys. Rev. C* **76**, 065204 (2007), arXiv:0707.3594 [hep-ph].

[65] F. Giacosa, A. Okopińska, V. Shastry, «A simple alternative to the relativistic Breit–Wigner distribution», *Eur. Phys. J. A* **57**, 336 (2021), arXiv:2106.03749 [hep-ph].

[66] F. Giacosa, «Multichannel decay law», *Phys. Lett. B* **831**, 137200 (2022), arXiv:2108.07838 [quant-ph].

[67] P. Ko, S. Rudaz, «Phenomenology of scalar and vector mesons in the linear σ model», *Phys. Rev. D* **50**, 6877 (1994); J.K. Kim, P. Ko, K.Y. Lee, S. Rudaz, «$a_1(1260)$ contribution to photon and dilepton productions from hot hadronic matter reexamined», *Phys. Rev. D* **53**, 4787 (1996), arXiv:hep-ph/9602293.

[68] M. Urban, M. Buballa, J. Wambach, «Vector and axial-vector correlators in a chirally symmetric model», *Nucl. Phys. A* **697**, 338 (2002), arXiv:hep-ph/0102260.

[69] D. Parganlija, F. Giacosa, D.H. Rischke, «Vacuum properties of mesons in a linear sigma model with vector mesons and global chiral invariance», *Phys. Rev. D* **82**, 054024 (2010), arXiv:1003.4934 [hep-ph].

[70] A.H. Fariborz, R. Jora, J. Schechter, «Toy model for two chiral nonets», *Phys. Rev. D* **72**, 034001 (2005), arXiv:hep-ph/0506170; A.H. Fariborz, «Isosinglet Scalar Mesons Below 2-GeV and the Scalar Glueball Mass», *Int. J. Mod. Phys. A* **19**, 2095 (2004), arXiv:hep-ph/0302133; M. Napsuciale, S. Rodriguez, «Chiral model for $\bar{q}q$ and $\bar{q}\bar{q}qq$ mesons», *Phys. Rev. D* **70**, 094043 (2004), arXiv:hep-ph/0407037.

[71] W. Bietenholz *et al.*, «Pion in a box», *Phys. Lett. B* **687**, 410 (2010), arXiv:1002.1696 [hep-lat].

[72] K. Langfeld, C. Kettner, «The Quark Condensate in the Gell-Mann–Oakes–Renner Relation», *Mod. Phys. Lett. A* **11**, 1331 (1996), arXiv:hep-ph/9601370.

[73] P. Kovács, G. Wolf, «Meson Vacuum Phenomenology in a Three-flavor Linear Sigma Model with (Axial-)Vector Mesons: Investigation of the $U(1)_A$ Anomaly Term», *Acta Phys. Pol. B Proc. Suppl.* **6**, 853 (2013), arXiv:1304.5362 [hep-ph].

[74] F. Giacosa, S. Jafarzade, R. Pisarski, «Anomalous interactions for heterochiral mesons with $J^{PC} = 1^{+-}$ and 2^{-+}», arXiv:2309.00086 [hep-ph].

[75] J. Gasser, H. Leutwyler, «Chiral Perturbation Theory to One Loop», *Ann. Phys.* **158**, 142 (1984). See also S. Scherer, «Introduction to chiral perturbation theory», *Adv. Nucl. Phys.* **27**, 277 (2003), arXiv:hep-ph/0210398,

[76] A. Koenigstein, F. Giacosa, «Phenomenology of pseudotensor mesons and the pseudotensor glueball», *Eur. Phys. J. A* **52**, 356 (2016), arXiv:1608.08777 [hep-ph].

[77] S. Jafarzade, A. Koenigstein, F. Giacosa, «Phenomenology of $J^{PC} = 3^{--}$ tensor mesons», *Phys. Rev. D* **103**, 096027 (2021), arXiv:2101.03195 [hep-ph].

[78] A. Athenodorou, M. Teper, «The glueball spectrum of SU(3) gauge theory in $3+1$ dimensions», *J. High Energy Phys.* **2020**, 172 (2020), arXiv:2007.06422 [hep-lat].

[79] E. Trotti, S. Jafarzade, F. Giacosa, «Thermodynamics of the glueball resonance gas», *Eur. Phys. J. C* **83**, 390 (2023), arXiv:2212.03272 [hep-ph].

[80] H.X. Chen *et al.*, «An updated review of the new hadron states», *Rep. Prog. Phys.* **86**, 026201 (2023), arXiv:2204.02649 [hep-ph].

[81] G.J. Gounaris, J.E. Paschalis, R. Kogerler, «The zero-spin glueballs: A new approach to relativistic bound states», *Z. Phys. C* **31**, 277 (1986); *Erratum ibid.* **33**, 474 (1987).

[82] V.A. Novikov *et al.*, «Charmonium and gluons», *Phys. Rep.* **41**, 1 (1978); M. Campostrini, A. Di Giacomo, Y. Gündüc, «Gluon Condensation in SU(3) lattice gauge theory», *Phys. Lett. B* **225**, 393 (1989).

[83] F. Giacosa, A. Pilloni, E. Trotti, «Glueball–glueball scattering and the glueballonium», *Eur. Phys. J. C* **82**, 487 (2022), arXiv:2110.05582 [hep-ph].

[84] W.J. Lee, D. Weingarten, «Scalar quarkonium masses and mixing with the lightest scalar glueball», *Phys. Rev. D* **61**, 014015 (2000), arXiv:hep-lat/9910008.

[85] F. Giacosa, T. Gutsche, V.E. Lyubovitskij, A. Faessler, «Scalar nonet quarkonia and the scalar glueball: Mixing and decays in an effective chiral approach», *Phys. Rev. D* **72**, 094006 (2005), arXiv:hep-ph/0509247.

[86] H.Y. Cheng, C.K. Chua, K.F. Liu, «Scalar glueball, scalar quarkonia, and their mixing», *Phys. Rev. D* **74**, 094005 (2006), arXiv:hep-ph/0607206.

[87] F. Brünner, D. Parganlija, A. Rebhan, «Glueball decay rates in the Witten–Sakai–Sugimoto model», *Phys. Rev. D* **91**, 106002 (2015), arXiv:1501.07906 [hep-ph]; *Erratum ibid.* **93**, 109903 (2016).

[88] CLQCD Collaboration (L.C. Gui *et al.*), «Scalar Glueball in Radiative J/ψ Decay on the Lattice», *Phys. Rev. Lett.* **110**, 021601 (2013), arXiv:1206.0125 [hep-lat].

[89] W.I. Eshraim, S. Janowski, F. Giacosa, D.H. Rischke, «Decay of the pseudoscalar glueball into scalar and pseudoscalar mesons», *Phys. Rev. D* **87**, 054036 (2013), arXiv:1208.6474 [hep-ph].

[90] BESIII Collaboration (M. Ablikim *et al.*), «Observation of a State $X(2600)$ in the $\pi^+\pi^-\eta'$ System in the Process $J/\psi \to \gamma\pi^+\pi^-\eta'$», *Phys. Rev. Lett.* **129**, 042001 (2022), arXiv:2201.10796 [hep-ex].

[91] F. Giacosa, J. Sammet, S. Janowski, «Decays of the vector glueball», *Phys. Rev. D* **95**, 114004 (2017), arXiv:1607.03640 [hep-ph].

[92] A. Vereijken, S. Jafarzade, M. Piotrowska, F. Giacosa, «Is $f_2(1950)$ the tensor glueball?», *Phys. Rev. D* **108**, 014023 (2023), arXiv:2304.05225 [hep-ph].

[93] F. Hechenberger, J. Leutgeb, A. Rebhan, «Radiative meson and glueball decays in the Witten–Sakai–Sugimoto model», *Phys. Rev. D* **107**, 114020 (2023), arXiv:2302.13379 [hep-ph].

[94] F. Hechenberger, J. Leutgeb, A. Rebhan, «Spin-1 glueballs in the Witten–Sakai–Sugimoto model», *Phys. Rev. D* **109**, 074014 (2024), arXiv:2401.17986 [hep-ph].

[95] K. Sil, V. Yadav, A. Misra, «Top–down holographic G-structure glueball spectroscopy at (N)LO in N and finite coupling», *Eur. Phys. J. C* **77**, 381 (2017), arXiv:1703.01306 [hep-th].

[96] C.A. Meyer, E.S. Swanson, «Hybrid mesons», *Prog. Part. Nucl. Phys.* **82**, 21 (2015), arXiv:1502.07276 [hep-ph].

[97] J.J. Dudek *et al.*, «Toward the excited meson spectrum of dynamical QCD», *Phys. Rev. D* **82**, 034508 (2010), arXiv:1004.4930 [hep-ph]; Hadron Spectrum Collaboration (J.J. Dudek *et al.*), «Toward the excited isoscalar meson spectrum from lattice QCD», *Phys. Rev. D* **88**, 094505 (2013), arXiv:1309.2608 [hep-lat].

[98] V. Shastry, C.S. Fischer, F. Giacosa, «The phenomenology of the exotic hybrid nonet with $\pi_1(1600)$ and $\eta_1(1855)$», *Phys. Lett. B* **834**, 137478 (2022), arXiv:2203.04327 [hep-ph]; V. Shastry, F. Giacosa, «Radiative production and decays of the exotic $\eta_1'(1855)$ and its siblings», *Nucl. Phys. A* **1037**, 122683 (2023), arXiv:2302.07687 [hep-ph].

[99] W.I. Eshraim, C.S. Fischer, F. Giacosa, D. Parganlija, «Hybrid phenomenology in a chiral approach», *Eur. Phys. J. Plus* **135**, 945 (2020), arXiv:2001.06106 [hep-ph].

[100] V. Baru *et al.*, «Evidence that the $a_0(980)$ and $f_0(980)$ are not elementary particles», *Phys. Lett. B* **586**, 53 (2004), arXiv:hep-ph/0308129.

[101] T. Branz, T. Gutsche, V.E. Lyubovitskij, «Strong and radiative decays of the scalars $f_0(980)$ and $a_0(980)$ in a hadronic molecule approach», *Phys. Rev. D* **78**, 114004 (2008), arXiv:0808.0705 [hep-ph].

[102] A.A. Petrov, «Glueball-meson molecules», *Phys. Lett. B* **843**, 138030 (2023), arXiv:2204.11269 [hep-ph].

[103] M. Boglione, M.R. Pennington, «Dynamical generation of scalar mesons», *Phys. Rev. D* **65**, 114010 (2002), arXiv:hep-ph/0203149hep-ph/.

[104] T. Wolkanowski, F. Giacosa, D.H. Rischke, «$a_0(980)$ revisited», *Phys. Rev. D* **93**, 014002 (2016), arXiv:1508.00372 [hep-ph].

[105] J.R. Peláez, «Nature of Light Scalar Mesons from their Large N_c Behavior», *Phys. Rev. Lett.* **92**, 102001 (2004), arXiv:hep-ph/0309292.

[106] J.R. Peláez, «From controversy to precision on the sigma meson: A review on the status of the non-ordinary $f_0(500)$ resonance», *Phys. Rep.* **658**, 1 (2016), arXiv:1510.00653 [hep-ph].

[107] J.R. Peláez, A. Rodas, J. Ruiz de Elvira, «Strange resonance poles from $K\pi$ scattering below 1.8 GeV», *Eur. Phys. J. C* **77**, 91 (2017), arXiv:1612.07966 [hep-ph].

[108] T. Wolkanowski, M. Sołtysiak, F. Giacosa, «$K_0^*(800)$ as a companion pole of $K_0^*(1430)$», *Nucl. Phys. B* **909**, 418 (2016), arXiv:1512.01071 [hep-ph].

[109] F. Giacosa, M. Piotrowska, S. Coito, «$X(3872)$ as virtual companion pole of the charm–anticharm state $\chi_{c1}(2P)$», *Int. J. Mod. Phys. A* **34**, 1950173 (2019), arXiv:1903.06926 [hep-ph].

[110] E. van Beveren *et al.*, «A low lying scalar meson nonet in a unitarized meson model», *Z. Phys. C* **30**, 615 (1986), arXiv:0710.4067 [hep-ph]; E. van Beveren *et al.*, «The nature of σ, κ, $a_0(980)$ and $f_0(980)$», *Phys. Lett. B* **641**, 265 (2006), arXiv:hep-ph/0606022; J.A. Oller, E. Oset, «Chiral symmetry amplitudes in the S-wave isoscalar and isovector channels and the σ, $f_0(980)$, $a_0(980)$ scalar mesons», *Nucl. Phys. A* **620**, 438 (1997), arXiv:hep-ph/9702314; *Erratum ibid.* **652**, 407 (1999); J.A. Oller,

E. Oset, J.R. Peláez, «Meson meson interaction in a nonperturbative chiral approach», *Phys. Rev. D* **59**, 074001 (1999) arXiv:hep-ph/9804209; *Erratum ibid.* **60**, 099906 (1999); *Erratum ibid.* **75**, 099903 (2007).

[111] F. Giacosa, «Dynamical generation and dynamical reconstruction», *Phys. Rev. D* **80**, 074028 (2009), arXiv:0903.4481 [hep-ph].

[112] Z.H. Guo, L.Y. Xiao, H.Q. Zheng, «Is the $f_0(600)$ Meson a Dynamically Generated Resonance? A Lesson Learned from the O(N) Model and Beyond», *Int. J. Mod. Phys. A* **22**, 4603 (2007), arXiv:hep-ph/0610434.

[113] R.L. Jaffe, «Multiquark hadrons. I. The phenomenology of Q^2Q^{-2} mesons», *Phys. Rev. D* **15**, 267 (1977).

[114] R.L. Jaffe, «Exotica», *Phys. Rep.* **409**, 1 (2005), arXiv:hep-ph/0409065.

[115] L. Maiani, F. Piccinini, A.D. Polosa, V. Riquer, «A New Look at Scalar Mesons», *Phys. Rev. Lett.* **93**, 212002 (2004), arXiv:hep-ph/0407017.

[116] F. Giacosa, «Strong and electromagnetic decays of the light scalar mesons interpreted as tetraquark states», *Phys. Rev. D* **74**, 014028 (2006), arXiv:hep-ph/0605191.

[117] F. Giacosa, «Mixing of scalar tetraquark and quarkonia states in a chiral approach», *Phys. Rev. D* **75**, 054007 (2007), arXiv:hep-ph/0611388.

[118] L. Olbrich, M. Zétényi, F. Giacosa, D.H. Rischke, «Influence of the axial anomaly on the decay $N(1535) \to N\eta$», *Phys. Rev. D* **97**, 014007 (2018), arXiv:1708.01061 [hep-ph].

[119] V. Koch, «Aspects of Chiral Symmetry», *Int. J. Mod. Phys. E* **6**, 203 (1997), arXiv:nucl-th/9706075.

[120] C.E. DeTar, T. Kunihiro, «Linear sigma model with parity doubling», *Phys. Rev. D* **39**, 2805 (1989).

[121] D. Zschiesche, L. Tolos, J. Schaffner-Bielich, R.D. Pisarski, «Cold, dense nuclear matter in a SU(2) parity doublet model», *Phys. Rev. C* **75**, 055202 (2007), arXiv:nucl-th/0608044.

[122] S. Gallas, F. Giacosa, D.H. Rischke, «Vacuum phenomenology of the chiral partner of the nucleon in a linear sigma model with vector mesons», *Phys. Rev. D* **82**, 014004 (2010), arXiv:0907.5084 [hep-ph].

[123] S. Gallas, F. Giacosa, G. Pagliara, «Nuclear matter within a dilatation-invariant parity doublet model: The role of the tetraquark at nonzero density», *Nucl. Phys. A* **872**, 13 (2011), arXiv:1105.5003 [hep-ph].

[124] R.A. Tripolt, C. Jung, L. von Smekal, J. Wambach, «Vector and axial-vector mesons in nuclear matter», *Phys. Rev. D* **104**, 054005 (2021), arXiv:2105.00861 [hep-ph].

[125] P. Lakaschus, J.L.P. Mauldin, F. Giacosa, D.H. Rischke, «Role of a four-quark and a glueball state in pion–pion and pion–nucleon scattering», *Phys. Rev. C* **99**, 045203 (2019), arXiv:1807.03735 [hep-ph].

[126] L. Olbrich, M. Zétényi, F. Giacosa, D.H. Rischke, «Three-flavor chiral effective model with four baryonic multiplets within the mirror assignment», *Phys. Rev. D* **93**, 034021 (2016), arXiv:1511.05035 [hep-ph].

[127] H. Satz, «The Thermodynamics of Quarks and Gluons», *Lect. Notes Phys.* **785**, 1 (2010), arXiv:0803.1611 [hep-ph]; H. Satz, «The Quark–Gluon Plasma: A Short Introduction», *Nucl. Phys. A* **862–863**, 1 (2011), arXiv:1101.3937 [hep-ph].

[128] J.T. Lenaghan, D.H. Rischke, J. Schaffner-Bielich, «Chiral symmetry restoration at nonzero temperature in the $\mathrm{SU}(3)_r \times \mathrm{SU}(3)_l$ linear sigma model», *Phys. Rev. D* **62**, 085008 (2000), arXiv:nucl-th/0004006.

[129] N.K. Glendenning, «Compact stars: Nuclear physics, particle physics, and general relativity», *Springer Verlag*, 2000.

[130] S. Lottini, G. Torrieri, «A Percolation Transition in Yang–Mills Matter at Finite Number of Colors», *Phys. Rev. Lett.* **107**, 152301 (2011), arXiv:1103.4824 [nucl-th].

[131] G. Torrieri, I. Mishustin, «The nuclear liquid–gas phase transition at large N_c in the Van der Waals approximation», *Phys. Rev. C* **82**, 055202 (2010), arXiv:1006.2471 [nucl-th].

[132] A. Heinz, S. Struber, F. Giacosa, D.H. Rischke, «Role of the tetraquark in the chiral phase transition», *Phys. Rev. D* **79**, 037502 (2009), arXiv:0805.1134 [hep-ph].

[133] R.D. Pisarski, F. Rennecke, «The chiral phase transition and the axial anomaly», arXiv:2401.06130 [hep-ph].

[134] M. Gazdzicki, M. Gorenstein, P. Seyboth, «Onset of Deconfinement in Nucleus–Nucleus Collisions: Review for Pedestrians and Experts», *Acta Phys. Pol. B* **42**, 307 (2011), arXiv:1006.1765 [hep-ph].

[135] NA61/SHINE Collaboration (H. Adhikary *et al.*), «Search for the critical point of strongly-interacting matter in $^{40}\mathrm{Ar} + {}^{45}\mathrm{Sc}$ collisions at 150 $A\,\mathrm{GeV}/c$ using scaled factorial moments of protons», *Eur. Phys. J. C* **83**, 881 (2023), arXiv:2305.07557 [nucl-ex]; M.I. Gorenstein, M. Gaździcki, W. Greiner, «Critical line of the deconfinement phase transitions», *Phys. Rev. C* **72**, 024909 (2005), arXiv:nucl-th/0505050.

[136] G. Pagliara, J. Schaffner-Bielich, «Stability of color-flavor-locking cores in hybrid stars», *Phys. Rev. D* **77**, 063004 (2008), arXiv:0711.1119 [astro-ph].